

ISSN 0236-2945

LIGHT & ENGINEERING

Volume 27, Number 3, 2019

**Editorial of Journal
“Light & Engineering” (Svetotekhnika), Moscow**

The purpose and content of «Light & Engineering» is to develop the science of light within the framework of ray, photometric concepts and the application of results for a comfortable light environment, as well as for visual and non-visual light technologies, including medicine. The light engineering science is a field of science and technology and its subject is the development of methods for generation and spatial redistribution of optical radiation, as well as its conversion to other forms of energy and use for various purposes.

The scope of journal includes articles in the following areas:

- Sources of light;
- Light field theory;
- Photometry, colorimetry and radiometry of optical radiation;
- Visual and non-visual effects of radiation on humans;
- Control and regulation devices for light sources;
- Light devices, their design and production technology;
- Light devices for the efficient distribution and transportation of the light energy: hollow light guides, optical fibers;
- Lighting and irradiation installations;
- Light signaling and light communication;
- Light remote sensing;
- Mathematical modelling of light devices and installations;
- Energy savings in light installation;
- Innovative light design solutions;
- Photobiology, including problems of using light in medicine;
- Disinfection of premises, drinking water and smell elimination by UV radiation technology;
- Light transfer in the ocean, space and other mediums;
- Light and engineering marketing;
- Legal providing and regulation of energy effective lighting;
- Light conversion to other forms of energy;
- Standardization in field of lighting;
- Light in art and architecture design;
- Education in field of light and engineering.

Journal "Light & Engineering" had been founded by Prof. Julian B. Aizenberg in 1993

**LIGHT &
ENGINEERING**

**СВЕТО
ТЕХНИКА**

Editorial of Journal "Light & Engineering/Svetotekhnika"

General Editor: Julian B. Aizenberg
Editor-in-Chief: Vladimir P. Budak
Deputy Chief Editor: Raisa I. Stolyarevskaya

Editorial Board Chairman: George V. Boos, Moscow Power Engineering Institute

Editorial Board:

Sergei G. Ashurkov, Editorial of Journal

Lou Bedocs, Thorn Lighting Limited, United Kingdom

Mikhail L. Belov, Scientific-Research Institute of Radioelectronics and Laser Technology at the N.E. Bauman Moscow State Technical University

Tony Bergen, Technical Director of Photometric Solutions International, Australia

Grega Bizjak, University of Ljubljana Slovenia

Peter Blattner, Head of Laboratory of Federal Institute of Metrology METAS Bern-Wabern, Switzerland

Alexander A. Bogdanov, OJSC, "INTER RAO LEDs Systems"

Wout van Bommel, Philips Lighting, the Netherlands

Peter R. Boyce, Lighting Research Center, USA

Lars Bylund, Bergen's School of Architecture, Norway

Natalya V. Bystryantseva, ITMO University, St. Petersburg

Stanislav Darula, Academy Institute of Construction and Architecture, Bratislava, Slovakia

Andrei A. Grigoryev, Deputy Head of the "Light and Engineering" Chair, MPEI, Moscow

Tugce Kazanasmaz, Izmir Institute of Technology, Turkey

Alexei A. Korobko, BL Group, Moscow

Saswati Mazumdar, Jadavpur University, India

Dmitriy A. Melnikov, Ministry of Energy of Russian Federation

Evan Mills, Lawrence Berkeley Laboratory, USA

Leonid G. Novakovsky, Closed Corporation "Faros-Aleph"

Yoshi Ohno, NIST Fellow, (CIE President 2015–2019), USA

Alexander T. Ovcharov, Tomsk State Arch. – Building University, Tomsk

Leonid B. Prikupets, VNISI named after S.I. Vavilov, Moscow

Lucia R. Ronchi, Higher School of Specialization for Optics, University of Florence, Italy

Alla A. Ryabtseva, Ophthalmology department of Moscow Regional Research and Clinical Institute "MONIKI"

Anna G. Shakhparunyants, General Director of VNISI named after S.I. Vavilov, Moscow

Nikolay I. Shchepetkov, SA MARchi, Moscow

Alexei K. Solovyov, State Building University, Moscow

Peter Thorns, Zumtobel Lighting, Dornbirn, Austria

Konstantin A. Tomsy, St. Petersburg State University of Film and Television

Leonid P. Varfolomeev, Moscow

Nicolay Vasilev, Sofia Technical University, Bulgaria

Jennifer Veitch, National Research Council of Canada

Pavel P. Zak, Emanuel Institute of Biochemical Physics of Russian Academy of Science (IBCP RAS)

Olga E. Zheleznyakova, Head of the "Light and Engineering" Chair, N.P. Ogarev Mordovia State University, Saransk

Georges Zissis, University of Toulouse, France

Moscow, 2019

Light & Engineering / Svetotekhnika Journal Country Correspondents:

Argentina	Pablo Ixitaina	National and Technological La Plata Universities
France	Georges Zissis	University of Toulouse
India	Saswati Mazumdar	Jadavpur University
Slovenia	Grega Bizjak	University of Ljubljana
Turkey	Tugce Kazanasmaz	Izmir Institute of Technology (Urla)
	Erdal Sehirli	Kastamonu University (Kastamonu)
	Rengin Unver	Yildiz Technical University (Istanbul)

Editorial Office:

Russia, VNISI, Rooms 327 and 334
106 Prospekt Mira, Moscow 129626

Tel: +7.495.682.26.54
Tel./Fax: +7.495.682.58.46
E-mail: lights-nr@inbox.ru
<http://www.l-e-journal.com>

Light & Engineering" is an international scientific Journal subscribed to by readers in many different countries. It is the English edition of the journal "Svetotekhnika" the oldest scientific publication in Russia, established in 1932.

Establishing the English edition "Light and Engineering" in 1993 allowed Russian illumination science to be presented the colleagues abroad. It attracted the attention of experts and a new generation of scientists from different countries to Russian domestic achievements in light and engineering science. It also introduced the results of international research and their industrial application on the Russian lighting market.

The scope of our publication is to present the most current results of fundamental

Scientific Editors:

Sergei G. Ashurkov
Alexander Yu. Basov
Evgene I. Rozovsky
Raisa I. Stolyarevskaya
Art and CAD Editor
Andrei M. Bogdanov
Style Editor
Marsha D. Vinogradova

research in the field of illumination science. This includes theoretical bases of light source development, physiological optics, lighting technology, photometry, colorimetry, radiometry and metrology, visual perception, health and hazard, energy efficiency, semiconductor sources of light and many others related directions. The journal also aims to cover the application illumination science in technology of light sources, lighting devices, lighting installations, control systems, standards, lighting art and design, and so on.

"Light & Engineering" is well known by its brand and design in the field of light and illumination. Each annual volume has six issues, with about 80–120 pages per issue. Each paper is reviewed by recognized world experts.

CONTENTS

VOLUME 27

NUMBER 3

2019

LIGHT & ENGINEERING

Maria M. Ilyevskaya Interrelation of Architectural Concepts and Principles of Artificial Lighting in the Moscow Concert Hall Zaryadye	4
Vladimir N. Anisimov Light Desynchronosis and Health	14
Alexander V. Spiridonov and Nina P. Umnyakova Inspection of the State (General and Instrumental) of Historical Translucent Structures of the Pushkin State Museum of Fine Arts	26
Victor V. Belyaev, Donatien Nessemon, and Andrei A. Belyaev Application of Display Technologies for Lighting	32
Merve Öner and Tuğçe Kazanasmaz Illuminance and Luminance Based Ratios in the Scope of Performance Testing of a Light Shelf-Reflective Louver System in a Library Reading Room	39
Xiufang Zhao, Xin Zhang, and Kai Cui Recreating the Tibetan Traditional Lighting in Local Modern Library: Research-Based Lighting Design in Yushu Library	47
Ksenia I. Nechaeva The Reconstruction Project of Illumination Devices at the Krasnoselskaya Station of the Moscow Metro	59
Behçet Kocaman and Sabir Rüstemli Comparison of LED and HPS Luminaries in Terms of Energy Savings at Tunnel Illumination	67
Mechmet Sait Cengiz The Relationship between Maintenance Factor and Lighting Level in Tunnel Lighting	75
Ana del Águila, Dmitry S. Efremenko, and Thomas Trautmann A Review of Dimensionality Reduction Techniques for Processing Hyper-Spectral Optical Signal	85
Vitold E. Pozhar, Alexander S. Machikhin, Maxim I. Gaponov, Sergei V. Shirokov, Mikhail M. Mazur and Alexei E. Sheryshev Hyper-spectrometer Based on an Acousto-optic Tuneable Filters for UAVS	99
Michael Young-gon Lee and Sergei V. Fedorov Double Beam Spectrophotometer for Simultaneous Measurements of the Upwelling Sea Radiance and the Incident Sea Irradiance	105
Olga E. Zheleznikova and Sergei V. Prytkov On the Issue of Transformation of Spatial Photometric Systems	111
Content #4	116

INTERRELATION OF ARCHITECTURAL CONCEPTS AND PRINCIPLES OF ARTIFICIAL LIGHTING IN THE MOSCOW CONCERT HALL ZARYADYE

Maria M. Ilyevskaya

TPO Reserve, LLC, Moscow Institute of Architecture (State Academy), Moscow
E-mail: research@reserve.ru

ABSTRACT

The article is focused on the analysis of the Zaryadye Concert Hall building in Moscow in terms of the significance of artificial lighting for the creation of the imagery and perception of this facility within the typology of entertainment music-oriented buildings. Through the example of modern places of entertainment, the author reveals a number of formal features (typological attributes), which, being common to buildings of this function, constitute the basis of their image and become obvious due to the realized lighting concept. The interpretation of these attributes in the interaction of architectural planning and lighting concepts in the Zaryadye Concert Hall is traced. In conclusion, the distinctive features of the building under consideration are determined. At the same time, they reflect a new understanding of concert halls as a building type, the changes related to the overall development of architecture, as well as the elements of the individual architectural language.

Keywords: Zaryadye Concert Hall, architecture of concert halls, places of entertainment, the lighting of public buildings, artificial lighting, building typology

1. INTRODUCTION

The Zaryadye Concert Hall in Moscow is the newest architectural work, officially opened on September 8 of 2018, and it became the first place in the Russian capital similar in function and

capacity to the opened in 2002 Moscow International Music Centre. It is important to note that the planning of the Zaryadye Hall took place against the background of the incredibly active construction of musical theatres and concert halls around the world, which makes the new discussion of this type of buildings relevant, if not comprehensive, at least in some aspects.

The concert halls as a special type of buildings have been repeatedly discussed both in Russian and foreign literature. In the national sources, the approach prevails related to the functional evaluation of the auditorium regarding its varieties and their connection with forms of concert activities. Abroad, a rapid reaction to the “musical building boom” in the architectural periodicals to be recorded, which published special issues dedicated to the new objects, and among them such journals as *Archi* (No. 22018), *Baumeister* (No. 32017), *Detail* (No. 32018). However, according to experts, the study of this area still lacks consistency, at least in the domestic interpretation [1]. Therefore, when evaluating the new Moscow object, it seems interesting to distinguish a set of features systematically characterizing it as a building type, first of all, in the perception of the viewer. The emotional feedback in the press after the opening of the Zaryadye Hall, establish an interesting base for this purpose.

The attempt of such architectural evaluation on pages of the *Light & Engineering Journal* is not coincidental. Going beyond the technical topics and commitment to the interdisciplinary approach

is one of the strategic tasks that the editorial board has set [2]. At the same time, it is crucial for architects to draw the attention of technical specialists to the humanitarian concerns related to their field, to the issues of architecture perception and to those aspects of architectural practice that are directly related to the choice of lighting solutions.

The significance of artificial lighting to identify the special nature of the subject to typology has already been discussed in the journal in respect to industrial facilities [3]. As for concert halls, this is a type of building, for which artificial light in most cases becomes a necessary condition for perception of architectural design. The main functional unit (auditorium/auditoria), with few exceptions, is closed to natural light, due to the acoustics requirements. Displaying by lighting the individual plasticity of the hall, as well as the relationship between the hall and the rest of the audience complex, becomes one of the key artistic goals. The appearance of the building in the city, of course, is determined by the urban development situation. But its urban image, perceived by the viewers, due to the work pattern of musical halls, is most often associated with the memorable light image of the building. That is the understanding of the architecture of a place of entertainment requires attention to lighting solutions, and, on the contrary, when choosing the lighting solutions it should be considered what typological features they highlight.

This article is aimed at analyzing the lighting solutions of the new Moscow Concert Hall in terms of their relationship with a number of plastic and spatial features that make up the *typological attributes* of concert halls. The *typological attributes* herein will be understood as organizing elements in the architecture of the building, which have been the subject of artistic development as a result of the building type evolution.

The research methods are selected such as architectural analysis with the inclusion of visual analysis of artificial lighting techniques and comparison of the considered building with other buildings within the typology, and in some cases besides concert halls object is comparing with opera buildings and musical theatres. The focus of the review is the audience complex, while the administrative and service unit is concerned only in connection with the description of the space-planning solution.

2. GENERAL URBAN PLANNING AND ARCHITECTURAL SOLUTIONS OF THE ZARYADYE CONCERT HALL

After the competition for landscape and urban planning concept of Zaryadye Park held in 2013, its implementation was entrusted to the winner of the first prize – a consortium led by *Diller, Scofidio + Renfro NY*, American architectural firm. The design of the concert hall within the park concept was assigned to the second prize winner, to the Moscow architectural bureau TPO “Reserve”.

2.1. The Site Conditions

The Zaryadye Concert Hall building closes the east side of the landscape urban complex “Zaryadye Park”, which is located in close proximity to the Moscow Kremlin on the territory of the historic Zaryadye district and on the site of the Hotel Russia dismantled in 2010, that is, between Vasilievsky Descent, Varvarka Street, Kitaygorod Passage and the Moscow River Embankment. The implementation of the concert hall design as a part of the park complex project entailed a number of conceptual, planning and structural limitations. The most significant are:

- Limitation for the vertical development of the building. This does not refer only and mostly to the urban height limits, but to the concept of the glazed spatial structure covering the hall, presented by American architects at the contest stage and given to the authors of the concert hall for further elaboration. In addition, the idea of a microclimatic recreation area on the concert hall roof also related to the contest concept by *Diller, Scofidio + Renfro NY* was to be realized. In other words, the concert hall building received geometrically pre-installed “fifth facade”, which excludes light openings on the side of the park as well as in the covering of the building.

- Limitation for development in width due to the car-parking space adjacent to the concert hall site and cut off by straight walls. These walls become the physical contour of the building, predetermining a large area of utility rooms without natural light, as well as position of a small hall.

- The location of the major hall within the site recorded at an early stage of the project. At the beginning of design process, the concept of visual opening of a large hall to a new “floating bridge” through a glazed opening of the end wall was devel-

oped, but it was rejected according to the acoustics requirements [4]. However, the orientation of the longitudinal axis of the hall was maintained, and it predetermined the development of the foyer space along the eastern wall of the building. On the southern facade a blind fragment of the wall emerged, requiring definition in respect of architectural and lighting aspects.

Thus, the design situation can be described as a rectangular niche, covered on the top, in which the hall is inscribed diagonally, occupying more than a third of the floor area. The area of the site under design is 18,450 m². The principal entrance is located in the northeast and is oriented towards the most vibrant pedestrian traffic from the Kitay-Gorod metro station; it is accentuated by a small square formed by the incurved facade surface under the overhanging part of the spatial structure. The primary area of perception of the building is the space about 25 m wide between the Kitaygorod wall and the eastern facade of the concert hall, partially open to the embankment and Zaryadye Park (Fig. 1).

2.2. Architectural Solutions

Being part of the park complex the building, however, can be considered as an independent architectural work of entertainment, as in terms of functional organization it has no continuous connection with park facilities (Fig. 2).

The foyer envelops the large hall on the north and east sides, developing on two levels and actively using the slope of the site towards the Moscow River. The outer contour of the foyer is completely glazed, and the adjacent interior areas are mainly



Fig. 1. Zaryadye Concert Hall in Moscow, view of the entrance area (photo: A. Naroditsky)

high, multi-light spaces. In the southern part of the building on the second level there is a viewpoint, overhanging above the lower level and oriented towards the embankment panorama. Cafes and bars are designed as open areas within the foyer.

The cloakroom is located under the entrance area of the foyer, in the underground part of the building.

The large hall with 1,588 seats is designed as a space with natural acoustics for musical performances of different genres with arena-type stage and the possibility of various transformation of the spectator area. The spectator area includes the stalls, the tiered stalls, the dress circle around the stage, as well as one level of the upper circle. The central axis length of the hall is about 50 m, the largest width is 33 m, and the height above the tiered stalls is 20 m.

The small hall is designed for 400 seats. It is thought for both rehearsals and chamber concerts, and has an irregular shape close to a trapeze. Its height is 14.5 m and its area on the lower level is 300 m². At a height of 5 m the hall is surrounded by a narrow gallery with additional spectator seats.

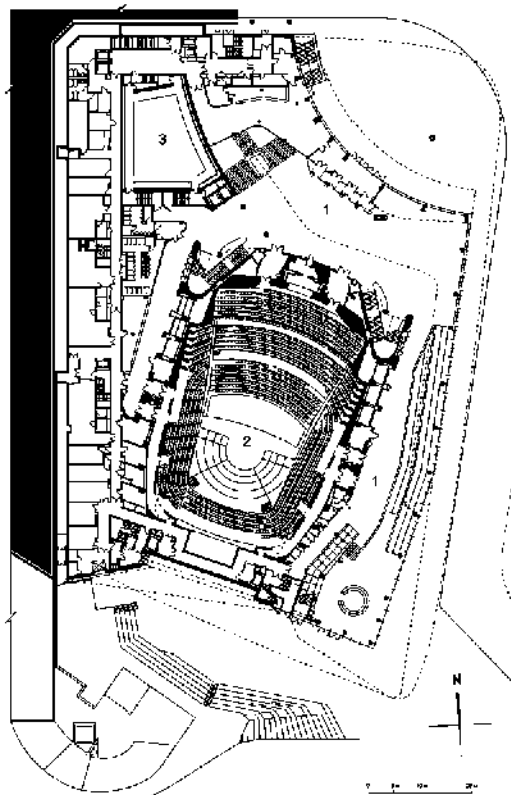


Fig. 2. Zaryadye Concert Hall in Moscow, scheme of the ground floor plan (TPO Reserve):
1 – foyer; 2 – main hall; 3 – small hall

The administrative unit is located above the second level of the foyer and is partially opened by the glazed front into the inner multi-light space.

Overall dimensions of the building are: length of the eastern facade (on the overhanging part) is 100 m, length of the southern facade (glass part) is 25 m, and blind part length is equal to 45 m. Height to the top of the glass parapet is from 18 up to 23 m (with regard for changes in topography). The total area of the building is 25,870 m².

3. THE SHAPING OF THE BUILDING LIGHT IMAGE IN THE URBAN ENVIRONMENT

The forced inbuilt configuration, mentioned above, could not but influence the choice of expressive means, including the approach to lighting. The idea of glowing “insides” of a large body, visible from the outside through the open hollows of relief (or rather, the roofs of built-in facilities), is common to the entire park complex. It involves, for example, such an interpretation of the building, where it appears as buried to a large extent in the construction of the park complex, and the illuminated interior is visible only on one side. Side facades are half hidden in relief, which requires a special ingenuity in their design. The same principles are applied to the architecture of other facilities of the park, mainly intended for entertainment. In the concert hall building these conditions entailed two solutions, each of which, even for the separate city places of entertainment, can be considered the typological attributes. This is the principle of the “*exposed interior*” on the east side and the application of the *media facade* on the south side (Fig. 3).



Fig. 3. General view from the southeast; on the southern facade there is a LED screen and the wall plastic is illuminated (photo: A. Naroditsky)

3.1. “Exposed Interior” as an Inviting Element

In Modernist architecture, the facade showing the depth of the interior is perhaps one of the crucial achievements associated with the new possibilities of constructions. In Postmodernist architecture, especially in relation to places of entertainment, it is one of the most often used solutions because of its performing and communicative features. By virtue of it, the performance begins already on the way to the building, when the viewer perceives the atmosphere of the foyer from the city space. Therefore, the lighting techniques supporting the idea of a “showcase facade” are no less developed than the space-planning solutions representing it. Such buildings as Metropolitan Opera in New York, USA (1966, architect *W. Harrison*), Winspear Opera House in Dallas, USA (2009, *Foster + Partners*), Stavanger Concert Hall, Norway (2012, *RATIO arkitekter AS*) are just a few examples of convincing disclosure of this topic in architectural and light terms.

As noted by the chief architect of *TPO Reserve* Vladimir Plotkin, the theme of the exposed interior, a complex illuminated sculpture visible from the outside through the glass, became decisive for the solution of the eastern facade [4]. This intention is perfectly read by observers. The author of an essay about the Zaryadye Hall Konstantin Savkin takes the idea of depth as a title, understanding it not only as a facade inviting idea, but also as the essence of this building [5].

Logic suggests that the greatest effect here is achieved with minimal illumination of the exterior facade plane and luminous interior. In the Zaryadye Hall these light relations are generally preserved. The authors refused to illuminate the glazed facade. In the entrance area, only local illumination of the canopy is used with LED luminaires built in the paving. In addition, in the canopy there are LED strip lights, illuminating the surface of the ground in front of the entrance¹. A special role in the facade design is played by light graphics in the interior, which will be discussed further, and a number of transparent fins that create a resemblance of

¹ Here and further technical data on light sources are provided in accordance with the project documentation on the “Concert Hall of Philharmonic Music for 1,500 seats, Varvarka Str., estate 6” volume 5.1.2 “Interior Lighting”, volume 5.1.3. “Architectural lighting of facades”.



Fig. 4. Light themes of facades: a – “exposed interior”; b – lighting of wall plastic on the southern facade (photo: M. Ilyevskaya)

a glass curtain refracting the light along the building perimeter.

Performed by the *TPO Reserve* architects, this rather popular facade interpretation reflects one of the basic items of the bureau’s artistic language: a kind of universal space concept in form of the structure of overlaid grids and separate filling elements (Fig. 4a) [6].

3.2. The Media Facade as a Manifestation of Commercial Component in the Typology of Concert Halls

It is also necessary to focus on the light solution of the southern facade of the concert hall facing the Moscow River, the only blind fragment of the visible part of the building. A large LED screen is placed in a niche resembling an acute-angled portal. According to the architects, this is a kind of technical replacement of the rejected idea of the hall opened in the park: the screen is intended for broadcasting the events from the main hall to the open air amphitheatre, as well as for informing about the program of the concert hall [4]. The screen has a variable height from 8 to 14 m, and a length of 22.4 m. The screen is based on LED modules with a physical pixel pitch of 10 mm, the screen brightness is not less than $6,000 \text{ cd/m}^2$.

² The technical data on the media facade are given in accordance with the project documentation of the “Concert Hall of Philharmonic Music for 1500 seats, Varvarka Str., estate 6”, volume 5.6.15 “Media facade”.

Media facades have already firmly entrenched in the urban environment: a “talking surface” – the surface of communication – is an element that refers to the advertising backlit panels of Las Vegas. But the entertainment and commercial component of the “pavilion in the entertainment garden”, being present along with the strict image of the “palace of music worship” in the typology of concert halls [1], leads the media facade to become a full attribute of buildings of this type. The architects, the authors of concert halls, do not refuse this means of clearly advertising nature, its potential for creating large-scale facade solutions combined with the ability to attract attention is very seductive. In this regard, it is worth mentioning again the Stavanger Concert Hall, which uses the LED screen in a similar situation to the Moscow Hall, as well as the Danish Radio Concert Hall in Copenhagen (2009, architect *J. Nuvel*), with the facade completely formed by the LED system, the Harpa Concert Hall in Reykjavik, Iceland (2011, architect *H. Larsen*), New World Centre in Miami Beach, USA (2011, architect *F. Gary*).

The concept of the walls framing the screen allows speaking about the next attribute of music halls. These walls are designed plastically as a system of thin vertical pilasters. The portal area corresponds to the organ’s area in the interior of the hall, so you can see again the projection of the internal content on the facade, this time by architectural details. Illuminated by a top-down system of spotlights of 12 white LEDs each, with correlated colour temperature $T_{cc} = 3,000 \text{ K}$, with a power of 27 W, this fine plastic continues to be perceived

in hours of darkness (Fig. 4b). But in addition to this “literary” reading, it is of much importance to outline the theme linking more deeply the architecture of concert halls with music, namely, the active use of rhythmic series in concepts of buildings of this type. We will discuss this in more detail in the next section.

4. IDENTIFICATION OF TYPOLOGICAL ATTRIBUTES THROUGH THE LIGHT SCENARIO OF THE INTERIOR OF THE SPECTATOR COMPLEX

In the internal arrangement of concert halls there are three major issues that can be considered as the attributes of type, namely: *reading the foyer as an autonomous spectacular space*; *architectural elaboration of “core-and-shell” relationships*; *active use of rhythmic rows*. Their disclosure in the Zaryadye Hall building through interior lighting shows how the context of a particular building affects their modification.

4.1. Foyer as an Autonomous Spectacular Space

The architecture of the foyer is a big issue in the evolution of places of entertainment with musical profile, which should be associated with the changes in relationship of the society to the music presentation activity over time. Speaking about the musical centres of the second half of the 20th century and the beginning of the 21st century, it is worth noting the trend of increasing autonomy of the foyer and extending of its functional understanding. “Less is

a bore” maxim, driven by the hand of architect and theorist R. Venturi, which determined the mentality of postmodern society, determines, among other things, the situation when the vision of foyer solely as the distributive space prefacing the main hall, even if elegantly designed, would be an anachronism. Such a foyer would seem “boring” today. It acquires the character of an open and universal space, which is expected to be architecturally complex and well staged. A possible condition of autonomy is the connection with the outer space, direct or visual. The foyer as if “given” to the city, not only serves a hall. As noted by Western architectural critics, the spectacular foyer and its role in the city today become the key to success for a musical institution no less, and sometimes more, than what is happening on the stage [7]. As a result, the foyer is increasingly becoming venues for events not related to concert activities, as was the case with the Zaryadye Hall, which long before the opening became a platform for Moscow Urban Forum 2018. A good example of how the foyer of a concert hall can turn today into architectural and light show, is the building of the *Elbphilharmonie* in Hamburg, Germany (2017, *Herzog & de Meuron*). And the true historical manifesto of the autonomous foyer is, from our point of view, the magnificent Opera and Concert Hall complex in Sydney, Australia (1959–1973, architect *J. Utzon*). The approaches to the development of a complex spatial scenario can be different, but the lighting, as well as in the space of the performance, plays the role of an emotional manipulator.

In analyzing the foyer of the Moscow Concert Hall, written feedback from visitors was essential



Fig. 5. Foyer lighting: entrance area, light graphics against the background of floodlighting (photo: A. Naroditsky)

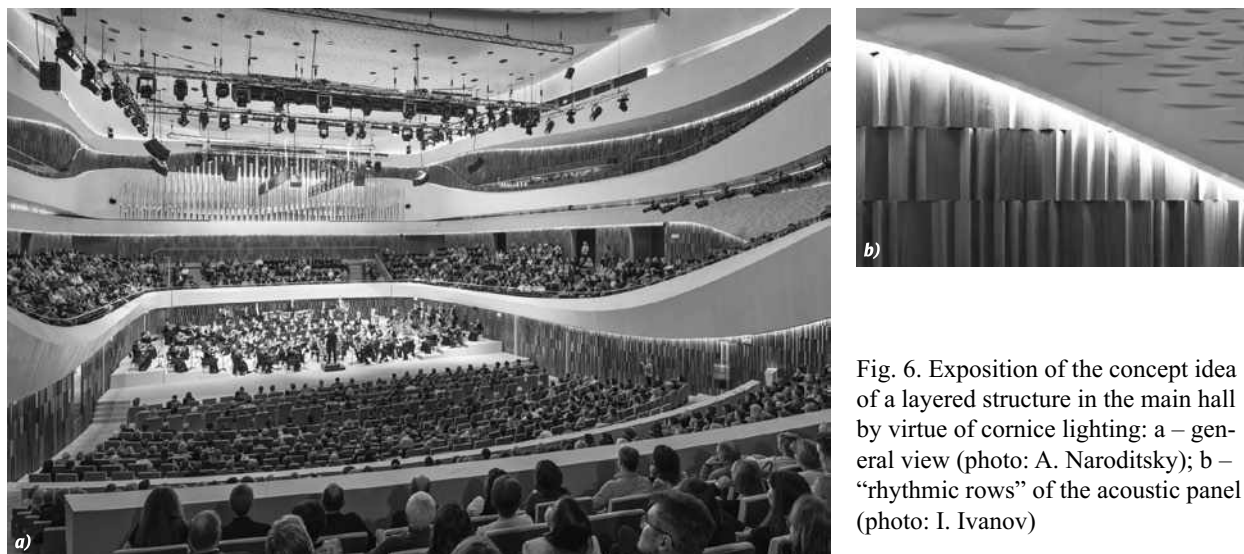


Fig. 6. Exposition of the concept idea of a layered structure in the main hall by virtue of cornice lighting: a – general view (photo: A. Naroditsky); b – “rhythmic rows” of the acoustic panel (photo: I. Ivanov)

reference. The thing attracting them is the perception of the foyer space as a labyrinth, a place with a confusing structure, a feeling of being “inside the mechanism” [8], appreciated, however, as “contemplative journey” [5]. In our opinion, the crucial role in such a picture is played by the lighting principle, although the complexity of utilities (stairs, ramps, balconies and viewpoints) cannot be underestimated, as well as the use of a large amount of materials with a reflective surface (polished granite on the floor, large stained glass surfaces, mirror panels in wall decoration). The light scenario can be described as “bright on bright”. In other words, against the background of matt, almost shadowless floodlight, more active elements of light graphics are applied (Fig. 5).

The floodlighting is provided by built-in LED luminaires of 13 W and $T_{cc} = 3000$ K in the suspended ceilings (the total number of such luminaires at all levels of the foyer is 878, and in the cloakroom is 425). The principal design concept was their visually disordered arrangement. In the multilight areas of the foyer, wall spotlights (30 W, radiation angle 32° , $T_{cc} = 3000$ K) focused downwards are also applied. The elements of light graphics (such as cornice lighting of ceiling levels, light strips on the ceiling in the cloakroom) are formed by hidden LED strips and emphasize the geometry of the ceilings.

The absence of an explicit light-and-dark scenario brings the foyer closer to commercial public spaces, creating an indirect response to the trend of universalization of this area. But this light solution opens another aspect: it is in such a uniform, matt light that the foyer elements, such as ramps,

supports, roof trusses, acquire a detached, abstract character, they are more like geometric bodies than functional architectural details. This adherence to mathematical thinking is a special component of the *TPO Reserve* architecture [9]. And in this regard, the autonomous performance of the foyer is one of the architects’ signs in the building.

4.2. Architectural elaboration of “Core-and-Shell” Relationships

Handling the “core-and-shell” relationships, where the core is the auditorium and the shell is the surrounding functions, is connected as an architectural task with the emergence of precise acoustic calculations and requirements for the hall. Modelling with large surfaces, the use of wooden finishing, the applying of micro-relief in the walls and ceiling surfaces predetermine the saturated colouristic and emphasized materiality of the hall. It is clear, that the decorative lighting of these details becomes an essential element of the interior. At the same time another trend is growing: the hall begins to be treated as a body (“core”) of one material inside the “shell”, which is the foyer of another material, usually contrasting. Lighting is used to visually separate the “core” and the “shell”. This is achieved either by intensive illumination of the outer surface of the hall walls facing to the foyer and having a special “precious” finishing, or by cornice (hidden) lighting of this surface in places of conjunction with the foyer constructions (floor slabs, stairs etc.). In modernist buildings, this theme is calm and sometimes absent; with the advent of Post-modernism, and later, of digital technologies, it be-



Fig. 7. Cornice lighting of acoustic panels in the small hall (photo: A. Naroditsky)

comes more dramatic. Direct examples of its implementation in the latest architecture are the Royal Opera building in Copenhagen, Denmark (2005, architect *H. Larsen*), mentioned above Winspear Opera House, Harbin Opera House, China (2015, *MAD Bureau*). Let us follow what its interpretation is in the Zaryadye Concert Hall.

Three groups of light sources are used in the lighting of the major hall, and for all lighting there is a light regulation system. In the acoustic ceiling there are luminaires of general and stage lighting³. To illuminate the space under the balconies the LED directional lights of 23 W with a radiation angle of 50° are built in the lower surface of balcony volume. Finally, the mahogany walls are illuminated with flexible LED luminaires (power 10.6 W/m, $T_{cc}= 3000$ K, colour rendering R_a index > 80) hidden behind the balconies and repeating their outlines by cornice lighting. The lighting of the main hall walls veneered with the same wood species on the foyer side, contrasting to the dominant white acrylic stone, is arranged in the same way.

It is the last lighting technique that is responsible in the Zaryadye Hall for maintaining the relationship between the “core” and the “shell”. The authors of the project describe this relationship as a layered, sequential disclosure of space from the hall to the foyer and further to outdoor environment [10]. The independence of multifarious layers is emphasized

by the illuminated gaps between them. In the foyer, the “core” does not give itself away other than by the similarity of the material with that of the inside wooden finishing of the hall – this solution is rather close to the modernist examples. And the appearance inside the hall of white strips of balconies referring to the “shell” is a specific feature of the Zaryadye Hall, indicating the figurative priority of the layer structure over the proper idea of the “core” (Fig. 6a). Curiously, this vision of space and its light solution also have analogues: National Concert Hall in Dublin, Ireland (2008, contest project by *3XN Architects Bureau*) and the Paris Philharmonic, France (2018, author of the original concept *J. Nouvel*).

4.3. Active Use of Rhythmic Series

Active use of rhythmic series is no less common attribute of musical halls. The original commonality of concepts in music and architecture makes it an almost inevitable expressive means, and at the same time its use in concert halls can have functional and figurative, as well as decorative task.

The functional aspect again refers to the requirements of acoustics. Acoustic calculation leads to the fact that in the architecture of the auditorium the large or small rhythmic elements appear to ensure the quality of sound, and you can read them in a dark hall only thanks to artificial light. We have already discussed the cornice lighting of wooden acoustic finishing in the hall. Thanks to it we perceive not only spatial layers, but also complex relief of repeated small modules, and realize its purpose

³ This group of lighting devices refers to the stage lighting project not covered in this article.

(Fig. 6b). It is also worth noticing the lighting solution in the small hall, where with the same cornice lighting by the LED strip the tiers of large acoustic panels are underlined (Fig. 7). Due to its lighting atmosphere, the small hall in Zaryadye is related to the hall in Bleibach, Germany (2014, *peter haimerl.architektur* bureau). While the rhythmic pattern, arising the association with textile drapery, displayed by surface-mounted luminaries of 6 LEDs in each (12.6 W, radiation angle is 41°) arranged in a dotted line in the lower surface of the balcony that is what makes this chamber space a subtle find of the Moscow musical complex.

Decorative understanding of rhythmic elements is also present in the building. The already mentioned illumination of the plastic of the southern wall is a good illustration of this aspect in the external detail. In the foyer, by means of rhythmic elements, both material and light, its special ambience is created. In an essay by art critic Yu. Tarabarina, the experience of this ambience sounds like the leitmotif of the building. “Hatching” is the concept, by which she denotes rhythmic elements of all kinds, from glass fins of stained-glass windows to mirror stripes of cladding, stands for de-materialisation of architecture [8]. They are not highlighted in a special way, but rather coexist and overlap in the uniform light environment of the foyer, as discussed above. Special mention should be made of the solution that has become a kind of hallmark of the building – it is LED backlight in the form of thin vertical lines, integrated into the acrylic stone along the entire length of balcony fencing of the second floor. The decorative role of this detail is underlined by the colder correlated colour temperature T_{cc} (8,000–9,000) K than the one used throughout the building.

5. CONCLUSION

With a moderate palette of used technical means and techniques of artificial lighting in the building of the Zaryadye Concert Hall the attributes are read, which for today still determine the concert halls as a building type. When comparing with other objects within the typology and studying the light solutions applied in them, regularities and changes are revealed that are associated both with the evolution of the building type itself and with the general development of the architecture. In addition, a number of individual peculiarities of the Zaryadye Hall are covered related to both the initial design condi-

tions and the author’s language of the architectural bureau; their connection with the lighting approach is traced.

The analysis revealed five major constitutional principles supported by lighting concepts:

- The technique of “exposed interior” as an inviting element;
- Application of a large-scaled media façade;
- Interpretation of the foyer as an autonomous space with rich architectural scenography;
- Identification of the architectural relationship between the volume of the hall and the foyer: the “core-and-shell” conception;
- Active use of rhythmic series both in facade plastic and in an interior.

The specificity of the building considered is that due to its in-built position in the park complex the artificial lighting becomes crucial for it. Some typological attributes are not only common for concert halls technique; they become the only convincing solution in this case. First of all, it concerns the exposition of the foyer through the glass facade by the intensive interior floodlight. In interior solutions, the same floodlighting is responsible for the visual consolidation of the interior “mechanism”, which is played on a narrow site of complex configuration. Numerous rhythmic elements of the foyer, placed in a uniformly illuminated environment, create the effect of overlaying different layers both on the facade and in the interior. In this solution an individual language of the architectural bureau is manifested, and at the same time, a figurative link with the music language is created.

The concept of layered space disclosure moves organically into the main auditorium, which is not displayed as a “core”, but interpreted as another layer exposed by illuminated gaps between visually independent wall elements.

At the same time, there are means showing one of the two historical roots of concert halls and characterizing this type of buildings as entertaining and commercial public space. In external solutions, they include the interpretation of a part of the facade as an information luminous surface. In interior, the foyer ambience is responsible for this component, with its openly installed LED-lamps of general lighting combined with the selection of finishing materials. An atmosphere which implicitly suggests a broader purpose of the foyer than just that of pending the concert – this is another sign of time uniting today’s places of entertainment.

The carried out formal analysis of the new Moscow Concert Hall can be useful for the systematic study of the concert halls typology in the aspect of form building, expressive means of architecture and emotional perception. For practicing architects, architectural lighting specialists and students of architectural universities, it can become an impulse for a new creative understanding of this complex and interesting building type.

REFERENCES

1. Kramer, A. Yu. Concert hall in Russian and European culture. Dis.cand... of culturology: 24.00.01- SPb., 2015, 195 p.
1. Kramer A. Yu. Koncertnyj zal v otechestvennoj i evropejskoj kul'ture. Dis.kand... kul'turologii: 24.00.01 – SPb., 2015, 195 p.
2. Sery, E. Expanded meeting of the editorial board of the Svetotekhnika magazine // Svetotekhnika, 2017, No. 6, p. 77.
2. Seryi E. Rasshirennoe zasedanie redkollegii zhurnala "Svetotekhnika" // Svetotekhnika, 2017, No. 6, p. 77.
3. Shchepetkov Nicolai I., Cherkasov George N., Novikov Vladimir A. Lighting of Engineering Structures and Industrial Facilities: New Aspects of the Topic // Light & Engineering, 2018, V.26, #3, pp.29–36.
4. Interview by Yu. Shishalova with Vladimir Plotkin // Project Russia, 2017, No. 4 (86), pp. 82–83.
4. Intervju Yu. Shishalovoi s Vladimirom Plotkinym // Proekt Rossia, 2017, No. 4 (86). pp. 82–83.
5. Savkin, K.M. Interpretation of depth // Arkhitekturnyi Vestnik, 2018, No. 5 (164), pp. 42–53.
5. Savkin K.M. Interpretacija glubiny // Arkhitekturnyi Vestnik, 2018, No. 5 (164), pp. 42–53.
6. Vladimir Plotkin: "The main thing is passion about form". Interview. *Reserve. Creative Union*, edited by Elena Gonzalez, Grigory Revzin, Populyarnaya Literatura, Moscow, pp. 35–43.
6. Vladimir Plotkin: "Glavnoe – pristrastie k forme". Intervju // Rezerv. Tvorcheskoe objedinenie, pod red. Gonsales E., Revzina G.M.: Populyarnaya literatura, pp.35–43.
7. Kaltenbach, F. Der Auftritt vor dem Auftritt | The Show before the Show // Detail, 2018, No. 3, pp. 24–29.
8. Tarabarina, Yu. The Crystal of Music. URL: <https://archi.ru/russia/80955/kristall-muzyki> (reference date: 6.11.2018).
8. Tarabarina, Yu. Kristall muzyki. URL: <https://archi.ru/russia/80955/kristall-muzyki> (reference date: 6.11.2018).
9. Ilyevskaya, M. TPO Reserve: In the Stream of Time // Arkhitekturnyi Vestnik, 2017, No. 4 (157), pp. 78–87.
9. Ilyevskaya, M. TPO Rezerv: v potoke vremeni // Arkhitekturnyi Vestnik, 2017, No. 4 (157), pp. 78–87.
10. Interview by M. Ilyevskaya with Sergey Gusarev // Arkhitekturnyi Vestnik, 2017, No. 4 (157), pp. 62–65.
10. Intervju M. Ilyevskoi s Sergeem Gusarevym // Arkhitekturnyi Vestnik, 2017, No. 4 (157), pp. 62–65.



Maria M. Ilyevskaya,

graduated from the Moscow Institute of Architecture in 1999. She has got Master of Advanced Studies in History and Theory of Architecture from the Swiss Federal Institute of Technology (Zurich, 2014). At present, she is architect, Head of Research and Communications Department, TPO Reserve, LLC, senior lecturer of the Science Centre "Architecture and Computer Technologies" Chair of the Moscow Institute of Architecture (State Academy), member of the Union of Moscow Architects

LIGHT DESYNCHRONOSIS AND HEALTH

Vladimir N. ANISIMOV

*N.N. Petrov National Medical Research Oncology Centre of the Ministry of Health
of the Russian Federation, St. Petersburg, Russia
Email: aging@mail.ru*

ABSTRACT

The review summarizes the modern knowledge of the impact of day-night, light-darkness rhythm disorders on the aging process and on the risk of development of the age-related conditions. Significant evidence has been obtained of that the constant artificial illumination and the daylight of the North has a stimulating effect on the occurrence and development of tumours in laboratory animals. It has been shown that long-term shift work, trans-meridian flights (jet-lag) and insomnia increase the risk of cardiovascular diseases, diabetes mellitus, and malignancies in humans. Particular attention is given to the studies where the relationship between light intensity, light wavelength and its ability to suppress the synthesis of melatonin produced at night in the pineal gland, are investigated. It has been established that melatonin synthesis is most effectively suppressed with blue light sources of a wavelength from 446 to 477 nm. The use of exogenous melatonin prevents premature aging of the reproductive system and the body as a whole prevents the development of immune-suppression, metabolic syndrome and tumours caused by light pollution. An urgent task is to develop recommendations for optimizing the illumination of workplaces and residential premises, of cities and towns as a prevention measure for premature aging and age-related pathology, which, ultimately, will contribute to the long-term maintaining of performance and improving the quality of life.

Keywords: night light, light pollution, circadian rhythm, melatonin, aging, cancer

1. INTRODUCTION

The most vital phenomenon of nature on the planet Earth is the alternation of day and night, light and darkness. The axial rotation of our planet, and at the same time, around the Sun, measures the days, seasons and years of our lives. We accumulate the knowledge increasingly regarding the role of the pineal gland as the main pacemaker of body functions. Light inhibits the synthesis and secretion of melatonin hormone in the pineal gland, and therefore the maximum blood level of this hormone in humans and animals of many species is observed at night, and the minimum level – during daytime hours. The convincing data regarding circadian rhythm gene expression violation during aging has emerged in recent years [1]. It is significant that with aging, the activity of the pineal gland is reduced, which is seen, first of all, by a rhythm disturbance and a decrease in melatonin secretion level [2]. If the epiphysis can be considered as a biological clock of the body, then the melatonin can be considered as a pendulum that runs these clocks; the decrease in the amplitude of the pendulum causes the clocks to stop. Perhaps it will be more accurate to compare the epiphysis with the sundial, in which melatonin plays the role of a shadow from the ancient astronomical instrument, i.e. the gnomon – a rod casting a shadow from the sun. In the afternoon the sun is high, and the shadow is short (the level of melatonin is minimal), and in the middle of the night, there is a peak of melatonin synthesis and its secretion into the blood from the pineal gland. At the same time, it is important that the melatonin is

synthesized in a daily rhythm, i.e. its measuring unit is the chronological metronome, namely, the daily rotation of the Earth around its axis [3]. If the pineal gland is the body's sundial, then, obviously, any changes in the length of daylight should have a significant impact on its functions and, ultimately, on the aging rate. The circadian rhythm is essential not only for the temporal organization of the physiological functions but also for the human life expectancy. In a number of works, it has been shown that the violation of photoperiods can lead to a significant decrease in the life expectancy of animals [4, 5].

2. EFFECT OF LIGHT ON THE SYNTHESIS OF MELATONIN BY THE PINEAL GLAND IN HUMANS AND ANIMALS

Day and night (light and dark) is the main synchronizer (*Zeitgeber*) that regulates melatonin synthesis in the appendage of the brain – the pineal gland (epiphysis). The endogenous rhythm managing the synthesis and secretion of melatonin is adjusted to the duration of night-time in various mammalian species, regardless of whether they are of nocturnal or daytime habits [6–9]. In people who are active throughout the day, the high melatonin concentration and excretion in epiphysis are observed over the night. In addition to its effect as a circadian clock adjusting agent, the light acts as a masking factor when the body is exposed to light during the usual light phase of the day. The photoreception system involved in the regulation of clocks is different from the pattern recognition system. The daily change of light and darkness adjusts the endogenous circadian clock in the special brain structure – the hypothalamus – to the astronomical duration of the day (24 hours). The congenital period of the hypothalamic clock is slightly longer than 24 hours. Retinal receptors containing photo pigment constitute about 1 % of retinal ganglion cells and directly respond to light, acting as a synchronizer to the hypothalamic suprachiasmatic nucleus. The photo-pigment is melanopsin, an opsin/vitamin A complex with a blue spectrum sensitivity peak at 480 nm [10]. The radiation effect of different wavelength on melatonin synthesis in epiphysis was investigated, as it was found that melatonin synthesis is suppressed in a rather wide range of wavelengths, from 420 nm up to 600

nm, but most effectively in the interval from 446 nm to 477 nm. Suppression of the nocturnal peak of melatonin synthesis by illuminance exposure (200–500) lx for 1 hour is the same for men and women and is proportional to illumination. Low illuminance (90–180) lx, which is often present in living rooms, is enough to suppress melatonin synthesis. In apparently healthy subjects, the maximum sensitivity to light is within the range of very short wavelengths (420, 440 and 470 nm) [11–14].

Photosensitivity, assessed by suppressing melatonin levels, partly depends on the subject's previous exposure to light. It increases after exposure to the dark or to the dull lighting, which suggests an adaptation of photoreceptors or a response to the previous light exposure.

It was shown in [15], that at illuminance 800 lx the use of protective glasses blocking the most active short-wavelength part of the spectrum (lower than 530 nm), prevents light-induced suppression of nocturnal melatonin content in saliva. At the same time, individuals maintain night melatonin levels similar to those under dim lighting, and subjective drowsiness, anxiety and ability to act are not disturbed. Bright light at night causes a phase shift and a switching of the circadian phase. A phase shift can be observed even with much less illumination (for example, at 180 lx, normal lighting in a residential area). Moreover, it has been shown that very dim lighting (20 lx) can synchronize the circadian system in humans, normalizing sleep, awakening, and meal times. The circadian phase shift caused by short wavelengths radiation (with two peaks at 436 nm and 456 nm) during a 4-hour exposure (8 lx, 29 $\mu\text{W}/\text{cm}^2$) after a normal awakening led to a melatonin profile phase shift comparable to that of white light (12000 lx, 4300 $\mu\text{W}/\text{cm}^2$), despite the fact that white light contains many more photons than short wavelength radiation [15].

In addition to information on turning on and off the daily photoperiod, melatonin provides information about the length of the day. Melatonin synthesis and secretion duration in animals and humans varies depending on the duration of the dark hours. The longer dark period of the day takes in the laboratory or the longer the night takes in nature, the longer melatonin synthesis and secretion – regardless of whether this period is the time of activity of nocturnal rodents or the time of rest of animals with daytime activity, including humans [6, 14]. In ordinary laboratory animals, it is not possible to increase

daytime melatonin levels when placed into a dark room, but there is strong evidence of a decrease in their melatonin night time levels after exposure to the short light flashes over the night. Most mammals use changes in the length of the day and night to determine seasonal changes, thus adjusting the seasonal and/or synchronizing the near-year behavioural rhythms. Seasonal differences in reproduction are directly controlled by the relative length of light and dark periods [6, 7].

In modern urban conditions of electrification, the daylight and night time duration seasonal changes and, accordingly, the duration of melatonin secretion in humans, are obviously masked. In a number of studies, it was acknowledged that at low and middle latitudes the seasonal changes in melatonin secretion are absent. In contrast, seasonal changes associated with longer melatonin secretion in winter were observed in sub polar and polar high latitudes, with significant changes in photoperiod and illumination level, and high daytime levels of melatonin [7].

Light is the most powerful circadian synchronizer in humans and can have a prominent influence on the phase and amplitude of a human circadian pacemaker. Relatively intense illumination over the night almost completely suppresses the night peak of melatonin synthesis and secretion. Table 1 summarizes data on the extent of the blood melatonin inhibition in humans exposed to light, produced by incandescent and fluorescent lamps with different intensity. Fluorescent lamps reduce the melatonin concentration more intensively. The illumination level in residential areas rarely exceeds 200 lx. The data regarding operating rules adopted in Russia of illumination level in different facilities are summarized in Table 2. It is easy to see that the light exposure of such intensity over the night can significantly suppress the blood melatonin level.

Studies of melatonin synthesis suppression with light made it possible to calculate a threshold illumination sufficient to decrease it by 15 %, which, on illumination with white light and 30-minute exposure, is about 30 lx at the cornea level. It is important to note that in residential areas, when additional light sources are turned on with a special purpose, for example, for reading, sewing on a sewing machine or washing, the illumination at the level of the cornea can reach as much as (150–200) lx.

In the literature reports the individual variability of sensitivity to light at night hours [2] was noted:

deeper melatonin suppression with brighter light, the ability of light to shift the melatonin rhythm phase, with bright light in the morning moving it forward, while in the evening it causes night melatonin peak to delay. A valuable biomarker for circadian rhythm disorders may be a quantitative measurement of the time dependence of the melatonin renal excretion level [2].

In turn, melatonin, depending on the stage of the circadian rhythm, can synchronize it and shift it to an earlier or later time. Low doses of melatonin (0.3–10) mg being administered during “biological day” when endogenous melatonin level is low, can cause drowsiness or sleep and decrease the body temperature [6]. The daytime single administration of 5 mg of highly soluble melatonin can shift the internal clock forward by 1.5 hours. The timely administration of melatonin (0.5–5) mg at 24-hour intervals, preferably before bed, can completely fine-tune the free-running circadian rhythm in most blind patients. Acting as circadian synchronizer between the central and peripheral “clocks”, melatonin optimizes phases in relation to the external time, thus providing the optimization of cellular and systemic processes and enhancing the action of defence systems, which significantly expands the ranges of its possible therapeutic use.

Noteworthy, the effect of light on melatonin synthesis may depend on the season and individual sensitivity to light. In winter, the light inhibits the level of human melatonin in saliva 2 times more intensely than in summer [17]. Interestingly, the Arctic seasonal workers who worked in December in the open air demonstrated the night melatonin secretion level 2 times higher than in April [18]. Authors suggest that the diffuse light reflected by snow in April is enough to reduce melatonin levels.

3. GEOGRAPHIC LATITUDE AND HEALTH

It is known that health and life expectancy indicators in different geographic regions can vary significantly. I.A. Gundarov and N.L. Zilbert hypothesized that there is a connection between public health indicators and such an important parameter as the location of the region relative to the equator [19]. To establish this, a geographic latitude was used as an indicator. The statistical analysis between 1986–1987 showed that mortality rate in USSR constituent republics increased almost in a linear

fashion progressively from the South to the North, with a correlation coefficient of 0.82 ($p < 0.01$). Even more marginal association was between geographic latitude and incidence of malignancy. According to the WHO data, the total mortality rate in 72 countries in Europe and America in 1980–1985 increased progressively with the increased distance from the equator, with a correlation coefficient of 0.65 ($p < 0.01$). The value of standardized mortality from malignancies between males of 45 countries in Europe and America in 1981–1985 differed 8.7 times: from 38.1 in Honduras to 330.0 in Hungary. The relationship with geographic latitude was shown with a correlation coefficient of 0.70 ($p < 0.01$). Also, a positive correlation with geographic latitude was observed for hypertension, atherosclerosis, and the incidence of hypercholesterolemia [19].

Considering that there is a long night in polar region, Erren and Pekarsky [20] suggested that the indigenous population of the Arctic region should have a reduced incidence of malignancy as compared to the residents of temperate latitudes. Indeed, the incidence of malignancies is reduced in Saami, a nationality living in the North of Europe [21]. At the same time, the mortality from breast cancer (BC) among Alaska Natives (Eskimos, Indians, and Aleuts) has tripled since 1969 – according to the authors, for an unknown reason [22]. In 2008 *Circumpolar Inuit Cancer Review Working Group* published the results of cancer study in polar Innu (umbrella term which replaced the term “Eskimo”), living in Alaska territory, in Canada and Greenland, between 1989 and 2003 as compared to the period between 1969–1988, i.e., for the total of 35 years [23]. It was noted that there is a significant increase in the incidence of BC, uterine corpus cancer, lung cancer and colon cancer, which is related with lifestyle changes of the natives due to its so-called westernization. For the period of 1974–2003, the incidence of BC in female natives of Alaska has been increased by 105 %, whereas in Caucasian females of the USA – by 31 %. In the same years, the incidence of uterine corpus cancer has increased among Alaska native females by 500 %, while among white Americans it has decreased by 30 %. The analysis showed that a significant increase in the incidence of breast and endometrial cancer in the Alaska natives can be best explained by environmental changes. The authors noted that in women of Alaska the incidence of obe-

sity and diabetes has significantly increased for 30 years, and this increase is associated with a change in dietary habits. However, along with the westernization of food, there is a significant increase in the level of light pollution due to the doubling of the population over the same time and the industrialization, which, in our opinion, can play a leading role in the observed phenomenon. According to IARC data for 1985 and 1992, the incidence of BC, uterine corpus cancer, ovarian cancer and colon cancer in females was higher in countries located closer to the poles (North and South), and less in equatorial countries [3, 24–26].

It should be considered that the differences found (or the absence thereof) are not necessarily related to the light regimen, and therefore, with geographic latitude. It is known that the above-mentioned malignancies have multiple etiological factors. As mentioned above, features of reproductive status, excess fat, and carbohydrates in the diet, etc. play their important role in the development of female reproductive system neoplasm. Therefore, despite the character of the light regimen, it is necessary to consider climatic conditions related to geographic latitude, the extent of industrialization and lifestyle features. In general, it is not possible to state certainly that the light regimen or geographic location are the key factors of malignancies development, but this statement should not be underestimated whatsoever [27, 28].

4. SHIFT WORK: TERMINOLOGY AND PREVALENCE

Shift work is referred to as a method of arranging the work process in a duty fashion where workers change each other at one workplace in a certain sequence, in accordance with approved schedule. In addition to these definitions, in scientific literature the term “Shift work” is commonly used, and normally includes any forms of workflow arrangement different from the standard daytime work (from 7–8 a.m. till 5–6 p.m.).

According to the International Agency for Research on Cancer (IARC) [29] data, there are several types of shift work:

- Constant work – employees regularly shift only for one period, for example, morning, day or night, or rotation takes place – employees change their job shifts more or less periodically;

- Continuous work – employees work all days of the week or carry out work intermittently on weekends or on Sundays;

- Night work – working hours include all or part of the night, and the number of working nights per week/month/year can vary significantly. The period of night work may differ across countries: from 8, 9 or 10 p.m. until 5, 6 or 7 a.m., or from 11 or 12 p.m. until 5–6 a.m.

Arrangement of shift work can also vary significantly [29], and this can variously affect the health of workers, leading to circadian rhythm disturbances and important physiological dysfunctions, including insomnia.

In modern industrial society, also called “24-hour”, “round-the-clock” society, shift and night work is becoming more and more common. Shift work is required in many technological processes (for example, power plants, oil refineries, and metallurgical production), social services (hospitals, transport, police and security services, fire fighting services, hotels, telecommunications), some industries and services (for example, in manufacturing of textile, paper, food, chemicals). According to the International Labour Organization, more than 2.5 million people officially have shift work, 2/3 of them located in Asia. In European countries, more than 17 % of employees are shift workers.

5. SHIFT WORK AND HEALTH

A frequent sequel of internal circadian desynchronise with external environmental rhythms is the development of various diseases. As shown in numerous studies, shift workers often develop malignant neoplasm, diabetes mellitus, peptic ulcer disease, hypertension and cardiovascular diseases, psychogenic disorders and many other diseases [4, 5, 30–34].

In all mammals, the cardiovascular system is a highly organized system in terms of timing. It was well documented in epidemiological studies that many cardiovascular pathological processes, such as myocardial infarction, stroke, arrhythmia, most frequently occur in the early morning hours, and this is the time when fatal outcomes are also more common.

In a survey covering 17 studies where the relationship between shift work and cardiovascular diseases was investigated, it was estimated that shift-working people have a 40 % increased risk of

cardiovascular diseases when compared with individuals with the daytime job [32]. The duration of the shift work is also important: the morbidity was higher in those who had it for more than 6 years.

Approximately 20 % of all workers cease working in shifts shortly after the start of such working due to serious health problems, 10 % do not have any problems associated with shift work during their entire work activity, whereas 70 % are faced with certain problems of varying severity, manifested as discomfort, everyday life troubles or diseases [29]. Some individual habits and features can modify the effects that shift work has on health. For example, it is believed that there are more smokers among shift workers, they more often consume caffeinated beverages or alcohol at night, eat more sweets and carbohydrates. They are more likely to have metabolic disorders, an increased risk of cardiovascular diseases and obesity [29].

During long-distance trans-meridian flights, circadian systems do not immediately adjust to the new local time. This requires several days, depending on the number of crossed time (hourly) zones, and the more zones are crossed, the more time is needed for normalization. It is believed that human circadian systems adjust to no more than (60–90) min per day [29].

Recovery is faster during the flights to the west (about 1-day recovery for 1-hour shift) than for flights to the east (about 1.5 hours for a shift of 1-hour time zone). Full recovery after 6-time zone travel takes 10 to 13 days, depending on the direction of the flight (to the west or east, respectively) [29]. In addition, aircraft crew members are affected by other additional factors such as cosmic radiation, electromagnetic fields, illumination, noise, acceleration, vibration, psychological stress, low mobility, high atmospheric pressure [36].

Seafarers often have a rotation (shift) working during the entire trip, and they also move through time zones, although not as quickly as aircraft crews do. Merchant seamen often use a 4-hour shift rotation, although the 6-hour shift is becoming increasingly popular. For oil workers, the rotation nature of working usually includes a 12-hour work shift for several weeks, followed by a rest at home. Similar problems are observed in truck drivers, the so-called “truckers”, train locomotive drivers and conductors on long-distance passenger trains.

In Japan, there was a study of the incidence of diabetes mellitus in 2,860 “white-collar workers”,

“blue-collar workers” with a fixed daytime job, and “blue-collar workers” in shift work. The relative risk of diabetes in shift workers was 1.33–1.73 times higher than in “daytime blue collars” and 2.01 times higher than in white-collar workers [37]. In shift “blue collars” body mass indices and cholesterol level were significantly higher than in daytime workers [38].

In [39], it was shown that shift work contributes to an increase in the incidence of GI disorders in car factory workers. Sleep disturbances reported in shift workers play an important role in the higher incidence of peptic gastric and duodenal ulcers in this population [40]. There are findings indicating a significant increase in the risk of duodenal ulcer development in shift workers infected with *Helicobacter pylori* [41].

The exact mechanisms of cardiovascular diseases development in shift workers are not completely understood, although circadian rhythm disorders and concomitant factors like smoking, irregular diet, and social issues are considered to play a key role, causing usual stress in shift workers [29, 42].

Desynchronisation of circadian clocks that can be caused by shift work, leads to hypertension, dyslipidemia, insulin resistance and obesity [29]. The serum level of total cholesterol and low-density lipoproteins in shift workers was significantly higher as compared with the controls, i.e. those working in daytime, which allowed shift working to conclude in a risk factor for employees.

Glucose tolerance has fluctuations from day to day, and the observed variability is due to inconstant cortisol level during the day. Glucose tolerance decreases in normal individuals through the day-time, and eating at night is, therefore, a cause of increased obesity and weight gain, which are often seen in shift workers [29]. Abdominal obesity, hypertriglyceridemia (> 1.7 mmol / l), low level of high density lipoproteins (< 1.03 mmol / l in men and < 1.29 mmol/l in women) and impaired glucose tolerance were detected more often in night shift workers, more susceptible to the development of the metabolic syndrome [43].

6. ILLUMINATION OVERNIGHT AND CANCER

A number of papers have convincingly demonstrated an increased incidence of spontaneous and

chemically induced malignancies in laboratory animals kept under the constant illumination conditions or those of the Arctic region [3–5, 26, 28, 44, 45].

Using satellites, the level of light pollution over night was investigated and evaluated in 147 Israel municipalities, after which, using the method of multiple regression analysis, the relationship between night illumination and the frequency of breast cancer and lung cancer in women were calculated. After allowance for corrections on the ethnic composition, number of births, population density and income level, a high degree of correlation was established between the intensity of night illumination and the frequency of breast cancer ($p < 0.05$), moreover, this association increased ($p < 0.01$), when statistically significant factors only were considered for the regression analysis. On the other hand, no association has been found between the night illumination intensity and the frequency of lung cancer [46]. It was noted that 73 % of the maximum breast cancer frequency estimates were in those public entities with maximum illumination at night.

Using the same approach, the relationship between night illumination and the frequency of the three most common malignant tumours (prostate, lung, colon cancer) in men in 164 countries was studied. A high positive association was found between the light exposure of the population at night and the incidence of prostate cancer, but not lung or colon cancer [47]. The authors explain the presence of the found association between prostate cancer and night time illumination by suppressing the level of melatonin and clock-genes dysfunction. The risk of prostate cancer in countries with the most intensive night illumination was 110 % higher than that in countries with the lowest light pollution.

Subsequently, the same authors compared the frequency of the five most common neoplasm in women in 164 countries with the level of night illumination and found a high positive correlation between illumination and the frequency of breast cancer [48]. No such correlation was found between night illumination and colon cancer, and malignancies of larynx, liver, and lungs. The breast cancer risk in countries with the highest night illumination was 30–50 % higher than in countries with the least illumination.

Several cohort studies have shown that women, who often turn on lights in the bedroom at night, have an increased risk of breast cancer [29, 49, 50].

An analysis of the effect of night-time bedroom illumination intensity performed in Israel found that this factor is very significant and increases the risk of breast cancer in women with a habit of sleeping with the lights on ($OR = 1.22, p < 0.001$) [48].

Comparing their own data with the results obtained in [49], the authors of [48] note that during the 15 years since this study (1992–95), the light pollution has been increased, and currently women are exposed to a more intensive illumination as energy-saving lamps emitting in the blue spectrum (at 460 nm) are increasingly used. It is emphasized that this is the first large-scale randomized study where a positive correlation between illumination in the bedroom (habit to sleep in the light), light overnight hours (light pollution) and breast cancer (BC) has been established, and where the evidence was provided that the relative risk of BC increases proportionally to the intensity of night-time illumination in the bedroom. Therefore, not only the shift work over night hours is a risk factor for BC, but also the habit of sleeping in the light [4, 5, 29].

According to the International Agency for Research on Cancer in 2000 BC accounted for the majority of cancer cases in developed countries. The most common malignancy among women – breast cancer – each year affects about 1 million women (22 % of all female malignancies with the number of deaths of 375,000). More than half of all new cases are reported in economically developed countries: around 335,000 in Europe and 195,000 in North America [51]. Breast cancer is still not the most common among women in developing countries, but even in those countries, there is a steady increase in incidence. Increasing risk of breast cancer is caused with high socio-economic status (annual income, education, housing, etc.), because it is related with such health indicators as the onset of menstrual activity and menopause, obesity, big height, alcohol consumption, late age of first birth, small number of births, hormone replacement therapy, dietary patterns, etc. Two more factors characteristic of developed countries that may be of importance: the increasing night illumination exposure [29] and low-frequency electromagnetic fields (50–60) Hz [52].

Much higher mortality rates from malignancies are reported in shift workers who worked in production for at least 10 years, compared with those employed only in day shifts. In Denmark, in a large controlled randomized study (about 7,000 subjects

in each group), it was shown that evening work significantly increases the risk of breast cancer in women aged 30 to 54 years. Among those working at night, the most reliable results were found among waiters of restaurants working on night shifts (300 cases). Similar observations were made during a survey of flight attendants in a large breast cancer risk cohort study in Finland. In California flight attendants, breast cancer was found 30 % more often and malignant melanoma was detected 2 times more often than in the rest of the population of California [29].

An epidemiological randomized study conducted in the US in 813 breast cancer female patients investigated the lifestyle features of these patients over the past 10 years compared with healthy women. At the same time, the light exposure at night was considered, based on the following parameters: night insomnia, lighting level in a bedroom at night and working in night shifts (at least 3 nights per month). It was found that the risk of cancer increases with increasing night insomnia, increased lighting level in a bedroom and when working on night shifts. In the latter case, the risk also increased with work experience [49].

According to [53] data from health research among nurses, which included questions on their experience, shift work, day, night and evening shifts, among nurses with more than 30 years of experience and shift work, the relative BC risk was 1.36 when compared to those nurses not working in shifts. Nurses who work for a long time with night shifts had a reduced level of melatonin and an increased level of oestrogen in the blood. The meta-analysis based on 13 studies, including 7 studies in workers of airlines and 6 studies in workers of other professions with night shifts, shown that the overall risk assessment was 1.48. The flight crew of airlines and women working on night shifts had a significant risk of developing BC.

The study, which focused on the health data of almost 45,000 nurses in Norway, found that working at night for 30 years or more poses the additional risk of breast cancer of 2.21. An increased risk of BC and colon cancer was found in Seattle residents who worked for a long time at night shifts [29].

The risk of colon cancer and rectal cancer was reported to increase in women working on radio and telegraph. The authors of [53] examined the Harvard data on the health research of 79,000 nurses

Table 1. The Degree of Suppression of the Night Melatonin Level Under the Illumination with Incandescent Lamps (IL) or Fluorescent Lamps (FL) [16]

Illuminance, lx	Suppression of melatonin concentration after turning on the light,%					
	After 30 min		After 60 min		After 90 min	
	IL	FL	IL	FL	IL	FL
0.1	0	0	0	0	0	0
0.3	0	0	0	0	0	1
1	0	1	1	1	1	1
3	1	2	2	3	2	4
10	3	6	5	9	5	10
30	8	14	11	19	13	20
100	19	29	25	36	27	39
300	35	47	42	53	45	55
1000	54	62	59	65	60	66
3000	65	69	68	71	69	71

and found that nurses working at night shifts have a higher risk of breast cancer. The authors also found that colon and rectal cancer are more common among workers who have at least 3-night shifts per month for 15 years or more. The mechanisms underlying this increased risk of cancer among night workers and flight crews may be similar. Probably, the circadian rhythms disturbance and the forced light exposure at night both lead to a decreased production of melatonin, which is a known biological blocker of the development of malignant tumours.

7. THE EFFECT OF MELATONIN ON THE DEVELOPMENT OF TUMOURS IN ANIMALS AND HUMANS

In experiments using various carcinogens and experimental designs, it was found that the use of melatonin has a suppressive effect on the development of tumours in animals. The spectrum of the anti-carcinogenic effect of melatonin is quite wide – it inhibits the carcinogenesis in the skin, subcutaneous tissue, breast, cervix and vagina, endometrium, lung, liver, and colon [27, 28, 55, 56]. Experimental data are in compliance with the results of clinical observations. So, the work of Canadian researchers provided the results of a meta-analysis of 10 randomized controlled studies of the effectiveness of melatonin for the treatment of solid cancer patients [58]. In total, 643 patients received treatment. The

use of melatonin reduced the relative risk of death within 1 year to 0.66, and no side effects of the drug were recorded.

Possible mechanisms of the inhibitory effect of melatonin on carcinogenesis have been intensively discussed recently [54]. Melatonin has been found to have effects on both systemic and tissue levels and on cellular and sub cellular levels. At the same time, the action of melatonin prevents processes leading to aging and cancer. In particular, at the system level, melatonin reduces the synthesis of hormones that contribute to these processes and stimulates the immune surveillance system. At the same time, the formation of oxygen free radicals is suppressed, and the antioxidant defence system is stimulated. Melatonin inhibits the proliferative activity of cells and increases the level of apoptosis, preventing the tumour onset and development. At the genetic level, it inhibits the effect of mutagens, and also suppresses the expression of oncogens [55, 57].

8. THE EFFECT OF MELATONIN ON LIFE EXPECTANCY

Numerous studies have shown the ability of melatonin to slow down the aging process and increase the lifespan of laboratory animals (fruit flies, flatworms, mice, rats) [26, 57]. Some optimism is raised by publications about the ability of melatonin to increase resistance to oxidative

Table 2. Some Russian Regulatory Values of Light Illumination in Public, Residential and Auxiliary Premises (SP52.13330.2016)

Type of room	Illuminance of working surfaces in general lighting, lx
Administrative buildings	
Computer rooms	200–400
Business and work facilities, offices	300
Conference rooms, meeting rooms	200
Recreations Coulouirs, lobbies	150
LABORATORIES	400
Institutions of general education, primary, secondary and higher	
Classrooms, schoolrooms, secondary school rooms	500
Sports halls	200
Classrooms, training rooms, laboratories of technical schools and universities	400
Classrooms and teachers' rooms	300
Recreations	200
Medical institutions	
Adult wards	100
Procedural, manipulation rooms	500
Operating rooms	500
Massage and physical therapy exercises rooms	200
Shops	
Supermarket retail spaces	500
Trading rooms of the shops without self-service	300

stress and reduce the manifestations of some age-related diseases, such as retinal macular dystrophy, Parkinson's disease, Alzheimer's disease, diabetes, etc. [55, 58]. Comprehensive clinical trials are needed for melatonin use in various diseases, which, as we believe, will significantly expand its use for the treatment and prevention of age-related desynchronization.

9. CONCLUSION

Data provided in a new atlas of artificial night sky lighting, suggest that 80 % of the world and 99 % of American and European populations live under light pollution [59]. 23 % of the Earth's surface between 75° N. and 60° S, 88 % of Europe and almost half of the United States are subject to light

pollution. The light exposure overnight has been increased and became an essential part of the modern lifestyle, being accompanied by many serious behavioural and health disorders, including premature aging, cardiovascular diseases, obesity, diabetes and cancer [14, 28, 29, 45, 60]. Obtained in animal experiments, strong evidence of carcinogenicity of light-induced desynchronization, caused by constant lighting or daylight of the North, served as a basis for recognizing circadian rhythm disorders by the International Agency for Research on Cancer as a factor increasing the risk of cancer in humans [29, 33]. In experiments using various carcinogens and experimental designs, it was found that the use of melatonin has a suppressive effect on the development of tumours of different localizations. Convincing experimental evidence has also been obtained

that the use of melatonin prevents premature aging of the reproductive system and the body as a whole prevents the development of immune-suppression, metabolic syndrome and different tumours caused by light pollution. The widespread introduction of LED light sources sets a problem of developing guidelines for optimizing the light mode of working and living areas, for lighting cities and other settlements, which will ensure long-term maintenance of working performance, high quality of life, and ultimately will contribute to the prevention of premature aging and the development of diseases, including malignant neoplasm.

REFERENCES

1. Panchenko, A.V., Gubareva, E.A., Anisimov, V.N. Circadian system and aging in rodent models. In: *Circadian Rhythms and Their Impact on Aging. Health Ageing and Longevity 7*. S.M. Jazwinski, V.P. Belancio, S.M. Hill, Eds. Springer International Publishing AG, 2017, pp. 103–128. DOI: 10.1007/978-3-319-64543-8_5.
2. Touitou, Y, Reinberg, A, Touitou, D. Association between light at night, melatonin secretion, sleep deprivation, and the internal clock: Health impacts and mechanisms of circadian disruption. *Life Sci.*– 2017, 173, pp. 94–106. DOI: 10.1016/j.lfs.2017.02.008
3. Anisimov, V.N. Light pollution, reproductive function and cancer risk // *Neuro Endocrinol. Lett.*– 2006, Vol. 27, pp. 35–52.
4. Anisimov V.N., Vinogradova I.A., Bukalev A.V. et al. Light desynchronization and risk of malignant neoplasms in humans: problem state // *Problems. oncol.* 2013, Vol 5, No. 3, pp. 302–313.
4. Anisimov V.N., Vinogradova I.A., Bukalev A.V. i dr. Svetovoi' desinkhronoz i risk zlokachestvenny'kh novoobrazovaniy' u cheloveka: sostoianie problemy' // *Vopr. onkol.*2013, Vol 59., No. 3, pp. 302–313.
5. Anisimov V.N., Vinogradova I.A., Bukalev A.V. et al. Light desynchronization and risk of malignant neoplasms in laboratory animals: problem state // *Problems. oncol.* 2014, Vol 60, No. 2, pp. 15–27.
5. Anisimov V.N., Vinogradova I.A., Bukalev A.V. i dr. Svetovoi' desinkhronoz i risk zlokachestvenny'kh novoobrazovaniy' u laboratorny'kh zhivotny'kh: sostoianie problemy' // *Vopr. onkol.* 2014, Vol. 60, No. 2, pp. 15–27.
6. Arendt, J. *Melatonin and the Mammalian Pineal Gland*. London: Chapman & Hall. 1995, 331 p.
7. Arendt, J. Biological rhythms during residence in polar regions//*Chronobiol. Internat*, 2012, Vol.29, (4), pp. 319–394.
8. Brainard George C. and Provencio I, Photoreception for the Neurobehavioral Effects of Light in Humans// *Light & Engineering Journal*, 2008, V.16, #1, pp.5–18.
9. Komarov F.I., Rapoport S.I., Malinovskaya N.K., Anisimov V.N. *Melatonin in norm and pathology*. M.: ID Medpractica-M, 2004, 308p.
9. Komarov F.I., Rapoport S.I., Malinovskaia N.K., Anisimov V.N. *Melatonin v norme i patologii*. M.: ID Medpraktika-M, 2004, 308p.
10. Brainard G.K., Provencio I. The perception of light as a stimulus for non-visual reactions in humans // *Svetotekhnika*. 2008, No. 1, pp. 6–13.
10. Brainard G.K., Provencio I. *Vospriiatie sveta kak stimula nezritel'ny'kh reakcii' cheloveka* // *Svetotekhnika*. 2008, No. 1, pp. 6–13.
11. Revel, F.G., Herwig, A., Garidou, M.-L. et al. The circadian clock stops ticking during deep hibernation in the European hamster // *Proc. Natl. Acad. Sci. USA*, 2007, Vol. 104, pp. 13826–13820.
12. Brainard, George C. and Hanifin, John P. *Exploring the Power of Light: From Photons to Human Health*// *Light & Engineering*, 2014, Vol. 22, #4, pp.4-14.
13. Kyba, C.C.M., Kuester, T., Sanchez de, Miguel, A. et al. Artificially lit surface of Earth at night increasing in radiance and extent // *Sci. Adv.*, 2017; 3: e17017258
14. Russart, K.L.G., Nelson, R.J. Light at night as an environmental endocrine disruptor// *Physiol. Behav.* 2018, Vol. 190, pp.82–89. DOI: 10.1016/j.physbeh.2017.08.029.
15. Gaston, K.J., Davies, T.W., Nedelec, S.L., Holt, L.A. Impact of artificial light at night on biological timings// *Ann. Rev.Ecol.Eviol.Syst.* 2017, Vol. 48, pp. 49–68.
16. Rea, M.S., Figueiro, M.G., Bullough, J.D., Bierman, A. A model of phototransduction by the human circadian system. // *Brain Res. Rev.* 2005, Vol. 50, pp. 213–228.
17. Higuchi, S., Motohashi, Y., Ishibashi, K., Maeda, T. Less exposure to daily ambient light in winter increases sensitivity of melatonin to light suppression // *Chronobiol. Int.* 2007, Vol. 24, pp. 31–43.
18. Leppaluoto, J., Sikkila, K., Meyer-Rochow, V.B., Hassi, J. Spring snow lowers human melatonin // *Int. J. Circumpolar Health*. 2004, Vol. 63. Suppl.2, pp. 161–163.
19. Gundarov I.A., Zilbert N.L. Study of regional differences in morbidity and mortality of the population in terms of geographical latitude syndrome // *Annals of AMN USSR*. 1991, Vol. 11, pp. 52–56.

19. Gundarov I.A., Zil'bert N.L. Izuchenie regional'ny'kh razlichii' v zabolevaemosti i smertnosti naseleniia s pozitsii' sindroma geograficheskoi' shiroti' // Vestnyk AMN SSSR. 1991, Vol. 11, pp. 52–56.
20. Erren, T.C., Piekarski, C. Does winter darkness in the Arctic protect against cancer? // Med. Hypothesis. 1999, Vol. 53, pp. 1–5.
21. Hassler, S., Soiminen, L., Sjolander, P., Pukkala, E. Cancer among the Sami – A review on the Norwegian, Swedish and Finnish Sami populations // Int. J. Circumpolar Health. 2008, Vol. 67, pp. 421–432.
22. Kelly, J.J., Lanier, A.P., Alberts, S., Wiggins, C.L. Differences in cancer incidence among Indians in Alaska and New Mexico and U.S. Whites, 1993–2002 // Cancer Epidemiol. Biomarkers Prev. 2006, Vol.15, pp. 1515–1519.
23. Circumpolar Inuit Cancer Review Working Group. Cancer among the circumpolar Inuit, 1988–2003. II. Patterns and trends // Int. J. Circumpolar Health. 2008, Vol. 67, pp. 408–420.
24. Bartsch, C., Bartsch, H., Peschke, E. Light, melatonin and cancer: current results and future perspectives // Biol. Rhythm Res. 2009, Vol.40, pp. 17–35.
25. Borisenkov MF, Anisimov VN Cancer risk in women: possible association with geographic latitude and some economic and social factors // Vopr. onkol. 2011, Vol. 57, No. 3, pp. 343–354.
25. Borisenkov M.F., Anisimov V.N. Risk raka u zhen-shchin: vozmozhnaia sviaz' s geograficheskoi' shiroti' i nekotory'mi e'konomicheskimi i sotcial'ny'mi faktorami // Vopr. onkol. 2011. Vol. 57, No. 3, pp. 343–354.
26. Vinogradova, I.A., Anisimov, V.N. Light regime of the North and age pathology. Petrozavodsk: PetroPress, 2012, 128 p.
26. Vinogradova I.A., Anisimov V.N. Svetovoi' rezhim Severa i vozrastnaia patologiiia. – Petrozavodsk: PetroPress, 2012, 128 p.
27. Anisimov, V.N., Popovich, I.G., Zabezhinski, M.A. et al. Melatonin as antioxidant, geroprotector and anticarcinogen // Biochim. Biophys. Acta. 2006, Vol. 1757, pp. 573–589.
28. Anisimov, V.N., Vinogradova, I.A., Panchenko, A.V. et al. Light-at-night-induced circadian disruption, cancer, and aging // Current Aging Science, 2012, Vol. 5, No.3, pp. 170–177.
29. IARC Monographs on the Evaluation of Carcinogenic Risks to Humans, Vol.98. Painting, Firefighting, and Shiftwork. Lyon: IARC, 2010, 804 p.
30. Taylor, P.J., Pocock, S.J. Mortality of shift and day workers 1956–68 // Brit. J. Industr. Med.1972, Vol. 29, pp. 201–207.
31. Stevens, R.G., Wilson, B.W., Anderson, L.E. Melatonin Hypothesis. Breast Cancer and Use of Electric Power". Columbus: Battelle Press. 1997, 760 p.
32. Knutsson, A. Health disorders of shift workers. // Occupat. Med. 2003, Vol. 53, pp. 103–108.
33. Straif, K., Baan, R., Grosse, Y. et al. Carcinogenicity of shift-work, painting, and fire-fighting // Lancet Oncol. 2007, Vol.8, pp. 1065–1066.
34. Gibson, E.M., Williams, W.P., Kriegsfeld, L.J. Aging in the circadian system: Considerations for health, disease prevention and longevity // Exp. Gerontol. 2009, Vol. 44, pp. 51–56.
35. Mosendane, T., Mosendane, T., Raal, F.J. Shift work and its effect on the cardiovascular system // Cra-diovasc. J. Afr., 2008, Vol. 19, pp. 710–715.
36. Wegmann, H.M., Esser, P., Klein, K.E. Significance of circadian rhythms for aviation and space operations // J. UOEH. 1985, Vol. 7, Supplement, pp.131–140.
37. Morikawa, Y., Nakagawa, H., Miura, K. et al. Shift work and the risk of diabetes mellitus among Japanese mae factory workers // Scand. J. Work Environ. Health. 2005, Vol. 31, pp. 179–183.
38. Morikawa, Y., Nakagawa, H., Miura, K. et al. Effect of shift work on body mass index and metabolic parameters // Scand. J. Work Environ. Health. 2007, Vol. 33, pp. 45–50.
39. Caruso, C.C., Lusk, S.L., Gillespie, B.W. Relationship of work schedules to gastrointestinal diagnoses, symptoms, and medication use in auto factory workers // Am.J. Ind. Med. 2004. Vol. 46, pp. 586–598.
40. Segawa, K., Nakazawa, S., Tsukamoto, Y., Kurita, Y., Goto, H., Fuku, A., Takano, K. Peptide ulcer prevalent among shift workers // Dig. Dis. Sci. 1987, Vol. 32, pp. 449–453.
41. Pietroiusti, A., Forlini, A., Margini, A., Galante, A., Coppeta, L., Gemma, G., Romeo, E., Bergamaschi, A. Shift work increases the frequency of duodenal ulcer in H. pylori infected workers // Occup. Environ. Med. 2006, Vol. 63, pp. 773–775.
42. Knutsson, A., Boggild, H. Shiftwork, risk factors and cardiovascular disease: review of disease mechanisms. // Rev. Environ. Health. 2000. Vol. 15, pp. 359–372.
43. Sookoian, S., Gemma, C., Fernandez Gianotti T., Burgueno, A., Alvarez, A., Gonzalez, C.D., Pirola, C.J. Effects of rotating shift work on biomarkers of metabolic syndrome and inflammation // J. Intern. Med. 2007, Vol. 261, pp. 285–292.
44. Vinogradova, I.A., Anisimov, V.N., Bukalev, A.V. et al. Circadian disruption induced by light-at-night accelerates aging and promotes tumorigenesis in rats // Aging (Albany, NY). 2009, Vol. 1, pp. 855–865.

45. Haim, A., Portnov, B.A. Light Pollution as a New Risk Factor for human Breast and Prostate Cancer., Dordrecht: Springer Sciences, 2013, 168 p.
46. Kloog, I., Haim, A., Stevens, R.G., Portnov, B.A. Light at night co-distributes with nident breast ut not lung cancer in the female population of Israel // *Chronobiol. Int.* 2008, Vol. 25, pp. 65–81.
47. Kloog, I., Haim, A., Stevens, R.G., Portnov, B.A. Global co-distribution of light at night (LAN) and cancers of prostate, colon, and lung in men // *Chronobiol. Int.* 2009, Vol. 26, pp. 108–125.
48. Kloog, I., Stevens, R.G., Haim, A., Portnov, B.A. Nighttime light level co-distributes with breast cancer incidence worldwide // *Cancer Cases Control.* 2010, Vol. 21, pp. 2059–2968.
49. Davis, S., Kaune, W.T., Mirick, D.K. et al. Residential magnetic fields, light-at-night, and nocturnal urinary 6-sulfatoxymelatonin concentration in women // *Am.J. Epidemiol.* 2001, Vol. 154, pp. 591–600.
50. Kloog, I., Portnov, B.A., Rennert, H.S., Haim, A. Does the modern urbanized sleeping habitat rose a breast cancer risk? // *Chonobiol. Int.* 2011, Vol. 28, pp 76–80.
51. Parkin, D.M., Bray, F.I., Deseva, S.S. Cancer burden in the year 2000. The global picture. *Eur. J. Cancer.* 2001, Vol. 37, pp. S4–S66.
52. IARC Monographs on the Evaluation of Carcinogenic Risks to Humans. Vol.80. Non-Ionizing Radiation, Part I: Static and Extremely Low-Frequency (ELF) Electric and Magnetic Fields. -Lyon: IARC, 2002, 438 p.
53. Schernhammer E.S., Laden F., Speizer F.E. et al. Night-shifts work and risk of colorectal cancer in the nurses' health study // *J. Natl. Cancer Inst.* 2003, Vol. 95, pp. 825–828.
54. Wegrzyn, L.R, Tamimi, R.M, Rosner, B.A. et al. Rotating night-shift work and the risk of breast cancer in the nurses' health studies // *Am.J. Epidemiol.* 2017, Vol. 186 (5), pp. 532–540. DOI: 10.1093/aje/kwx140.
55. Reiter, RJ, Rosales-Corral, S, Tan, D.X, Jou, M.J, Galano, A., Xu, B. Melatonin as a mitochondria-targeted antioxidant: one of evolution's best ideas. *Cell Mol Life Sci.* 2017, Vol. 74, № 21, pp. 3863–3881. DOI: 10.1007/s00018–017–2609–7.
56. Guidice, A., Crispo, M., Polo, A., Grimaldi, M. et al. The effect of light exposure at night (LAN) on c carcinogenesis via decreased nocturnal melatonin synthesis.// *Molecules*, 2018, Vol. 23, 1308 p. DOI: 10.3390/molecules2306.1308.
57. Anisimov, V.N. Effect of melatonin on longevity // In: *Modulating Aging and Longevity / Rattan S.I.S., Ed. London: Kluwer Acad. Publ., 2003, pp. 239–260.*
58. Mills E, Wu P, Seely D, Guyatt G. Melatonin in the treatment of cancer: a systematic review of randomized controlled trials and meta-analysis. *J Pineal Res.* 2005, Vol. 39, № 4, pp. 360–6.
59. Falchi, F., Cinzano, P., Duriscoe, D. et al. The new world atlas of artificial night sky brightness // *Sci. Adv.* 2016, Vol 10, № 6, pp. e1600377, DOI: 10.1126/sciadv.1600377.
60. Davies, T.W., Smyth, T. Why artificial light at night should be a focus for global change research in the 21st century // *Glob. Change Biol.* 2018, Vol. 24, pp. 972–882. <https://doi.org/10.1111/gcb.13927>.



Vladimir N. Anisimov,

Prof., Dr. of Medical Sciences, Corresponding Member of the Russian Academy of Sciences, Head of the Scientific Department of Carcinogenesis and Oncoherontology of the National Medical Research Centre of Oncology named after N.N. Petrov, Ministry of Health of Russian Federation

INSPECTION OF THE STATE (GENERAL AND INSTRUMENTAL) OF HISTORICAL TRANSLUCENT STRUCTURES OF THE PUSHKIN STATE MUSEUM OF FINE ARTS

Alexander V. Spiridonov and Nina P. Umnyakova

*Research Institute of Building Physics of Russian Academy
of Architecture and Construction Sciences, Moscow
E-mail: spiridonov@aprok.org*

ABSTRACT

The article is focused on the general and instrumental survey of historical translucent structures in the Pushkin State Museum of Fine Arts in 2018. It is shown that they don't complying with the current requirements, neither in heat transfer resistance nor in air permeability. The improvement recommendations have been developed. It is noted that in case of preservation of metal window frames (according to the requirements of the law on protection of cultural heritage sites) the large-scale computer calculations should be performed to determine the best ways of window restoration.

Keywords: restoration, historical translucent construction, frame, sash, survey, testing, heat transfer resistance, air permeability, condensate, recommendations

In 1990–2000, many people lamented, seeing the destruction of entire quarters of old buildings in many large and small Russian cities. Often the sites “necessary” for new construction were simply burned out. In their place the elite housing, huge shopping and entertainment malls, office centres appeared, and the spirit of the old cities was lost. For example, the charming cosy places of Zamoskvorechye in Moscow, two-three-storey buildings with amazing balconies in Kazan (when preparing for its millennium anniversary) and many others disappeared. (By the way, many cast iron bal-

conies appeared later (some say) in the dachas of rich Tatarstan officials.)

Fortunately, the situation has changed dramatically – today there is just a boom of construction restoration. In Moscow alone, more than 300 old buildings were renovated in 2017. Externally, they look beautiful, according to ancient drawings and photographs, and inside the amazing halls are refurbished up.

Unfortunately, very often on the renovated facades “false teeth” can be found – plastic windows (mostly white), which in no way fit into the beauty of buildings of the 18th – early 20th centuries: because then there were no window structures made of PVC profiles.

This is due to the fact that one of the requirements for modern reconstruction (in addition to restoring the old facade) is to increase the energy efficiency of old buildings to current indications. And it is very difficult to do this with old windows for several reasons:

- Modern window technologies provide very high indicators of thermal and luminous efficacy of structures, which even at the beginning of the 20th century, the engineers and the architects could not dream of;

- All technologies of old windows production are lost – to replace the rotten and lost parts often needs to “reinvent the wheel”;

- Full restoration of historical translucent structures with bringing their characteristics to the mod-

ern level will be much more expensive than the windows, which domestic builders used to install in typical modern buildings.

That is why there are many restored old buildings with white PVC windows in almost all cities (for some reason most of all in St. Petersburg [1]), which should not be. By the way, it is in St. Petersburg very often at night the old windows and stained-glass doors are stolen (so that there is nothing to compare with, probably).

It is difficult to find interesting domestic publications on the restoration of historical translucent structures (on the Internet for such a request you get a lot of proposals not for reconstruction, but for replacement of windows). The authors were able to find only one such article [2]. At the same time, our colleagues abroad understand the importance of preserving the historical heritage. In particular, *Historical Windows of New York, Inc.*, is successfully functioning in the not so old New York.

Probably, it is necessary to establish the supervision over the restoration of translucent structures in complex works on old buildings and to change the price approach to these works – the quality restoration of windows cannot be cheap.

The authors had the opportunity to participate in the survey of historical translucent structures of the major building of the Pushkin State Museum of Fine Arts in the first half of 2018, and to develop recommendations for their improvement.

The works were carried out as part of the restoration works for this site under the general name “Complex reconstruction, restoration and adaptation to modern museum technologies of the major building of the Pushkin State Museum of Fine Arts (Moscow, Volkhonka Str., Bld. 12)” [3].

The museum was built on the initiative of Ivan V. Tsvetaev by architect Roman I. Klein. Most of the funds for its construction were donated by the Russian philanthropist Yuri S. Nechaev-Maltsov.

The Museum of Fine Arts named after Emperor Alexander III (so it was called before the Revolution) was opened in a solemn ceremony on May 31 (June 13), 1912 (Fig. 1).

Today, after the transfer to the Museum of many unique collections (including famous collectors, Moscow Old Believers merchants Sergey I. Shchukin and Ivan A. Morozov), it is the largest collection of foreign art in the Russian Federation.

The major building of the Museum is recognized as a cultural heritage site of federal importance and is subject to the state protection.

Many engineering structures have not been repaired since the building was put into operation (that is, more than 100 years), have become relatively unusable and, mainly, do not comply with the requirements of current construction regulations.

Due to the fact that a decision was made to establish Volkhonka Street and the adjacent streets of the Museum Quarter, the nearby buildings were handed over to the Pushkin State Museum of Fine Arts, where, like in the major building, large-scale reconstruction is being performed.

The goals of our work were to survey the existing historic windows on the first floor in order to identify the possible causes of condensate formation and to develop anti-condensation recommendations and a set of measures to modernize existing windows.

In the light openings of the first floor of the major building there are windows with steel sashes



Fig. 1. The Museum of Fine Arts named after Emperor Alexander III before opening in 1912



Fig. 2. Historical windows in the major building of the Pushkin State Museum of Fine Arts:
a – view from the outside, *b* – metal bonding (“ladder”) between external and internal sashes



Fig. 3. Condensate formation on the inner surface of translucent cladding

made at the beginning of the last century (Fig. 2). They are external and internal massive steel sashes with a single glass thickness of 6 mm, spaced by 0.5 m. Most of the translucent first floor structures installed around the perimeter of the building have the dimensions of about 1560 (width) × 3740 (height) mm.

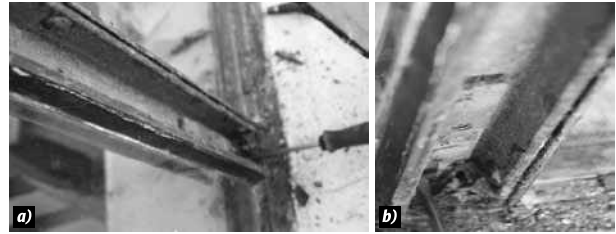


Fig. 4. Corrosion effect on one of the impostes of the inner frame (*a*) and the main (vertical) mullion of the inner frame (*b*)

Historical windows installed in the major building of the Pushkin Museum of Fine Arts as well as most other its structures are the cultural heritage sites and their replacement is impossible under the protection terms.

The surveys were conducted several times in different periods of the year – from February to June 2018. When conducting a visual examination on February 26, at the external air temperature $t_e = -15\text{ }^\circ\text{C}$, the internal air temperature $t_i = +20\text{ }^\circ\text{C}$ and the relative humidity of the internal air (52–63)%. In almost all rooms on the inner surface of all windows, there was abundant condensation from top to bottom, flowing down to the window sill and even to the floor (Fig. 3).

The condensate on the interior surfaces of translucent structures is absolutely unacceptable in the premises where the works of art are exhibited. In addition, moisture on the windows and slopes contributes to the appearance of mildew and fungi on the inner slopes of windows, which is also not useful for paintings – they can also be infected.

The survey of historical translucent structures revealed the following (Figs. 4 and 5):

- Structures are made of iron, repainted multiple times, but never (judging by their condition) treated with special anti-corrosion compositions;



Fig. 5. Elements of historical translucent structures

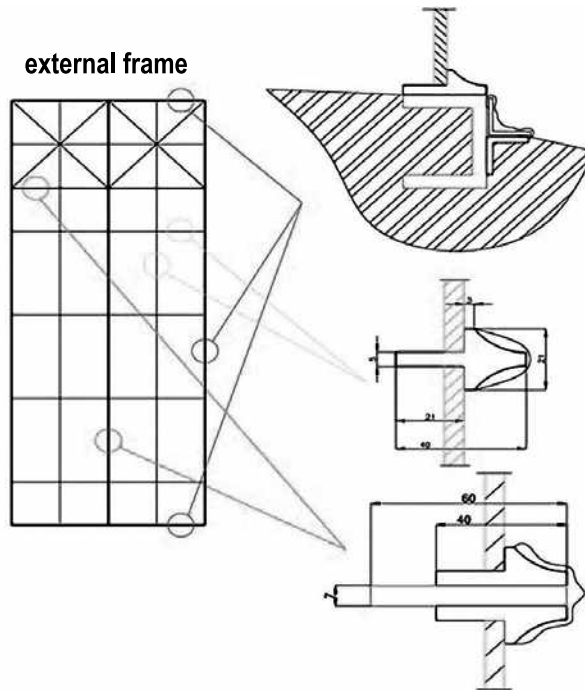


Fig. 6. Dimensions of external frame parts of historical translucent structure

- External and internal frames are made of sufficiently material-intensive corner iron, U-bars, T-bars, I-beams and shaped profiles;
- Ordinary transparent glass with a thickness of 6 mm is installed on external and internal frames;
- Translucent structures are installed in light openings without thermal insulation layers;
- The basic vertical imposts of window structures are very massive, and there are very strong corrosion processes inside;
- Under the blind casing on the internal frame structures, which are made with the use of sufficiently massive corner iron, the extensive corrosion damage is detected (probably the inner angle elements are to be replaced – they are almost decayed);

– In order to provide natural ventilation of exhibition premises in the early last century in translucent structures the ventilation windows were provided, which – in addition to exclusively original fittings – today (with the equipped air conditioning systems in the near future) are completely useless and even harmful.

According to the results of field surveys of historical translucent windows, their basic general dimensions and dimensions of structural details were obtained (in Fig. 6 the elements of the external frame are shown).

As a result of numerous field surveys of historical windows of the first floor of the major building of the Pushkin Museum of Fine Arts, it became clear that it is necessary to carry out additional instrumental surveys and calculations for development of reasonable recommendations for restoration of historical translucent structures¹.

Detailed measurements of historical windows (Fig. 6) will be extremely useful for restoration works.

The NIISPh of RAACS (Russian Academy of Architecture and Construction Sciences) proposed to conduct a field survey of the existing structure in one of the premises of the Pushkin State Museum of Fine Arts at sub-zero t_e (which was carried out on 26.02.2018 at $t_e = -15^\circ\text{C}$), and the evaluation of numerous possibilities of reconstruction of historical translucent structures by means of computer modelling.

In order to determine thermally homogeneous areas of the examined translucent cladding and to detect infiltration areas, a field survey was conducted using thermal imaging filming by the *NEC TH-910*

¹ They are in a terrible condition: Rust (almost on all structures), slits, inoperable fittings, etc.

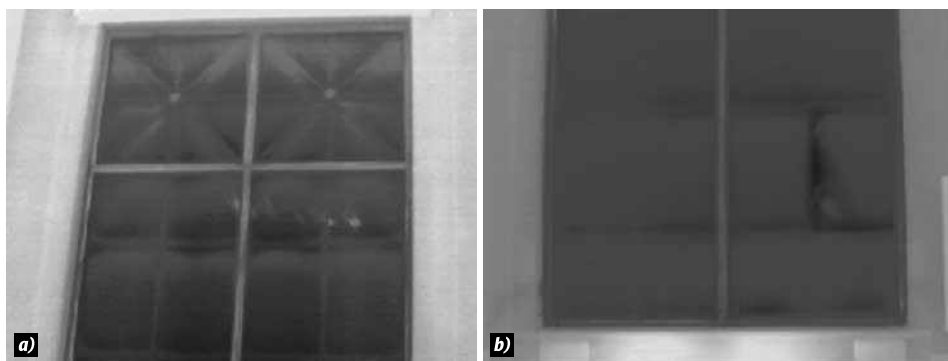


Fig. 7. Thermograms of upper (a) and lower (b) parts of unshadowed historical translucent structure at $t_e = -15^\circ\text{C}$ and $t_i = +20^\circ\text{C}$

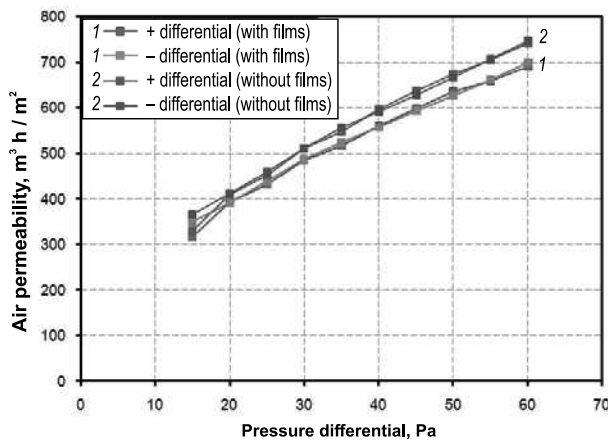


Fig. 8. The values of air permeability of the premises at positive and negative Δp

series thermal imager, in accordance with the relevant requirements [4, 5]. Some thermograms of the examined structures are shown in Fig. 7.

To determine the reduced R_o heat transfer resistance of translucent structure, a full-scale testing was carried out using heat flow and temperature meters in accordance with national standards [6]. The measurements were carried out within the period from 28.03.18 to 02.04.18. To perform the calculation, the period with the established temperature differential was selected: 28.03.18 23:00–29.03.18 04:00. During this period t_e and t_i were -10 and $+19.6$ °C respectively. The testing result is: $R_o = (0.37–0.39)$ m² °C/W.

Table 1. Dependence of Temperature in the Air Layer of Translucent Structure on Height

Height, m	Temperature, °C
2.9	9.5
1.5	7.0
0.76	4.8

The temperature distribution in the interglass space of the historical translucent structure is given in Table 1.

The testing of the historical translucent cladding for air permeability was carried out in the utility service room of the restoration workshop. The doors and other possible air infiltration areas were sealed before the testing. The “Blower Door” complex was installed in the doorway. The testing was carried out according to national standard [7]. Positive and negative differential air pressure Δp equal up to ± 60 Pa respectively were set during the full-scale testing. At each Δp value air permeability measurements were made. Then, on the basis of the obtained data, the air permeability values of the window at different Δp were calculated (Fig. 8 and Table 2).

As a result of the conducted surveys of historical translucent structures, it became obvious that they do not comply with the current requirements, neither on heat transfer resistance nor on air permeability. In case of preservation of metal window frames (according to the requirements of the law on protec-

Table 2. Air Permeability of Translucent Cladding at Positive Pressure Differential Δp

Δp , Pa	Volume air flow, m ³ /h	Mass air flow, G_a , kg/h	Air permeability	
			by volume, m ³ / (h · m ²)	by mass, kg / (h · m ²)
15	16	19.1	2.7	3.3
20	18	21.5	3.1	3.7
25	20	23.9	3.4	4.1
30	23	27.5	3.9	4.7
35	33	39.5	5.7	6.8
40	33	39.5	5.7	6.8
45	35	41.9	6.0	7.2
50	40	47.8	6.9	8.2
55	44	52.6	7.5	9.0
60	47	56.2	8.1	9.6

tion of cultural heritage sites) the large-scale computer calculations should be performed to determine the best ways of window restoration.

The authors express deep gratitude to the staff of the NIISPh (A. Verkhovsky, S. Potapov, V. Bryzgalin and E. Dalichik) and GC ROBITEK, LLC (N. Rumyantsev and I. Istomina) for assistance in carrying out field surveys of historical translucent structures of the Pushkin State Museum of Fine Arts.

REFERENCES

1. Replacement of windows in architectural monuments. // Oknamedia, publication 27.01.2017.
1. Zamena okon v pamiatneykakh arhitektury'. // Oknamedia, publikatsiia 27.01.2017.
2. Shestov A. Windows as the core element of the historical building. // ARDIS, No. 2 (54), 2013.
2. Shestov A. Okna kak vazhnei'shii' e'lement istoricheskogo zdaniia. // ARDIS, No. 2 (54), 2013.)
3. "Complex reconstruction, restoration and adaptation to modern museum technologies of the major building of the Pushkin State Museum of Fine Arts (Moscow, Volkhonka Str., 12)" [Documentation prepared by FSUE Central Scientific and Restoration Design Workshops].
3. "Kompleksnaia rekonstruktsiia, restavratsiia i prispособlenie pod sovremenny'e muzei'ny'e tekhnologii glavnogo zdaniia Gosudarstvennogo muzeia izobrazitel'ny'kh iskusstv imeni A.S. Pushkina (g. Moskva, ul. Volhonka, d. 12)" [Dokumentatsiia podgotovlena FGUP "Central'ny'e nauchno-restavratsionny'e proektny'e masterskie"]
4. GOST R54852–2011 "Buildings and structures. The technique of thermal imaging quality control of thermal insulation of cladding".
4. GOST R54852–2011 "Zdaniia i sooruzheniia. Metod teplovizionnogo kontroliia kachestva teploizoliatcii ograzhdaiushchikh konstruktsii".
5. Levin, E.V., Okunev, A. Yu., Umnyakova, N.P., Shubin, I.L. Fundamentals of Modern Construction Thermography/ Edited by I.L. Shubin. M.: NIISPh of RAACS, 2012, 176 p.
5. Levin E.V., Okunev A. Iu., Umniakova N.P., Shubin I.L. Osnovy' sovremennoi' stroitel'noi' termografii / Pod obshch. red. I.L. Shubina. M.: NIISF RAASN, 2012, 176 p.
6. GOST 26602.1–99 "Window and door blocks. Test methods for heat transfer resistance" and GOST R54853–2011 "Buildings and structures. Test method for heat transfer resistance of cladding by means of a heat meter".
6. GOST 26602.1–99 "Blokii okonny'e i dverny'e. Metody' opredeleniia soprotivleniia teploperedache" i GOST R54853–2011 "Zdaniia i sooruzheniia. Metod opredeleniia sopro-tivleniia teploperedache ograzhdaiushchikh konstruktsii' s pomoshch'iu teplomera".
7. GOST 31937–2011 "Buildings and structures. Test methods for air permeability of cladding in field conditions".
7. GOST 31167–2009 "Zdaniia i sooruzheniia. Metody' opredeleniia vozduhopronitcae-mosti ograzhdaiushchikh konstruktsii' v naturny'kh usloviakh".



Alexander V. Spiridonov,

Ph.D. in Technical Sciences, graduated from the Moscow Power Institute (MPEI) in 1975, majoring in "Lighting and light sources". At present, he is the Chief Research Fellow of the NIISPh of RAACS, President of the Association of Manufacturers of Energy Efficient Windows (APROK), Laureate of the RF Government Prize in Science and Technology



Nina P. Umnyakova,

Ph.D. in Technical Sciences, Associate Professor. graduated from the Moscow Civil Engineering Institute. At present, she is Deputy Director of the NIISPh of the RAACS. Her research interests are thermal protection of buildings, energy saving, evaluation of thermal protection qualities of cladding in the presence of reflective thermal insulation

APPLICATION OF DISPLAY TECHNOLOGY FOR LIGHTING

Victor V. Belyaev^{1, 2}, Donatien K. Nessemon¹, and Andrei A. Belyaev²

¹ *RUDN University (Russian University of Peoples' Friendship), Moscow*

² *Moscow Region State University (MGOU), Moscow*

E-mail: vic_belyaev@mail.ru, nessemon@yandex.ru, aa.belyaev@mgou.ru

ABSTRACT

The article is devoted to contemporary overview of development of a number of display technologies, which have been applied or may be applied for creation of new prospective light engineering solutions. The emphasis is on OLED-based technologies and liquid crystals-based technologies. Examples of their application in automotive industry and architecture are given with consideration of various economic indicators and hygienic and usability limitations.

Keywords: light engineering, optoelectronics, lighting specifications, solid and organic LED, display technology, nanotechnology

Nowadays, development of light engineering has been being significantly promoted by new inventions in different areas, primarily in electro-optics and optics. This leads to appearance of new market niches for devices with increased light engineering specifications or improved functionality. A classic example is light emitting diodes (LED) and LED luminaires. Their application is safer, more environmentally-friendly and more ergonomic from different points of view than application of other lighting devices [1].

Such area of science and technology as information displaying systems or displays has a good outlook for lighting engineering. Some technological solutions for displays, including organic light emitting diodes (OLED), had been originally designed for formation of flat images without application of backlighting but turned out to be prospective for

creation of flat and very thin light sources (LS) [2]. Another important technology for flat screens is liquid crystals technology (LC). Because back lighting is necessary for LC displays (LCD), development of this technology required development of many types of accessories for formation and control of a light beam: FL, LED, light-guiding plates and other elements.

Development of nanotechnology led to appearance of materials influencing on luminous efficacy and chromaticity of existing LSs or optical elements. Among the most well-known are quantum dots materials which have already been manufactured.

Development of display technology requires different usability studies: careful study of human vision system and impact of different LSs with different chromaticity and capability of light adjustment on it. Among the rapidly developing areas there are car displays, displays for industrial and military applications, etc., where light control is an important element.

This review briefly examines the contemporary level of development of different display technologies which have been applied or may be applied for creation of new prospective light engineering solutions.

The world leading companies, such as *Konica Minolta*, *LG Chem*, *AcuityBrands*, *OLEDWorks*, *BMW*, *Audi*, etc., are developing and manufacturing different types of OLED-based lighting devices (LD) with new functional capabilities as compared with conventional ones [2]. The OLED-based LDs may be flat and flexible and very thin at the same time, as well as be capable to be placed on sur-

Table 1. Prospective Specifications of White LED Light Sources

Characteristics	Target and practiceable limit
Luminous efficacy of radiation	350 lm/W
Internal quantum efficiency	95 %
Luminous efficacy of a pixel	180 lm/W with luminance of 3,000 cd/m ²

faces of almost any shape and flexion. Their big advantage is capability to vary their radiation spectra in space and time. Modern OLED technologies allow LDs creation with rather high luminance and luminous efficacy adopted for application in extreme environment, for instance, in motor cars some part of which are under high mechanical and temperature loads.

In the field of semiconductor lighting technology, the LED LSs, which have been becoming cheaper and cheaper are dominating, but illumination based on OLED LSs with characteristics and capabilities supplementing the previous has been rapidly developing and becoming more commercialised. With OLED, it's possible to construct large-area LSs with diffuse radiation and excellent colour rendering. And application of plastic substrate allows manufacturing of very thin and lightweight LD with any shape and flexion. Unlike the most of conventional LDs, OLED-based LD do not cause dazzling and exclusion of such components as diffusers significantly reduce their prices, which, by the way, positively affects the luminous efficacy of LD.

Nowadays, many companies manufacture OLED-based illumination panels for a number of applications including one of the major ones – lighting of motor cars. Such companies as *Audi*, *BMW* and others have shown that special OLED-based LDs provide more design freedom than others mostly thanks to OLED panels with different shape and extremely uniform illuminance distribution [3]. Also not without interest are applications of plastic OLED-based LDs in airplane interiors.

The target and prospective indicators of LD's based on white OLED are shown in Table 1 [3].

As for profitability of these LDs, according to the Department of Energy of the USA [4], as compared with conventional ceiling luminaires, the OLED-based flat luminaires used in corridors reduce power consumption by 73 %, which at the level of 2020 will allow saving up to USD \$1.7 billion per year. The ownership forecasts for 2020 for

4 types of ceiling luminaires presented in Fig. 1 show that at equal level of illumination of a 6 m² office space for 10 years (more precisely, taking office non-operational hours into account, 20,800 hours of operation), the luminaire based on a combination of LED and OLED is more economically efficient than the OLED-based luminaire. The latter here is inferior not only to the LED-based luminaire but even to the fluorescent luminaire. It is anticipated that the cost of 1,000 lm will be equal to \$30 for fluorescent luminaires, \$24 for LED-based luminaires, and \$100 for OLED-based luminaires in 2020.

The US Department of Energy has compiled 2025 roadmaps for luminous efficacy and the cost of manufacturing of OLED panels (Tables 2 and 3). It is anticipated that the general colour rendering index R_a will exceed 80 and the correlated colour temperature T_{cc} will be equal to 3,000K. Within a decade, the luminous efficacy should increase by 2.5 times due to improvement of materials and control devices (CD) efficiency. This should be achieved by multiple increase of investments in facilities for manufacturing of OLED panels with their technical and economical specifications comparable with LCD panels. Moreover, the cost of all materials and production operations should be significantly reduced. As a result, the cost of manufacturing of 1 m² of an OLED panel should reduce by 33 times within 10 years.

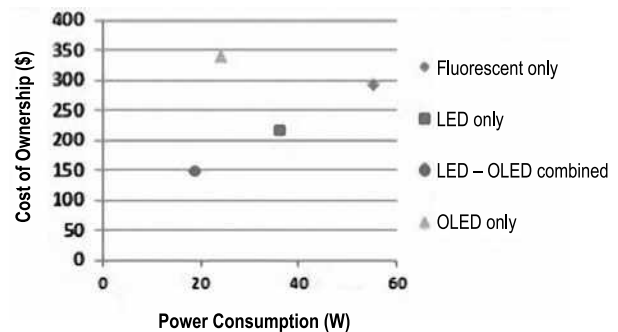


Fig. 1. Ownership cost estimation of ceiling illuminaires with FL, LED, OLED and combination of LED and OLED for office spaces (as of 2020)

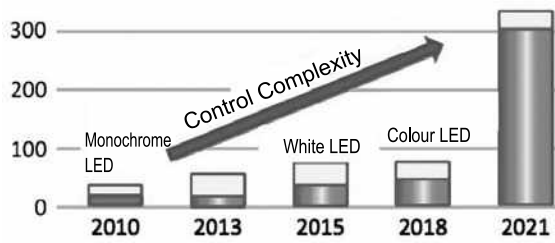


Fig. 2. Number of LED’s for interior lighting of one premium class motor car (according to data of BMW)

In study [5], capabilities of comfortable illumination options formation adjustable for different environments are overviewed. The strategy of energy efficient lighting is aimed to achievement a required level of illuminance and spectrum of the light in the right place at the right time. Herewith, such adjustable luminaire should contain a bright source of white light and a non-bright source of amber light integrated with the illuminance and an occupancy sensors. Signals from the illuminance sensor are used for turning off of both LS’s at daytime and for turning on at night. Signals from the other sensor are used for turning on of bright white light in presence of a person and it turning off during absence of a person.

Today automobile manufacturers keep demanding increase of functionality of LED for support of innovative features of their cars and ease of information reading from the relevant LED devices during daytime. While in 2010 there were 50 LEDs in a typical car for sale, their number should ex-

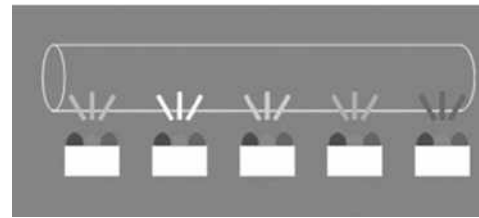


Fig. 3. Colour lighting of motor car interior with mono-chrome or polychrome LED’s with application of a light guide and a colour adjusting device

ceed 300 by 2021 (Fig. 2) [6]. Such increase occurs primarily by application of LEDs with three major colours (red, green and blue) connected in the united LS. In this case, it is necessary to develop relevant CD’s with pulse-duration modulation to obtain required colours, which adds non-required complexity as compared with systems applying platforms with white and monochrome LEDs dominated in the market several years ago.

Fig. 3 shows that interesting capabilities of motor car illumination with different chromaticity and intensity are obtained by application of light guides with end or side location of monochrome or polychrome LEDs.

OLED-based LSs are flexible, light-weight and thin, but despite such unique features, there are serious problems in development of this market. For market expansion, *Konica Minolta* has proposed the *True Value* concept for flexible OLEDs [4]. This concept considers “uniform light radiated by a surface with an extremely thin installation space” as

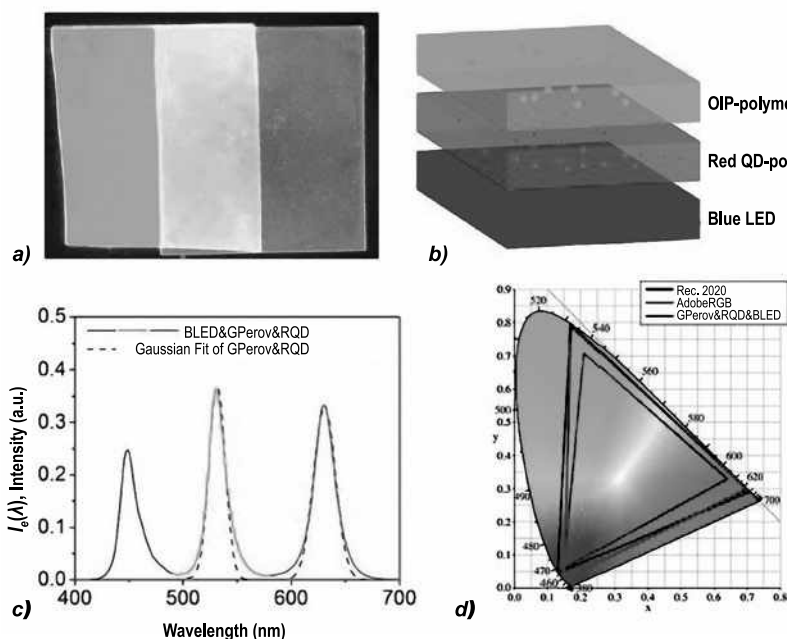


Fig. 4. Application of special composite film as a dimmer for backlighting of a wide colour spectrum display: *a* – composite film with red quantum dots and polystyrol as well as green $MAPbBr_3$ and polystyrol under impact of UV radiation; *b* – the diagram of white light generation by means of above mentioned films integration with a blue LED; *c* – white radiation spectrum of a system with above mentioned films (green and red) used as a radiation converter of blue LED. The dashed lines are Gaussian approximations of the green and red components of the spectrum; *d* – the chromaticity diagrams of the white LED system (blue line), of the system with *Adobe RGB* spectrum (grey line) and of the system complying with the CIE recommendation for 2020 (black line) as compared with the CIE chromaticity diagram for 1931

Table 2. 2025 Roadmap for OLED-based LD's

Characteristics	2015	2017	2020	2025	Target
Luminous efficacy (of a panel), lm/W	60	100	125	160	190
Optical efficiency,%	100			90	
CD efficiency,%	85			90	95
LD efficiency,%				81	86
Luminous efficacy of LD, lm/W	51	85	106	130	162

Table 3. 2025 Roadmap for Manufacturing Cost of OLED Panels

Parameter	2015	2016	2018	2020	2025
Base area, m ²	0.17	0.17	1.38	2.7	5.5
Capital investments, million \$USD	75	75	200	300	400
Production cycle duration, min	3	2	1.5	1	1
Performance, thousand m ² per annum	14	25	300	1,000	2,400
Life cycle cost, \$/m ²	1050	600	125	60	35
Cost of organic materials, \$/m ²	200	150	100	35	15
Cost of non-organic materials, \$/m ²	200	200	120	50	30
Cost of work, \$/m ²	150	100	20	10	5
Other costs, \$/m ²	75	50	15	10	5
Full cost without product yield taken into account, \$/m ²	1,675	1,100	355	160	90
Product yield,%	50	60	70	80	90
Full cost, \$/m ²	3350	1850	550	200	100

the main value. This value is increased by three main drivers: “weight reduction”, “*Twilight* light control” and “opportunity to touch LD without burning oneself”; in case of transparent LD's, there can be another driver: “invisible magic”.

As a result, different flexible OLED-based LD's can be built-in in ordinary objects, such as umbrellas, hand fans, clothes, overhead moving structures, and so on.

Apart from classical quantum dots, perovskite mineral nanoparticles are widely applied in fluorescent materials. In particular, there is a report [7] about a recent invention of organic and non-organic hybrid perovskites (ONHP) added to compound polymer films with exceeded efficiency of photolu-

minescence, higher monochromaticity (spectral line half-width is <20 nm), unprecedented water and heat resistance, applicability for backlighting in LCD screens as well as for sensors and light therapy. LEDs based on quantum dots and ONHP (*QLED*) already created and being manufactured, and their colour gamut, energy efficiency and cost can be better than those of OLED (Fig. 4). It is anticipated that for *QLED*-based LS luminous efficacy will exceed 359 lm/W and R_a will be equal to at least 91.

But the service life of such devices is still less than 30,000 h which is required for application in LDs. Currently it is equal to 2000 h with luminance of 500 cd/m² and 7000 h with luminance equal to 100 cd/m² [8].

Table 4. Impact of Adjustment of T_{cc} on Maximum Acceptable Duration of Retina Irradiation t with illuminance of 500 lx

T_{cc} , K	Planckian radiator	LED	OLED
	t , s		
2,000	407	370	369
3,000	146	155	153
5,000	63	74	70
8,000	40	50	47

OLEDWorks LLC has developed the second generation of high-performance amber-colour OLED panels for medical institutions [9]. As compared with the first generation panels, their luminance efficacy is increased to 60 lm/W by using phosphorescent materials. Moreover, their laminar design increases service life and uniformity of glow.

Pixelligent Technologies LLC has developed the technology of manufacturing of *PixClear*[®] material on the basis of dispersions and nanocomposites with nanocrystals of ZrO_2 , which allows the light extraction ratio to exceed 100 % for OLED-based LSs [10]. These materials have significantly increased refractive index of monomers and polymers with content of nanoparticles of ZrO_2 up to 90 %. Wherein, visible transparency of the material is high.

Usually LCD devices are used for formation or processing of images. But recent years, LCD devices for application in headlights of motor cars or architectural lighting has been intensively developed. LCD materials for such applications should be more resistant against extreme environment as well as against very bright light. To obtain required optical specifications when using in architectural lighting, LCD should have very high double refrac-

tion with high light-resistance. The German company *Merck* has developed such LCD mixtures, whereas *Hella KGaA Hueck & Co* [11, 12] has designed a luminaire with application of such LCD for operation in extreme environment (Fig. 5). The new monochrome structure is distinguished by availability of double light polarization (vertical and horizontal), and its polarization efficiency is 76 %. The LS is a LCD-matrix panel with relatively low resolution.

The structures allowing consumers to adjust them on the basis of their personal needs have been becoming more popular in the market. One of the ways to resolve this problem is to build in a dimmer. A good example is the *Hue* series of smart lighting devices by *Philips Lighting*. Not long ago, *LensVector* developed methods of changing the shape of light spot from local lighting. LCD elements can be used for adjustment of light direction or its focusing (Fig. 6) [12].

The study being fulfilled in the National Tsing Hua University (Hsinchu, Taiwan) shows that it is not necessary to consider only the luminous efficacy and energy efficiency to obtain “proper” lighting for a user [13]. The scientists had studied the process of suppression of melatonin secretion under influence of three types of LSs (a Planck radiator, LED

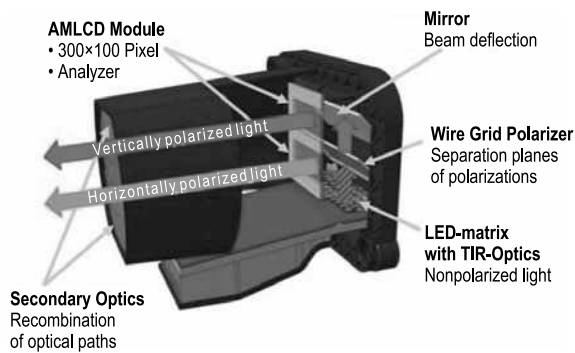


Fig. 5. Diagram of the structure of a directional luminaire with a LC light source

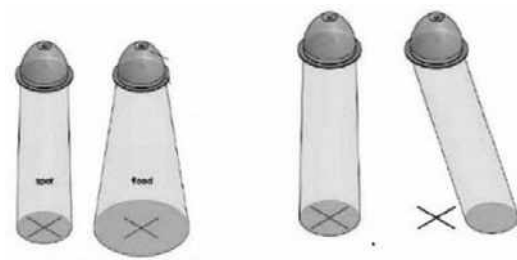


Fig. 6. Two concepts of light guides for architectural application: focusing or shape changing and direction adjustment

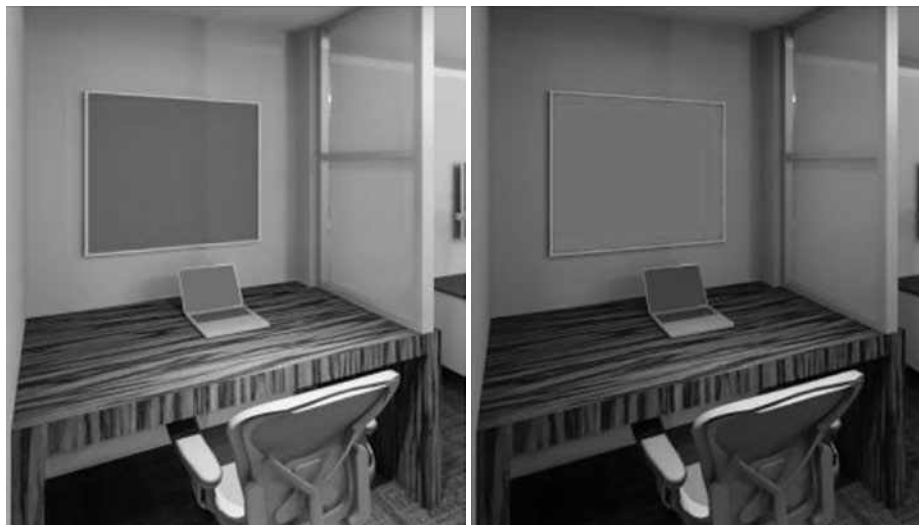


Fig. 7. Example of application of a self-glowing display panel for creation of efficient (blue) and inefficient (red) light (in terms of circadian rhythms) depending on the time period

and OLED) with T_{cc} varying between 2,000 and 8,000 K. Table 4 shows maximum acceptable values of retina irradiation for these three LSs in terms of photobiological safety [14].

Usually it is believed that the white light with T_{cc} of about 6000 K is more suitable for displays of TV's, monitor units and mobile phones than the light with T_{cc} equal to 7,000 K (with relatively higher content of blue colour).

The combination of the "proper" light and energy-saving technologies allows to avoid sleep disruption and risk of retina damage or diseases.

The Lighting Research Centre of the Rensselaer Polytechnic Institute (USA) conducted a study of synchronisation of circadian rhythms of different groups of people including those suffering various neurological disorders with local time [15]. The study also included research of potentially useful impact of lighting display panels on sleep and feeling. In the pilot experiments, a 70-inch display panel by Japanese company *Sharp* was used, the publication does not specify whether it was a plasma panel or a LCD panel. In the course of the one-week experiment, the people suffering Alzheimer disease sat at the table made of a lighting display panel during the light day from 7 in the morning till 6 in the evening. At the specified time, they had meal at this table. The table could be used also as a sensor screen for games and entertainment. As a result, sufficient improvement of sleep and reduction of depression and irritation were witnessed. The glow of the panel was either blue or red depending on the time period (Fig. 7), which allowed the circadian rhythms adjustment. Moreover, there were vertical display panels in the room so that their light could

reach retina. This cannot be always reached if LS is located on the ceiling.

CONCLUSION

The article contains a brief overview of contemporary safe, environmentally friendly and ergonomics technologies based on LED and OLED and application of some new composite materials. New fields of application of such devices are overviewed with consideration of economical prospects; possibility to apply such technologies in medicine is noted.

ACKNOWLEDGMENT

The work is conducted as part of the project No. 17-47-500752 of the Russian Foundation for Basic Research and the Government of the Moscow Region (with partial support).

REFERENCES

1. Yunovich, A.E. LED's and their Application for Lighting / Edited by Prof. Ju.B. Aizenberg. Moscow: Znak, 2011.
1. Iunovich A.E'. Svetodiody' i ikh primenenie dlia osveshcheniia / Pod red. Prof. Ju.B. Aizenberga. M.: Znak, 2011.
2. Usov, Nicolai N. Prospective Use of Organic Light Emission Diodes for Information Displays and for Illumination //Light & Engineering Journal, 2012, Vol.20, #1, pp.9-23.
3. Hack, M., Weaver, M. S., Brown J.J. Status and Opportunities for Phosphorescent OLED Light-

ing / SID Symposium Digest of Technical Papers, 2017, pp. 187–190.

4. Nagata A., Mitsui S., Iwamatsu N., Suzuki A., Kubota R., Hiraga A., Yamamoto N., Takemoto N., Tsujimura T. The “TRUE VALUE” of Flexible OLED – One and Only Design and Experience / Ibid, pp. 691–694.

5. Papamichael K. Adaptive Lighting for Energy-Efficient Comfort and Wellbeing / Ibid, pp. 306–309.

6. Automotive Interior Lighting Control Redefined. URL: <https://www.led-professional.com/resources-1/articles/interior-automotive-lighting-control-redefined>, 28.12.2017 (reference date: 21.08.2018).

7. Dong Y. Solution Processable Luminescent Nanomaterials for Display, Lighting and Beyond / SID Symposium Digest of Technical Papers, 2017, pp. 272–275.

8. Dong Y. et al. / Ibid, pp. 270–273.

9. Lee D., Spindler J., Kondakova M., Pleten A., Boroson M. Amber OLED Lighting Technology Development and Application / Ibid, pp. 91–94.

10. Guschl P.C., Wang X., Weinstein M.A. Ink-Jet Printing of High-Index Zirconia Nanocomposite Materials / Ibid, pp. 942–944.

11. Reinert-Weiss C.J., Baur H., Nusayer S.A.A., Duhme D., Fruehauf N. Development of active matrix LCD for use in high-resolution adaptive headlight // Journal of the SID, 2017, Vol. 25, No. 2.

12. BMBF (Bundesministerium für Bildung und Forschung Germany), Announcement of the project “Vol-ladaptive Lichtverteilung für eine intelligente, effiziente und sichere Fahrzeugbeleuchtung (VoLiFa 2020)”. URL: <http://www.photonikforschung.de/forschungsfelder/beleuchtungled/intelligente-beleuchtung/> (reference date: 01.06.2018).

13. Jou J.-H., Singh M., He Z.-K., Su Y.-T. Definition and Design of a Good Light / SID Symposium Digest of Technical Papers, 2017, pp.1812–1813.

14. GOST R IEC62741–2013 (IEC62471:2006) Lamps and lamp systems. Photobiological safety.

15. Figueiro M.G. Biological Effects of Light: Can Self-luminous Displays Play a Role? // Information Display, 2018, Vol. 34, No. 1, pp. 6–9.



Viktor V. Belyaev,

Prof., Dr. of Technical Science, graduated from MFTI with specialty in Automation and Electronics in 1974. At present, he is a Head of the Theoretical Physics Chair of MGOU and Professor of Mechanics and Mechatronics Department of the RUDN Engineering Academy. Fellow of the Society for Information Displays (SID)



Donatien K. Nessemon,

a translator in the field of professional communication (French and Russian languages). In 2012, Graduated from the RUDN Foreign Languages Institute



Andrei A. Belyaev,

environmentalist, graduated from MGOU with specialty in environmental geology in 2015. Engineer of the Education and Research Laboratory for Theoretical and Applied Nanotechnology of MGOU

ILLUMINANCE AND LUMINANCE BASED RATIOS IN THE SCOPE OF PERFORMANCE TESTING OF A LIGHT SHELF-REFLECTIVE LOUVER SYSTEM IN A LIBRARY READING ROOM

Merve Öner¹ and Tuğçe Kazanasmaz²

¹ *The University of Pisa, Pisa, Italy*

² *Izmir Institute of Technology, Izmir, Turkey*

E-mail: m.oner@studenti.unipi.it

ABSTRACT

Uncontrolled daylight brings visual and thermal problems that may result in negative interactions with user comfort, productivity, well-being, and human health. Library spaces, in which reading, writing, and computer task activities are performed, need to be well designed in terms of daylight performance to enhance user satisfaction. The focus of this study is to make a performance test of a light shelf-reflective louver system to improve the visual performance conditions of a library reading room. First, the instrumental monitoring of existing daylighting conditions was performed. Second, Relux model was prepared to evaluate luminance patterns and illuminance distribution. Third, a new light shelf-reflective louver system was proposed based on the insufficiencies of the simulation results. The performance of the new system was found highly satisfactory based on the findings of enhanced luminance patterns and uniformity ratios especially at the points near the windows.

Keywords: daylighting, visual performance, library, illuminance, luminance, light shelf, reflective louver

1. INTRODUCTION

Libraries are the spaces where people fulfil both their learning and working activities; so, visual performance ought to be considered initially. These kinds of spaces have to be responsible for users

to execute their work efficiently with no deficiency in visual acuity or comfort considering the whole aspects of performance issues associated with lighting [1]. Required illuminance values are needed to be satisfied; luminance/contrast relationship is to be well controlled with luminance ratios, which are determined by illuminance and reflectance of surroundings in the visual field. Eyes can adapt to varying luminances rapidly in a properly designed visual environment; their tiredness can decrease as well.

A well-daylit library stimulates success, increases the duration of stay, enhances well-being, and regulates the seating distribution [2, 3]. Benefits of daylight have become more significant in library planning within the context of visual comfort for various intended usages such as paperwork, computer-based work, bookshelf browsing, and reading books, journals, and digital sources [4, 5]. The amount of daylight for different purposes is associated with the luminance of surfaces within the field of view [6]. To obtain good visibility, an adequate amount of light for the task and the glare control are ought to be precisely existing [7].

Daylight redirecting systems provide such solutions to block the excessive illuminance that causes glare and heat gain problems and supply daylight to deep spaces [8]. Kontadakis et al. tested movable mirrors fixed on a light shelf that are able to track the sun in a south facing deep office. Illuminance increased during both 152 % in summer and 12.5 % winter solstices comparing to the actual case

Table 1. Photometrical Features of the Surfaces

Surface	Reflectance/Transmittance [%]
Walls	73
Floor	37
Ceiling	78
Desks	47
Glazing	80

[9]. Dogan and Stec developed a horizontal light shelf with a row of mirror tiles that can be tilted in two-axis according to sun movement. They observed almost 20 % daylight performance improvement and decrease in glare [5].

This study focuses on the evaluation of visual performance conditions in terms of illuminance and luminance distributions in an academic library, due to the above considerations and lack of studies to improve the visual quality of users in library spaces. The aim is to examine the effectiveness of a light shelf and reflective blinds in such problematic zones that are exposed to unsatisfied or excessive luminance and illuminance distributions on both VDU and paper tasks.

2. METHODOLOGY

2.1. Library Reading Room

The experiments were conducted in the library of Izmir Institute of Technology (38.19°N,

26.37°E). It has an orientation along the 60° east of south axis. The reading room (L 29.70m x W 19.00m x H 4.30m) has north-east, south-west, and north-west oriented facades, which are fully glazed. The workplane layout is divided into three zones: two seating zones and the center zone with bookshelves (Fig. 1).

Material characterization was performed on-site using luminance/illuminance based technique to practically and basically get information about materials on-site due to the literature [10]. An illuminance meter and a luminance meter were used (Table 1). The equation of Lambertian reflectance was the basis for the reflectance calculation. The windows consist of double layer glazing, whose transmittance was measured and calculated due to the literature [11].

2.2. Validation Process

Horizontal illuminance was chosen as the indicator, where the paper task was performed. Measurements were carried out with an illuminance meter on June 20 and July 20. In total, 131 measurement points were set with a height of 0.76 m above the ground. The readings were afterwards compared with illuminance outputs from Relux-based simulation model, which was generated with identical building characteristics. The coefficient of determination (R^2) values ranged between 51 % and 78 % for all simulations on the above dates indicating the acceptable accuracy of the simulation model. Keeping in mind the large floor area of the experimental

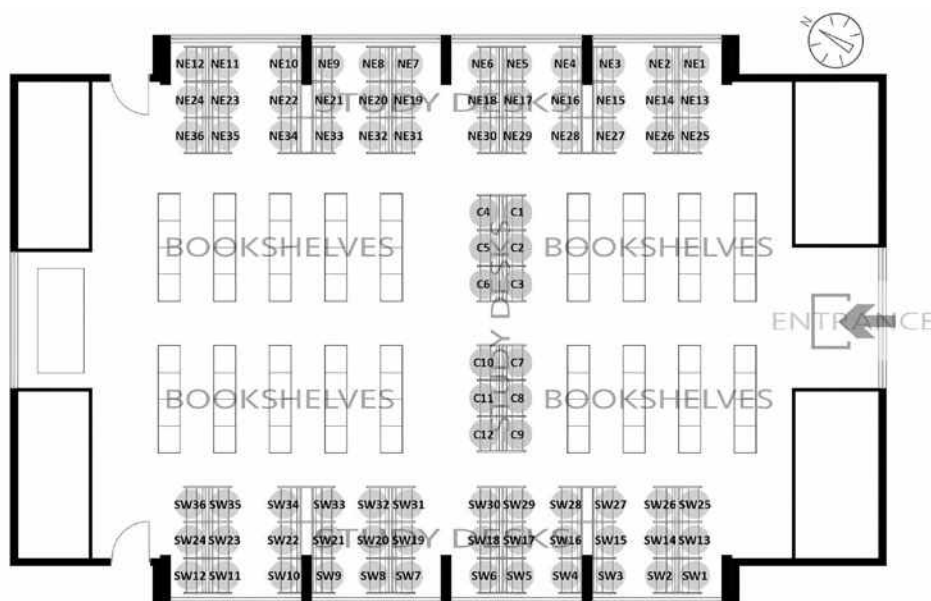


Fig. 1. Measurement locations: NE1-NE36 (north-east points), SW1-SW36 (south-west points), and C1-C12 (centre zone)

Table 2. Statistical Results of Errors

	R^2	MPE	CV(RMSD)
June 20, 2.00 pm	0.51	10 %	21.1 %
July 20, 11.00 am	0.67	20 %	21.7 %
July 20, 12.30 pm	0.78	20 %	19.8 %
July 20, 3.30 pm	0.71	55 %	31.1 %

space and furniture, the error margin may be considered acceptable. Further, mean percentage error (MPE) values and coefficient of variation (relative mean square deviation) (CV(RMSD)) are calculated to indicate the averaged error and deviation of measured to simulated illuminance values (Table 2).

2.3. Identification of the Problem

The library reading room was analyzed in Relux under CIE intermediate sky with sun, on the solstice and equinox dates at 12:30 pm within the scope of illuminance and luminance based ratio standards of library spaces. A total of 84 points were studied at a height of 0.76 m on the centre of each study desk, which was arranged with a computer screen and a white paper placed in front of the occupant (Fig. 1). The objective in this section is to identify the problem in daylight distribution measuring horizontal illuminance on the workplane and luminance pattern analysis in the visual field.

2.3.1. Luminance Pattern Analysis and Determination of the Most Problematic View Points

Luminance distribution of each viewpoint was analysed on the solstice and equinox days at 12:30 pm. Three points were determined as receiving the least uniform luminance distribution due to recommended luminance ratios. To achieve this, luminance on screen, white paper, desk, partition, wall, general surrounding, and sidewall adjacent to the window were evaluated according to the luminance maps of each view (Fig. 2).

Luminance map analysis showed that particularly southwest perimeter zone had the most critical luminance distribution within the visual field, which ranged from 13 cd/m² to 2050 cd/m². Three viewpoints (SW3, SW10, SW12) with the least uniform luminance pattern were identified, which were unsurprisingly located near the south-west facing window (Fig. 2). In the case of SW3, i.e, the luminance ratio between the VDU task and the side wall adja-

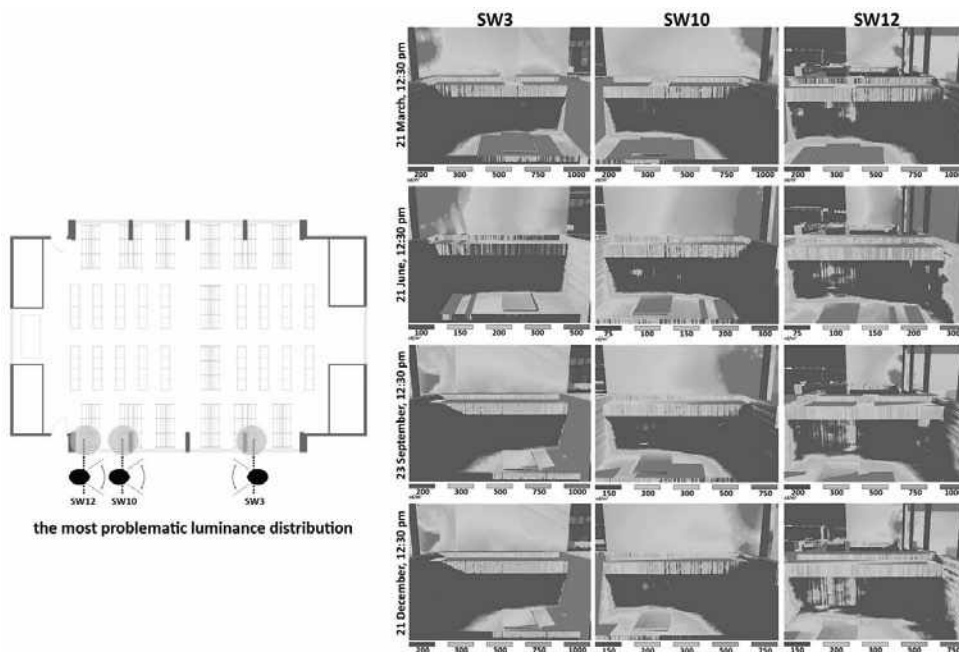


Fig. 2. Viewpoints with the poorest luminance distribution and luminance maps

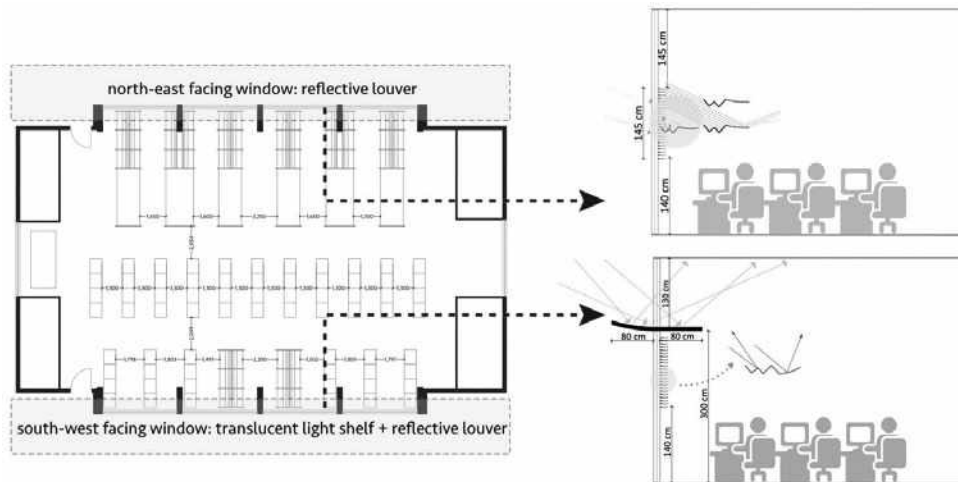


Fig. 3. Daylighting strategy on the plan layout and the cross sectional views showing its shape and principle

cent to the window was found 1:43 on December 21 at 12:30 pm, which is excessively high comparing to the recommended 1:10 ratio. In all cases, the luminance ratio between the paper task and VDU task ranged from 1:12 to 1:158, which again violates the recommendations and leads to an unsatisfactory perception for the library users.

2.3.2. Illuminance on Workplane and Uniformity

Illuminance in all cases shows an uneven distribution with a wide range of variation from very low levels to thousands. Peaks of illuminance occur at points (SW1-SW12), which were placed next to the south-west facing glazings. Rapid decreases are observed with the distance from the windows in the same zone (SW25-SW36). Illuminance distribution of north-east oriented points (NE1-NE36) appears relatively more uniform ranging from 46 lx to 1180 lx, while it shows the lowest values, i.e. between 95 lx and 396 lx, at the centre zone. To conclude, uniformity on the workplane throughout the room inherently appears poor, which is considerably lower than the standards (recommended illuminance for paper-based tasks in libraries in IES standards is between 500–1000 lx; useful daylight illuminance in workspaces is between 100–2000 lx) (Table 3).

2.4. Daylighting Strategy Proposal

New daylighting strategies were proposed for south-west facing (a light shelf made of translucent material with a reflective coating shelf and reflective louvers) and north-east facing windows

(reflective louvers) to improve illuminance and luminance distributions (Fig. 3). The systems are chosen based on the conclusions drawn from the literature and actual products [12–14]. A light shelf was positioned to the south-west facade throughout the glazing at 3.00 m from the floor with a depth of 1.6 m. The light shelf modelled as external and internal was defined as specular with a reflectance value of 85 %. The internal reflective louver chosen from Retrolux Archive [14] components with a reflectance value of 85 % for the south-west facing window were placed between 1.40 m and 2.85 m above the ground. It provides shading additionally. Each lamella has 13 mm depth, and the spacing between two lamellas is 0.5 cm. The identical reflective louver system was applied to the north-east facing window as well.

3. RESULTS

3.1. Luminance Based Findings

The luminance ratios within the field of view have substantially found the balance regarding visual performance standards. The shading-redirecting function of the system played a strong role in that sense. Viewpoints SW3 and SW10 were the worst ones due to the very bright side wall surfaces just in front of the viewers, which are fully covered by sun patches. Improving the impact of the redirecting system on luminance distribution on the wall surface is much stronger and clearer in SW3 and SW10 than SW12. Nevertheless, the shading-redirecting effect of the system can be seen well in all three viewpoints perceiving the surfaces within the field of views with a more balanced luminance distribu-

Table 3. Illuminance on Workplane and Uniformity Ratios (E : illuminance, avg: average, min: minimum, max: maximum, U : uniformity).

12:30 pm	E_{avg} (lx)	E_{min} (lx)	E_{max} (lx)	$U_1(E_{min}/E_{max})$	$U_2(E_{min}/E_{avg})$
March 21	1358	114	6610	0.017	0.083
June 21	430	48	1060	0.045	0.111
September 23	1686	97	7970	0.012	0.057
December 21	910	46	4700	0.009	0.050

tion. The excessive daylight on desk surfaces is balanced in all viewpoints providing a clear visual perception on the writing/reading task area.

The system functions as desired, i.e. on September 23 for SW10 and SW12, but less for SW3 that slightly observes sun patch traces on the wall surface particularly in the winter solstice. The most dramatic reductions in luminance ratios defined on screen, on paper, and on partitions were observed during the equinoxes. Luminance ratio between the paper task and desk partition on 21 March changed from 13.5:1 to 1.9:1 (SW12), 14:1 to 2.9:1 (SW10), 13:1 to 1:1.6 (SW3), which are providing recommended ratio ($\leq 5:1$) based on the standards. Lumi-

nous variability is slightly higher in SW3 than in the others, but still within the recommended values; i.e. desk-to-side wall luminance ratios are 1:3 in SW12, 1:3 in SW10, and 1:3.8 in SW3 in spring equinox. Or, paper-to-desk ratios in spring equinox are found to be reasonably good indicators of the performance of shading-redirecting system as respectively 1.6:1 in SW12, 1.6:1 in SW10, and 1.8:1 in SW3.

Luminance values were substantially fixed with respect to the recommended ratios, except the ratios between screen and paper luminance when compared to the actual case. Paper-to-screen ratio is identified as between 1:2.5 to 1:3 in standards; however, results are higher, i.e. spring equinox indicated

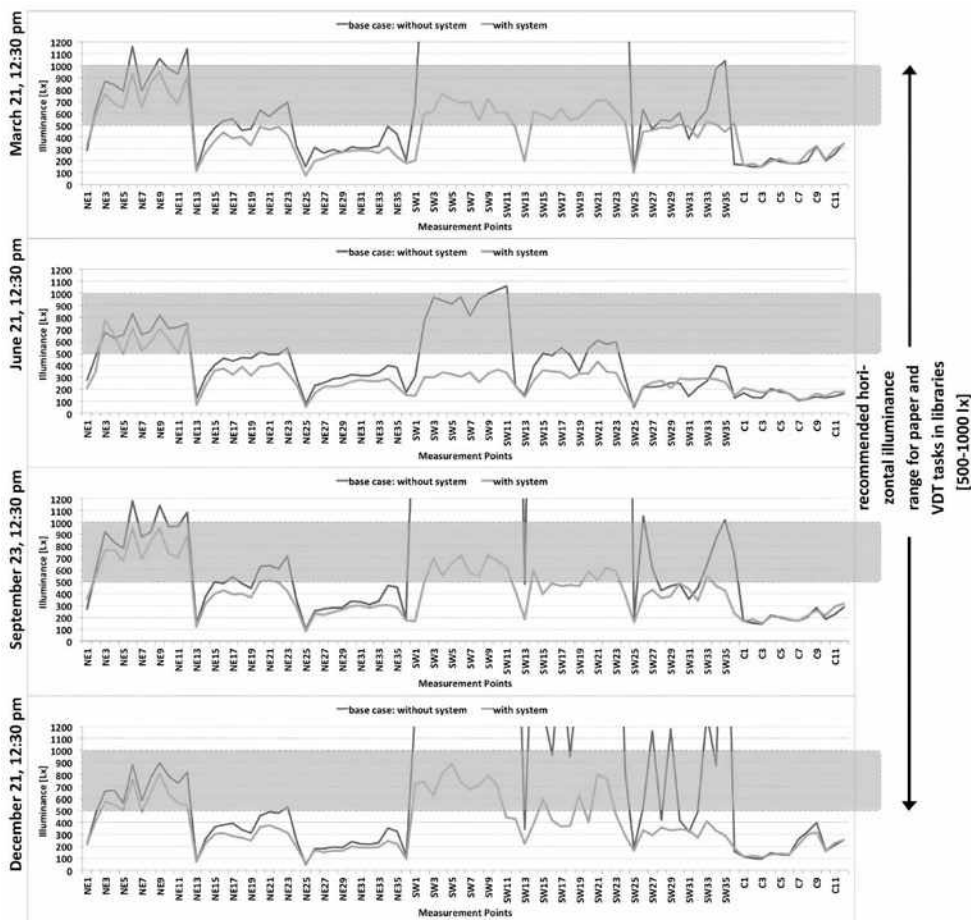


Fig. 4. The illuminance based effect of daylighting strategy on measurement points

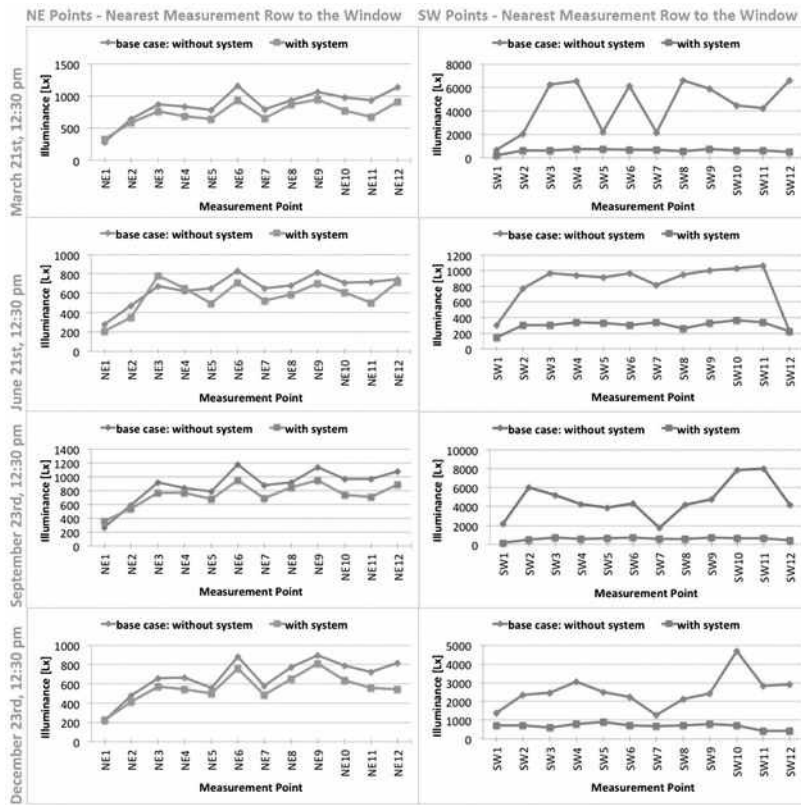


Fig. 5. Illuminance variation of the points near the windows (NE1-NE12 and SW1-SW12)

that the average paper-to-screen ratio decreased from 1:174 to 1:15 for SW12, from 1:191 to 1:35 for SW10, from 1:216 to 1:42 for SW3, which are considerably high.

3.2. Illuminance and Uniformity Based Findings

Illuminance on almost every point experience diminution in all cases, resulting in a decrease in the average horizontal illuminance (Fig. 4). These findings may be considered adversely since the percentage of points between recommended values falls; i.e. from 1358 lx to 454 lx (−66 %) on March 21, from 430 lx to 302 lx (−29 %) on June 21, from 1686 lx to 431 lx (−74 %) on September 23, from 910 lx to 378 (−58 %) lx on December 21, respectively. Yet, considering the recommendations of useful daylight illuminance values (100–2000) lx, the average horizontal illuminance of March 21, September 23, and December 21 have come close to the recommended range after the retrofitting applications. Almost 80 % of the calculated region below the IES standards satisfies the useful daylight illuminance range with a reasonable daylight availability. The potential reason, why only a few points are within the recommended range in June, can

be explained with the high solar altitude during the summer solstice, which was already insufficient before the daylighting strategy. Illuminance falls the most dramatically at near window locations, but not at the centre zone. The system actually works as planned by mostly diminishing the excessive amounts of illumination near windows and not much affecting the points that are far from the windows.

Illuminance based improvement of 24 measurement points near the window (NE1-NE12 and SW1-SW12) are shown in Fig. 5 emphasizing the shading efficiency of the daylighting strategy. The most striking change appears in terms of illuminance variation, particularly on southwest points. The system balanced the illuminance distribution among the aforementioned measurement points as it was expected, i.e. the trendlines on March 21, June 21, September 23, and December 21 appear to be almost linear throughout the majority of southwest points, but not much in the sense of northeast points. Illuminance range of northeast points was already between 220–1160 lx, which is an acceptable range according to the standards. In this case, the main consideration while applying the reflective louver system was to deliver daylight to the deeper parts of the space instead of blocking

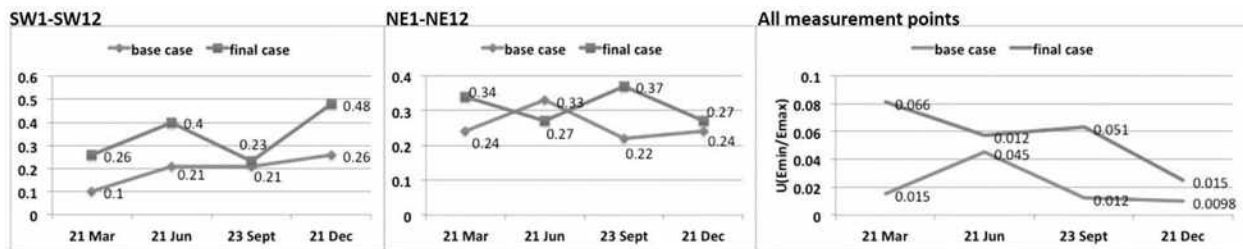


Fig. 6. Uniformity ratios before and after the daylight strategy (base and final case)

the sunlight. The system was successful to satisfy higher uniformity in every season in the third measurement row (NE25-NE36), specifically in December showing the strong redirecting effect of the system. The majority of northeast points remained very close to the base case illuminance, neither showing noticeable decrease nor increase, as desired at the beginning.

Fig. 6 illustrates the uniformity ratios (E_{min}/E_{max}) across the whole space in solstices and equinoxes. Even the worst uniformity ratio of the base case performed an improvement of 53 %, which belongs to the winter solstice, while the rest of the experiment days showed an improvement between 166 % and 340 %. Still being below the current uniformity standards, these ratios are found to be acceptable considering the large floor area of the case and the high number of measurement points. Specifically, better uniformity ratios are attained, except in NE in June.

4. CONCLUSION

The application of a translucent light shelf and reflective louvers improved the uniformity of both illuminance and luminance distribution by minimizing the incoming daylight near the window and maintaining or slightly maximizing it at the deep.

The most striking improvement observed after the daylight system application was the luminance distribution, since it blocks the excessive daylight filtering inside the space and redirects it to the deeper parts of the library. Specifically, the system with its shading-redirecting impact performed the best during equinoxes improving the unbalanced luminance distribution on surfaces within the visual field, i.e., the ratio of paper-to-desk partition was found to be significantly improved (79–85 %) and provided the recommended ratios.

The system notably maintained the target illuminance specifically on the most problematic measurement points, which are the nearest row to the

window. Reaching up to 80 % of improvement rate when compared to the base case, 75 % of these points satisfied the IES standards that are required for meeting visual tasks, while 100 % of them were calculated within the UDI range. Uniformity ratios were positively and significantly correlated with the more balanced illuminance distribution across space. Though still can not meet the required uniformity ratios of IES standards, an improvement of (53–340) % was observed when compared to the base case. To satisfy the target uniformity ratio in such spaces with a fairly large floor area is a challenging and almost impossible task to accomplish. The improvement of the uniformity ratio here may remain to be a successful step.

In overall, the big picture gives the clues on how a proper design of a daylighting system provides a noticeable improvement in visual performance of a library having these building specifications; yet, one should keep in mind that in some cases even the proposed design solutions are not able to guarantee the ratios suggested in literature.

REFERENCES

1. Pniewska A., Brotas L. Daylight and productivity in a school library // Proceedings of CISBAT 2013, 2013, Lausanne, Switzerland, Vol. 1, pp. 341–346.
2. Reinhart C., Selkowitz S. Daylighting – Light, form, and people // Energy and Buildings, 2006, Vol. 38, #7, pp. 715–717.
3. Konis K. Evaluating daylighting effectiveness and occupant visual comfort in a side-lit open-plan of office building in San Francisco // Building and Environment, California, 2013, Vol. 59, pp. 662–677.
4. Keskin Z., Chen Y., and Fotios S. Daylight and seating preference in open-plan library spaces // The International Journal of Sustainable Lighting, 2015, #1, pp. 12–20.
5. Dogan T., Stec P. Prototyping a facade-mounted, dynamic, dual-axis daylight redirection system // Lighting Research and Technology, 2016, pp. 1–13.

6. Baker N., Steemers K., Compagnon R., and Parpairi K. Daylight Design of Buildings // London: James & James Science Publisher, London, 2002.
7. Solar Heating and Cooling Programme (SHCP), Daylighting in buildings: design tools and performance analysis, 1999. URL: http://www.ieo-shc.org/task_21/publications/
8. Kazanasmaz T., Fırat Örs P. Comparison of advanced daylighting systems to improve illuminance and uniformity through simulation modelling // Light and Engineering, 2014, Vol. 22, #3, pp.56–66.
9. Kontadakis A., Tsangrassoulis A., Doulos L., and Topalis F. An active sunlight redirection system for daylight enhancement beyond the perimeter zone // Building and Environment, 2017, Vol. 113, pp. 267–279.
10. Jakubiec J.A. Building a database of opaque materials for lighting simulation // Proceedings of PLEA 2016 Los Angeles – 36th International Conference on Passive and Low Energy Architecture, 2016, Los Angeles, California, USA.
11. Bayram G., Kazanasmaz T. Simulation based retrofitting of an educational building in terms of optimum shading device and energy efficient lighting criteria // Light and Engineering, 2016, Vol. 24, #2, pp. 45–55.
12. Moazzeni M.H., Ghiabaklou Z. Investigating the influence of light shelf geometry parameters on daylight performance and visual comfort, a case study of educational space in Tehran, Iran // Buildings, 2016, Vol. 6, #4, pp. 1–16.
13. Freewan A.A. Maximizing the lightshelf performance by interaction between lightshelf geometries and a curved ceiling // Energy Conversion and Management, 2010, Vol. 51, #8, pp. 1600–1604.
14. Retrosolar. Information about Retrolux. URL: http://www.retrosolar.de/flash/ani_rlx_e.html [Accessed 11 June 2017].



Tuğçe Kazanasmaz,

Ph.D. in Building Science from Middle East Technical University (METU). She has 18 years academic experience in architectural lighting, building physics, and energy efficient design. At present, she is a Professor in the Department of Architecture in İzmir Institute of Technology, Turkey



Merve Öner,

M. Sc. in Architecture from Izmir Institute of Technology in 2017. She holds her undergraduate degree obtained from Yaşar University as B. Sc. (Eng) in Architecture in 2012. Her research topics are architectural lighting and computer based simulations. She is still a Ph.D. candidate in the Department of Energy Engineering, Systems, Territory, and Construction in University of Pisa, Italy since 2017

RECREATING THE TIBETAN TRADITIONAL LIGHTING IN LOCAL MODERN LIBRARY: RESEARCH-BASED LIGHTING DESIGN IN YUSHU LIBRARY

Xiufang Zhao¹, Xin Zhang², and Kai Cui³

¹ *Brandston Partnership Inc., New York, USA*

² *Tsinghua University, Beijing, China*

³ *China Architecture Design & Research Group, Beijing, China*

*E-mail: zhaoxf07@gmail.com; zhx@mail.tsinghua.edu.cn;
yingqizhang@aliyun.com*

ABSTRACT

This paper demonstrates the research-based lighting design process of Yushu Library, a new library built after the 2010 Yushu Earthquake. The design goal is to recreate the Tibetan traditional lighting in this local modern library without sacrificing functional needs. The research methodology is comprised of a literature review, site visit and measurement, user interview, and daylighting simulation.

Keywords: lighting design, Tibetan traditional architecture, lighting evaluation, daylighting simulation

1. PROJECT BACKGROUND

1.1. Post-Earthquake Reconstruction

The 2010 Yushu Earthquake registered a magnitude of 6.9 Mw and originated in Yushu Tibetan Autonomous Prefecture, Qinghai Province, China. Over 85 % of buildings in Gyegu, the seat of Yushu County, were destroyed. The post-earthquake reconstruction plan included a library, a theatre, a cinema, and a cultural centre. Yushu Library was designed and built serving as the core project in rebuilding the town and community after earthquake [1].

1.2. Unique Traditional Architectural Lighting

In China, Yushu is in Lighting Climate Zone I, which has an average daylight illuminance of 28,000 lx [2]. At an elevation of 3,700 meters, Yushu has a harsh alpine subarctic climate with 2496 sunshine hours annually. The sunshine hour was defined as the period, during which direct solar irradiance exceeds a threshold value of 120 W/m² [3]. The cold climate, the large temperature difference between day and night, and strong ultraviolet radiation have historically led to an inward architectural form with small windows and thick walls to prevent heat loss and an atrium to get an access to daylight in public buildings [4].

This traditional architecture form creates a unique lighting, which is experienced daily by local residents, 97 % of whom are Tibetan and have Tibetan culture deeply rooted in their daily life. The new Yushu Library is designed for the local users to enjoy a modern library, which embodies a traditional Tibetan architectural environment through space geometry, interior furnishings, and lighting. This is a library in Yushu and for Yushu and would not be the same as a library in Beijing, New York, or London.

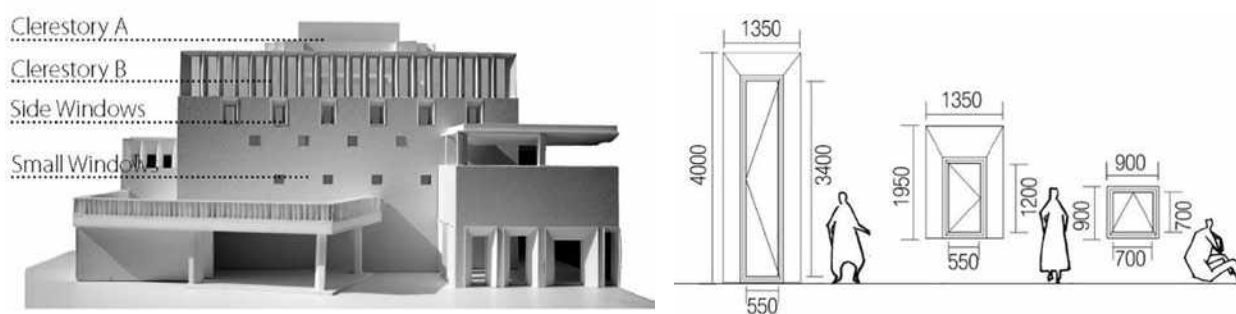


Fig. 1. Yushu Library physical model and window system

1.3. A Current Design Problem

The obvious difference between new and traditional architectural lighting is a rising issue in Yushu post-earthquake reconstruction projects. New public buildings kept traditional space form and decoration style, but their lighting directly followed the national standards in China [5, 6]. By simply following the standards, designers on some projects introduced excess daylight or electrical lighting into new buildings. This increased the illuminance level and decreased the luminance contrast, which is on the contrary of Tibetan traditional lighting.

For electrical light, the standard [6] requires 300 lx for library reading rooms. According to the recommended light levels from the IESNA Lighting Handbook [7], the light level in a Library – Reading / Studying is (300–500) lx. For daylight, the standard [5] requires minimum 2 % Daylight Factor for library reading rooms. In [8], Section 2.2.2.1, it states that “An average daylight factor below 2 % generally makes a room look dull; electric lighting is likely to be in frequent use.” [5] is aligned with [8].

If the characteristics of a traditional lighting could be quantified, could a new lighting be designed to resonate with traditional lighting? This is the question we asked in the beginning of this research-based design.

2. CONNECTION BETWEEN THE NEW LIBRARY AND THE TRADITIONAL CHANTING HALL

2.1. Yushu Library

Yushu Library has four floors with a gross area of 4300 m² (Fig. 1). Architects learnt from traditional Tibetan architecture and kept the architec-

tural elements including small windows and atrium, which provided a solid foundation of further design to recreate traditional lighting. The window size increases from the bottom to the top, and the atrium is the library core space with a clerestory as the main daylight path. There are 3 reading programs in the library (Table 1).

2.2. Case Selection on Traditional Tibetan Lighting

Traditional Tibetan architecture is a broad definition, which includes public religious buildings and private residential buildings, among which Tibetan Buddhist monastery buildings are the most well-studied type. Monasteries concentrate religious consciousness, aesthetic concept, local context, and advanced building technology for the time [4]. Among Tibetan Buddhist monastery buildings, a Chanting Hall is a significant public venue for religious activities and events, where monks read daily and villagers read during religious events. The visual tasks in a chanting hall are similar to the ones performed in a library by users. The chanting central area is similar to the atrium in Yushu Library in terms of function and space geometry.

The traditional Tibetan lighting is a result of how architecture responds to local climate and cultural context. Small windows in thick walls, a clerestory for daylight access, high luminance contrast, low average illuminance, and dark areas shape the lighting in a traditional Tibetan building. The daylight path of a typical chanting hall is distinctive. In most of the chanting halls, the clerestory around the lifted roof is the daylight path for chanting area.

The Damkar Main Chanting Hall is located at the Damkar Monastery, which was initially built in about 1190 (the Song Dynasty) and has been used for local religious events and daily chanting since

Table 1. Reading Programs in Yushu Library

Reading Area	Number of seats	Daylight Source	Can daylight achieve 300 lx standard?
Atrium centre	24	atrium clerestory	No
Around atrium	72	atrium clerestory	No
Wall niche	76	side windows	Yes

then. The Main Chanting Hall and Yushu Library have similar visual tasks and daylight path. Site visit, measurement, interview, and simulation were performed to evaluate lighting of the Damkar Main Chanting Hall.

3. METHODOLOGY: THE BRIDGE FROM RESEARCH TO DESIGN PRACTICE

The project goal is recreating the traditional lighting in the new library via evaluating the lighting in both the traditional chanting hall and the new library. The methodology has been developed for general instances, in which local traditional context and elements are valued by both users and designers of the new buildings. The methodology layout is:

- a) Quantify the local traditional daylighting through simulation and field measurement;
- b) Transfer the traditional daylighting into the new building and fulfil the light level requirement in a modern library;
- c) Evaluate the design environment in the library through simulations on both daylight and electrical light, and adjust the furniture layout, interior material, and fixture control schedule to achieve the designed effect and reduce energy consumption.

The methodology guides research steps and design actions in order to apply research discoveries

in design practice. Fig. 2 maps the integration of research and lighting design.

4. LIGHTING RESEARCH FOR MAIN CHANTING HALL

4.1. Objects of Study

Yushu Library has an atrium with four floors, but by the current lighting standards, daylight only cannot provide enough illuminance for the ground floor reading area. Electrical lighting is needed as a supplement to daylight during open hours. The object of research is the atrium space (Fig. 3) (Table 2).

The models of the Main Chanting Hall and Yushu Library were built in Rhinoceros based on building measurements and drawings and calibrated with field measurements.

4.2. Field Measurement and User Interview

Field measurements taken in the Main Chanting Hall included Daylight Factor (DF), material reflectance and transparency, and a close observation of user behaviour. DF was measured for further calibration of model simulation result, since the digital model was simplified by excluding decoration and structure details. Material reflectance was measured by spectrophotometer, which provided material parameters in the simulation.

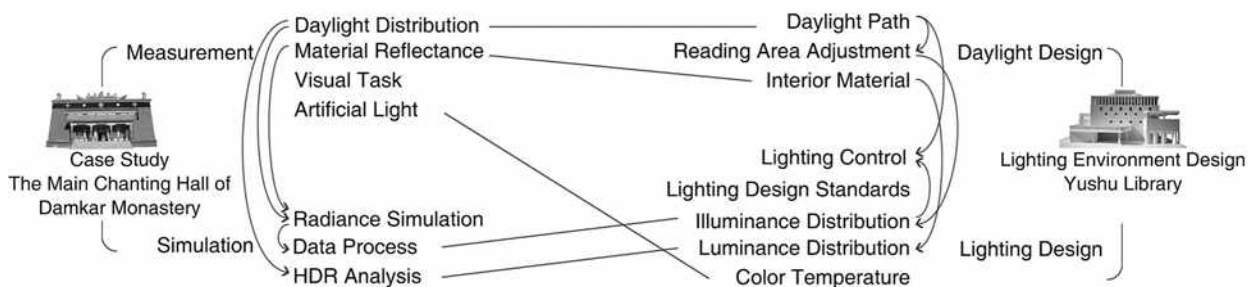


Fig. 2. Methodology map of research-based design

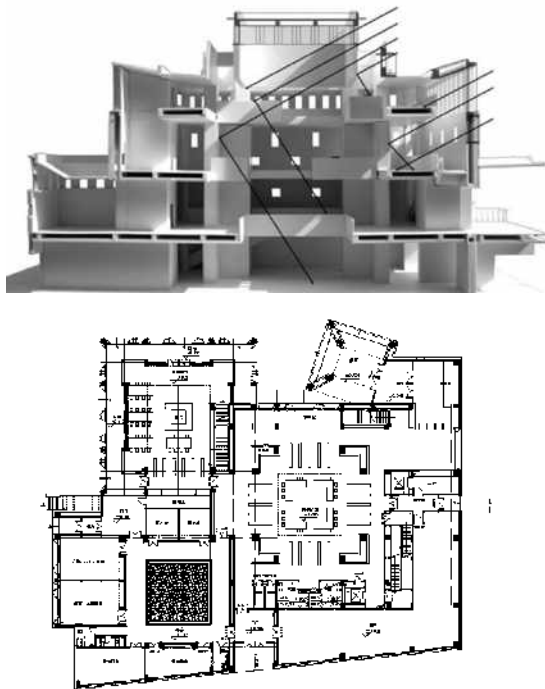


Fig. 3. Yushu Library section, first floor plan, and daylight path

The average DF in the Main Chanting Hall is 0.22 %, and the standard-required minimum DF for library reading rooms is 2 % [5]. However, the monks use the centre of the atrium for chanting, where the daylight condition is the best with direct sunlight. The chanting time is when direct sunlight reaches the centre of the atrium. The illuminance of the reading area could achieve 200 lx at noon on a sunny day. When it gets dark in the afternoon, the main tasks are cleaning and maintenance. Fig. 4 shows the daylighting difference between



Fig. 5. Chanting material and typical chanting position in the Main Chanting Hall



Fig. 4. 12:00 pm (a) and 4:00 pm (b) at the Main Chanting Hall (December 8, 2012)

chanting time and maintenance time in a day. It also revealed the limitation of DF as an indicator of daylight availability.

Observation and interview of users (15 monks as daily users) provided first-hand information on how users react to lighting. All interviewees said the daylight was enough for chanting. While chanting, monks sit on seats that are 400 mm tall. All words are in Tibetan Uchen script in about size 11, and the reflectance of the paper is 0.91 (Fig. 5).

4.3. Daylight Autonomy and Illuminance Pattern

Diva for Rhino was used in the simulation for annual daylight evaluation in the Main Chanting Hall. The calculation of annual daylight autonomy (DA) was based on the local weather data from EnergyPlus weather file of Yushu, Qinghai [9]. Annual daylight autonomy takes the local climate into consideration, which is critical to this project: the local climate provides generous sunlight almost all the year, which shaped the unique architectural space and its lighting. For DA (50 lx), only the centre of the atrium, where monks sit and chant, has a higher daylight autonomy of 50 %. The perimeter along the wall is the dark area with only 10 % daylight autonomy, but it is only used for circulation.

In Fig. 6, annual daylight autonomy revealed that the large cloth decorations in the Main Chanting Hall played an important role in reflecting direct sunlight from the south-facing clerestory, to provide an even and bright reading area in the centre.

For quantifying daylight information, the chanting hours on typical days were taken as study hours: 9 am to 12 pm on March 20–22, June 20–22,

Table 2. Comparison of Main Chanting Hall and Yushu Library on Building Definition

Building	Main Chanting Hall	Yushu Library
Location	33°0' N97°8' E	33°0' N97°0' E
Year of built	1190, 1981 (rebuilt)	2012
Floor	4	4
Ground floor atrium area	633 m ²	784 m ²
Ground floor seats	24	24
Users	Monks and local residents	Monks and local residents

September 20–22, and December 20–22. The accumulated illuminance of each point during the study hours was from the data file generated by the annual daylight autonomy simulation. The accumulated illuminance of chanting hours on those sample days was used to extract daylight illuminance pattern. On the horizontal surface, the average accumulated illuminance of each area was the average of 9 test points in the Reading area (R) and 30 test points in the Circulation area (C). Accumulated daylight illuminance ratio of R: C is from 8.5:1 to 10:1.

On the vertical surface the average accumulated illuminance of each area was the average of 4 test points in the Top area (T), 4 test points in the Clerestory area (C), and 4 test points of the Bottom area (B). The Clerestory area was affected by direct sunlight, so the ratio was not constant. Accumulated daylight illuminance ratio of T: B is from 4:1 to 6:1.

These illuminance ratios of the Main Chanting Hall were used as references for the illuminance ratio of the Yushu Library.

4.4. HDR Analysis and Luminance Pattern

HDR (High Dynamic Range) analysis was applied in the luminance analysis in the Main Chanting Hall. In HDR photos of the Main Chanting Hall clerestory, the ceilings and cloth decorations had

the highest luminance, while the wall of the circulation area has the lowest luminance. In HDR photos of the Main Chanting Hall atrium, the Buddha statue has the highest luminance level. Monks that sit nearer to the Buddha statue have higher luminance on their faces. The ratio of luminance on the main surfaces is shown in Fig. 7. These luminance patterns were used as luminance reference for lighting design of Yushu Library.

5. LIGHTING DESIGN PROCESS

Architects rely on space geometry and furniture finishing to express local context. Lighting designers rely on the combination of daylight and electrical lighting to achieve the same goal. The traditional Tibetan lighting of the Main Chanting Hall is the basis for lighting design of Yushu Library (Table 3).

After quantifying the daylight illuminance and luminance pattern in the Main Chanting Hall, the lighting design process began with a concept and went through inter-disciplinary coordination, fixture selection, and installation. It was finished with on-site adjustment to demonstrate the found patterns while fulfilling the lighting design code requirements. After designing based on the illuminance and luminance pattern from Main Chanting Hall, Dialux was used for testing illuminance and lumi-

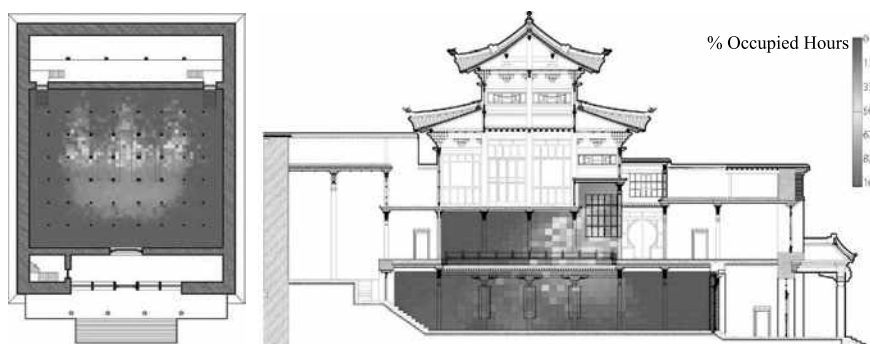


Fig. 6. Daylight distribution on horizontal surface (DA 50 lx) and vertical surface (DA 100 lx)

Table 3. The Relationship between Daylight and Electrical Light for Both the Main Chanting Hall and Yushu Library

	Daylight		Electrical Light	
	Research on the Main Chanting Hall	Design for Yushu Library	Research on the Main Chanting Hall	Design for Yushu Library
Space Geometry and Daylight Path	High atrium with clerestory, small side windows	High atrium with clerestory, small side windows	N/A	N/A
Reading Area and Daylight	Sitting area in the center of the atrium (best daylight autonomy area)	Revise the seating area based on daylight autonomy simulation	Monks use candle or LED lamp with battery pack at night.	Supplement of electrical task light at seat
Work Plane Illuminance	Measured 200 lx during chanting time (average of illuminance at 24 chanting seats)	Standard 300 lx	Candles are lit along the statues, not intended for reading	Supplement of electrical light to reach to the illuminance level required by the standards
Reading Time	9:00 am – 5:00 pm	9 am – 12 pm in summer; 9:30 am – 12:30 pm in winter	N/A	N/A
Visual elements (luminance ratio)	Clerestory, ceiling, and floor illuminance ratio 40:2:1	Revised wall material to adjust the reflectance	N/A	Enhanced clerestory illuminance

nance level of the library with the lighting design plan and selected lighting fixtures to test and adjust the lighting design.

Based on the result of electrical lighting simulation, the illuminance ratio of the reading area and the circulation area in the Yushu Library was 6:1. During daytime with daylight from the atrium, this ratio would increase, closer to the ratio in the Main Chanting Hall (from 8.5:1 to 10:1). Both the reading and the corridor area illuminance fulfilled the illumination requirements (300 lx and 100 lx). For vertical surfaces, the illuminance ratio of the ceiling and floor areas was 4:1, which was close to the ratio in the Main Chanting Hall (from 4:1 to 6:1). The simulated luminance condition in Yushu Library has a similar pattern with the HDR luminance condition in the Main Chanting Hall.

Yushu Library was opened to local residents and monks in December 2013. Fig. 8 shows the daylighting in the Yushu Library.

6. CONCLUSION AND DISCUSSION

The reproduction of traditional lighting in a new building is achieved based on close collaboration with architects through creating similar light-

ing distributions, revising the daylight path, adjusting key surface reflectance, and changing reading area locations. However, the eyes of the users are used to new visual tasks, some of which did not exist when the traditional buildings were built, such as reading on computer screens. Further discussion on the suitability of this methodology from traditional lighting to modern lighting design is needed for these new visual functions.

In the early phase of design, lighting designer, architect, and the client had a discussion over the possible glare control and daylight harvesting. However, first of all, the budget for this project is limited due to the limited total funding for all reconstruction projects in Yushu after the catastrophic earthquake. Electrical shades or dimmable lighting fixture controlled by daylight sensors are out of question due to the low budget. Second, local users are in fond of sunlight. During interviews with local monks at the Damka Monastery, we found the direct sunlight went through the clerestory and shine upon the reading area in chanting hours. Most users found direct sunlight provided the connection between interior artificial environment and exterior natural environment. Third, this library has 172 seats available around the atrium and facade with

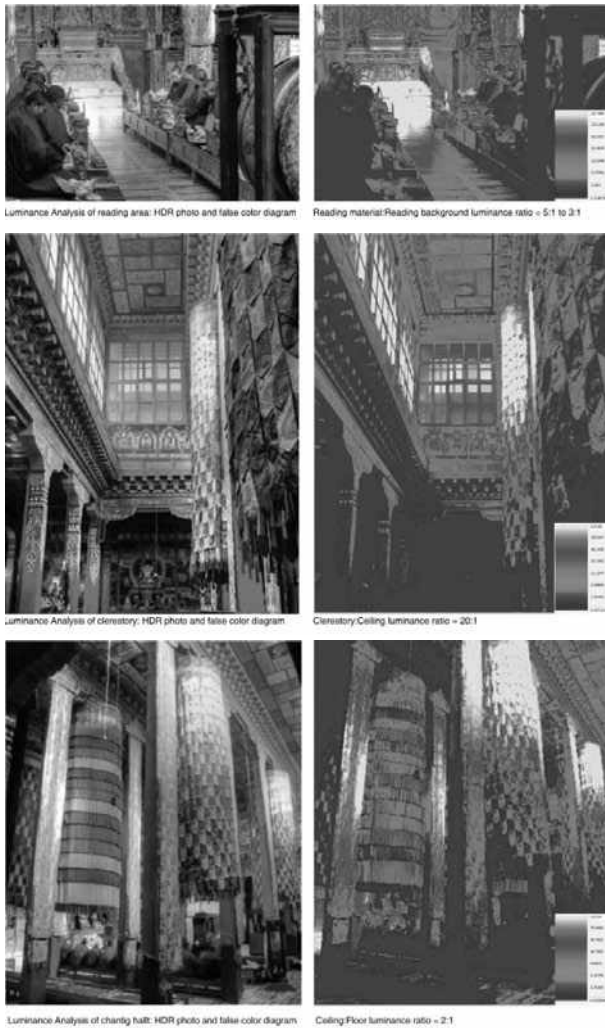


Fig. 7. HDR analysis on luminance in the Main Chanting Hall

daylight access. Compared with the number of daily users there are always seats available if one area is subject to severe glare.

The quantitative study of traditional lighting provides a solid base of design with comparable and quantified criteria such as illuminance and luminance. A multi-tool based methodology was developed and tested to achieve the best performance of lighting in the new library. Daylight only, in this library, cannot fulfil the modern requirement for reading. Introducing electrical light can provide much flexible time and location for the reading tasks. HDR analysis is close to what people see, but it was an instantaneous record: typical conditions have to be chosen carefully to represent the actual condition in a year. However, introducing electrical light will also raise the concern on sacrificing traditional lighting. Careless accommodation of daylight and dependence on artificial light could lead to the



Fig. 8. Photos of Yushu Library (Credit: Rui Zeng)

loss of the traditional environment in a building. It was also the trigger of the research and practice on this methodology. All front of house electrical lighting fixtures are with >80 CRI LED or fluorescent source. Atrium and reading areas are utilizing 3000K colour temperature to provide the warm white light. At the perimeter of clerestory, 4000K colour temperature light is used to wash the vertical surface below clerestory, to form the contrast between reading area and clerestory, and to echo the cold white tune from the skylight.

Back in 2012 when the daylight simulation for this project was conducted, Daylight Factor was the only parameter for daylight evaluation in standards for China, while further evaluation parameters were not included in standards or recommendations in other countries. However, Daylight Factor is not utilized in prevailing standards now (2018). IESNA has published a standard on approved method [9]. Some established and much-used methods of certifying the sustainability of buildings, such as LEED (Leadership in Energy and Environmental Design), makes recommendations for daylight. According to [10], it is required to achieve a Spatial Daylight Autonomy (sDA 300 lx, 50 %) in 55 % (2 pts) or 75 % (3 pts) with Annual Sunlight Exposure (ASE1000 lx, 250 h) below 10 % in all regularly occupied floor areas to earn the Daylight Credit.

7. ACKNOWLEDGEMENTS

Thanks to the architects from Cui Kai Studio, China Architecture Design & Research Group, who provided architectural insight and expertise that greatly assisted the research. Thanks to Junmei Zhaxi from THUPDI Tibetan cultural heritage preservation and research studio for assistance with the drawings of Damkar Main Chanting Hall and local contacts. We would also like to show our gratitude to the monks and nuns in Damkar Monastery for sharing their user experience and wisdom with us during the course of this research.

REFERENCES

1. Yushu Post-earthquake Recovery and Reconstruction Master Plan // Yushu Post-earthquake Recovery and Reconstruction Group, 2010.
2. He Y. and Lin Y. Analysis of China's Daylighting Climate with P-G-D Diagram // Journal of Civil, Architectural & Environmental Engineering, 2010, Vol. 32, #1, pp. 107–110.
3. Measurement of Sunshine Duration, Guide to Meteorological Instruments and Methods of Observation // World Meteorological Organization, 2008.
4. Xu Z. Introduction to Tibetan Traditional Architecture // China Architecture and Building Press, Beijing, 2004.
5. Standard for Daylighting Design of Buildings GB50033–2013 // National standard of the people's republic of China, 2013, 40 p.
6. Standard for Lighting Design of Buildings GB50034–2013 // National standard of the people's republic of China, 2013, 58 p.
7. DiLaura D., Houser K.W., Mistrick R.G., and Steffy G.R. The IESNA Lighting Handbook. Reference & application, 10th edition // Illuminating Engineering Society, 2011, 1328 p.
8. LG10 Lighting Guide 10: Daylighting and window design // CIBSE, 1999.
9. IES LM-83–12 IES Spatial Daylight Autonomy (sDA) and Annual Sunlight Exposure (ASE) // Illuminating Engineering Society, 2013, 14 p.
10. LEED v4, 2013. URL: <https://new.usgbc.org/leed-v41>.



Xiufang Zhao,

LC, LEED AP. Senior Lighting Designer, Brandston Partnership Inc.



Xin Zhang,

Ph.D., IALD. Associate Professor, Department of Architecture and Technology, School of Architecture, Tsinghua University, Beijing, China



Kai Cui,

Academician of China Engineering Academy, Chief Architect, China Architecture Design & Research Group, Beijing, China

Victor V. Belyaev, Donatien Nessemou, and Andrei A. Belyaev
Application of Display Technologies for Lighting

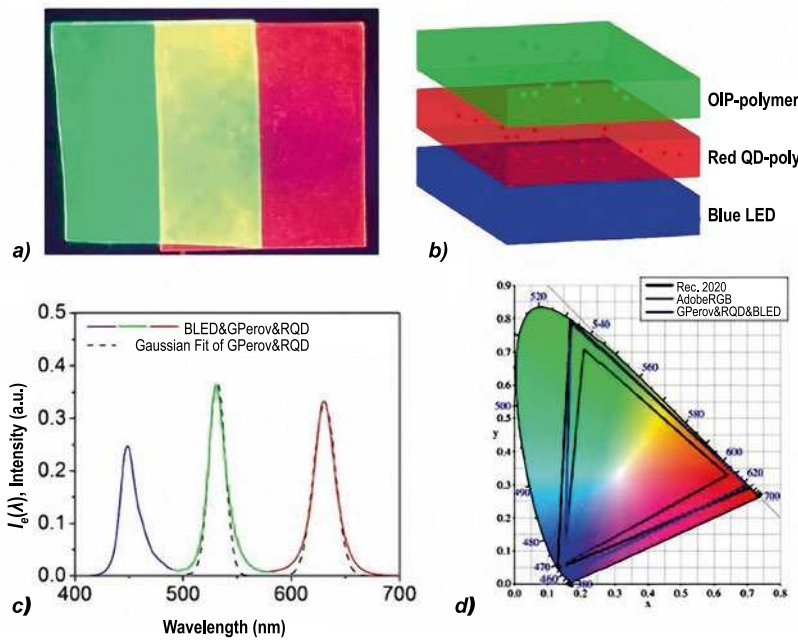


Fig. 4. Application of special composite film as a dimmer for backlighting of a wide colour spectrum display: *a* – composite film with red quantum dots and polystyrol as well as green $MAPbBr_3$ and polystyrol under impact of UV radiation; *b* – the diagram of white light generation by means of above mentioned films integration with a blue LED; *c* – white radiation spectrum of a system with above mentioned films (green and red) used as a radiation converter of blue LED. The dashed lines are Gaussian approximations of the spectrum; *d* – the chromaticity diagrams of the white LED system (blue line), of the system with *Adobe RGB* spectrum (grey line) and of the system complying with the CIE recommendation for 2020 (black line) as compared with the CIE chromaticity diagram for 1931

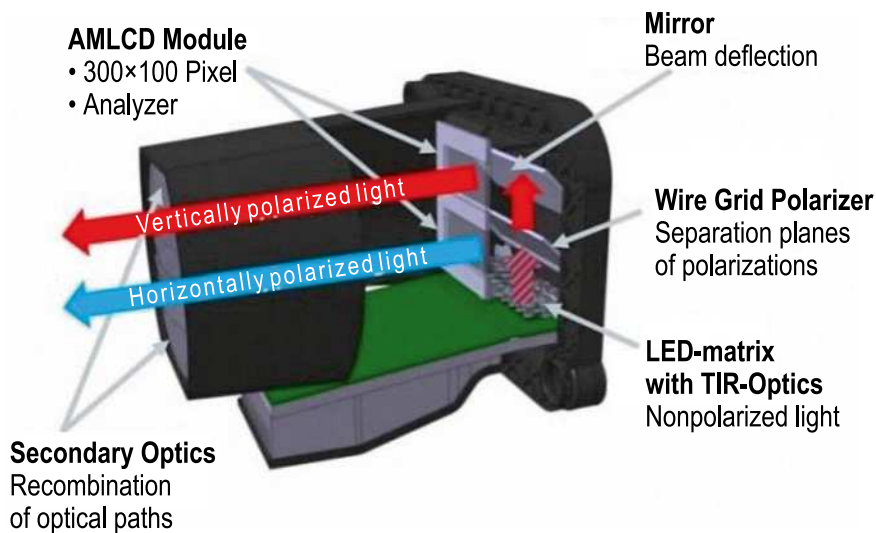


Fig. 5. Diagram of the structure of a directional luminaire with a LC light source

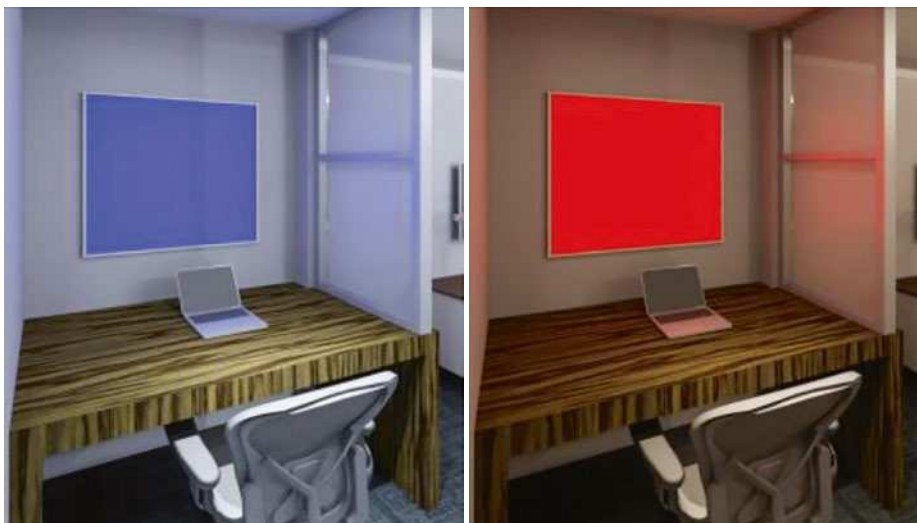


Fig. 7. Example of application of a self-glowing display panel for creation of efficient (blue) and inefficient (red) light (in terms of circadian rhythms) depending on the time period

Maria M. Ilyevskaya

Interrelation of Architectural Concepts and Principles of Artificial Lighting in the Moscow Concert Hall Zaryadye



Fig. 1. Zaryadye Concert Hall in Moscow, view of the entrance area (photo: A. Naroditsky)



Fig. 5. Foyer lighting: entrance area, light graphics against the background of floodlighting (photo: A. Naroditsky)

**Interrelation of Architectural Concepts and Principles of Artificial Lighting
in the Moscow Concert Hall Zaryadye**



Fig. 6. Exposition of the concept idea of a layered structure in the main hall by virtue of cornice lighting: a – general view (photo: A. Naroditsky); b – “rhythmic rows” of the acoustic panel (photo: I. Ivanov)

The Reconstruction Project of Illumination Devices at the Krasnoselskaya Station of the Moscow Metro



Fig. 3. Appearance of the connecting passage stairway at Krasnoselskaya station: (a) 1935, (b) 2018

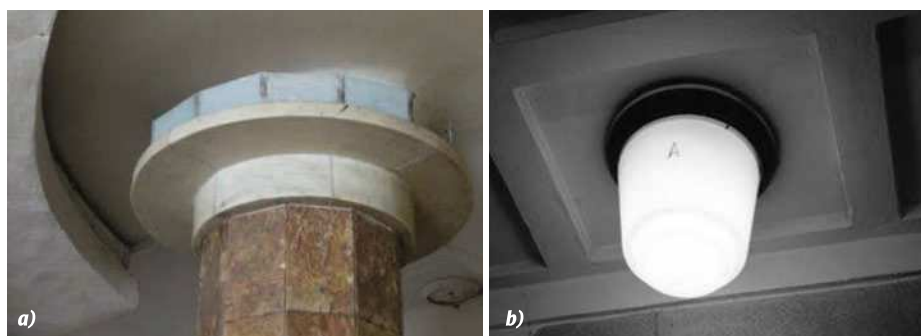


Fig. 4. First LDs of Krasnoselskaya station that survived to date: (a) opal plates used for lighting decoration of the stair flight, (b) luminaries of the connecting passage

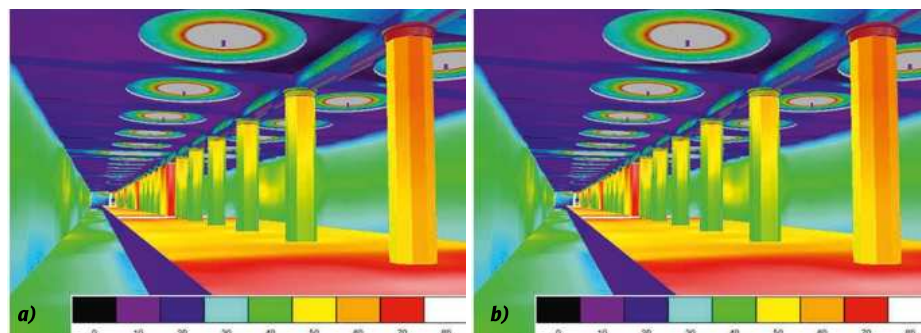


Fig. 5. Results of lighting calculation for the LI in 1935: (a) platform hall, (b) connecting passage

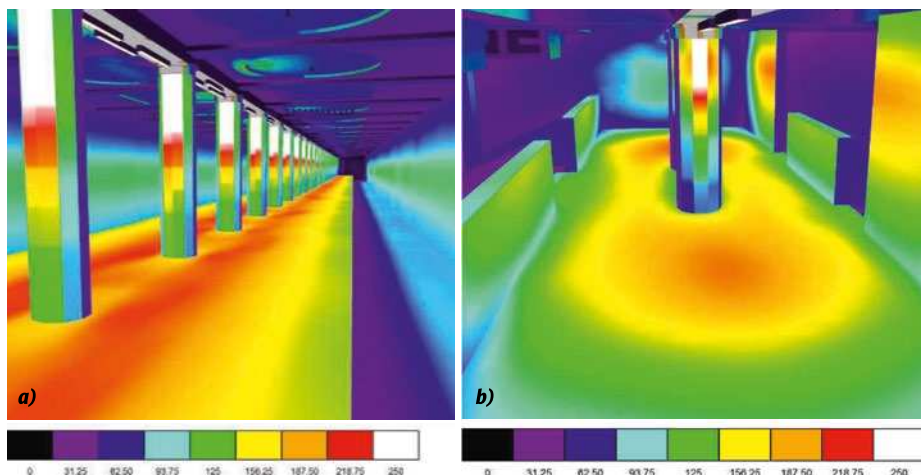


Fig. 6. Results of lighting calculation for the LI in 2018: (a) platform hall, (b) connecting passage

THE RECONSTRUCTION PROJECT OF LIGHTING DEVICES AT THE KRASNOSELSKAYA STATION OF THE MOSCOW METRO

Ksenia I. Nechaeva

ILEC “BL GROUP” LLC, Moscow, Russia
E-mail: ksunechaeva@yandex.ru

ABSTRACT

The current state of the Moscow Metro station of the first priority that became operational in 1935 does not allow it to be called a cultural heritage site. This is due to the fact that lighting modernisation carried out by the Moscow Metro was based on fluorescent lamps. Such lamps are more energy efficient compared to incandescent lamps, which were used in original lighting devices specified in the Station Lighting Project developed by architects and designers. However, they significantly changed the station appearance, transforming the originally designed station with entire well-visible architectural tectonics¹ from the standpoint of lighting into a simple, flat, unremarkable, and little loaded station of the Moscow Metro.

This paper describes a method of lighting reconstruction at Krasnoselskaya station by means

of original lighting devices that meet modern standards and requirements for cultural heritage sites. The historical analysis on the development of the station lighting environment was conducted during its operation in order to understand what kind of station was conceived by its architects, what changes occurred with its lighting over time, and how it influenced the station appearance and safety of passenger transportation.

Keywords: Moscow Metro lighting, lighting reconstruction, lighting device, illuminance, unified glare rating, lighting installation, dome lamp

1. INTRODUCTION

Lighting modernisation at spaces of the first-priority Moscow Metro stations representing cultural heritage sites is a very special task. In this case, the main problem is that the station appearance should correspond to the original appearance in order to preserve the status of a cultural heritage site (Fig. 1); however, this is rarely seen today: modernisation aimed at improving energy efficiency of lighting installations (LIs) often significantly

¹ The tectonics is a constructional-spatial pattern, a structure, a building installation (a platform hall in this case), and a real relation between a stress-bearing structural unit and a bearing carrier.

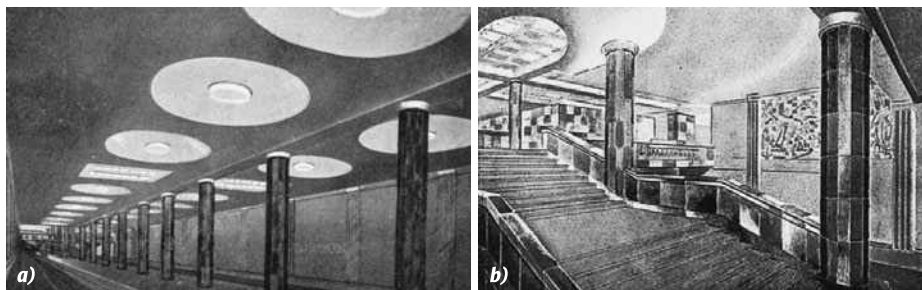


Fig. 1. Project draft of Krasnoselskaya station: (a) platform, (b) stair flight of the connecting passage



Fig. 2. Appearance of the platform at Krasnoselskaya station: (a) 1935, (b) 1950, (c) 1970, (d) 2018

changed the station appearance which was not for the better (Fig. 2). Meanwhile, lighting modernisation has led to the fact that existing LIs do not meet any modern lighting regulations [1], which is absolutely unacceptable. After all, the Moscow Metro today is a space, where thousands of people move every day, and ensuring their safety is the primary task for lighting reconstruction.

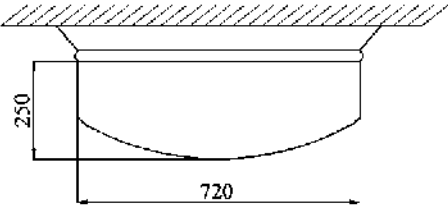
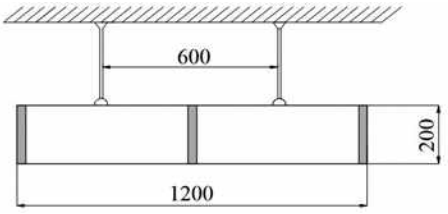
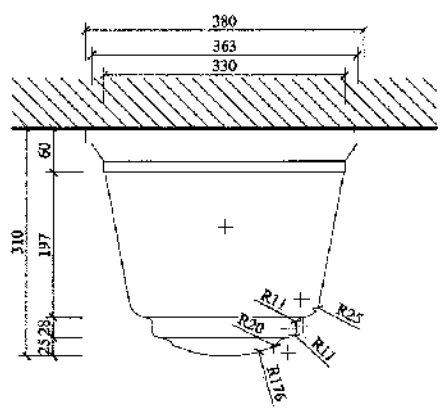
A similar situation happened with one of the first stations of the Moscow Metro – Krasnoselskaya. Lighting modernisation of Krasnoselskaya station has led to the fact that the current state of the station does not allow it to be called a cultural heritage site. In order to return the station to this status, a complete lighting reconstruction is required that is impossible without answering the following questions: what kind of station was conceived by its architects and designers? What lighting devices (LDs) and light sources were used? What illuminance values were its designers looked at? How did the station lighting environment change during the whole operation period? The archival documents of 1935 helped to give answers to these and many other questions [2].

Krasnoselskaya station was opened on 15 May 1935 with 12 more first-priority Moscow Metro stations. According to architects from Workshop 2 of the *People's Commissariat of Heavy Industry* – B.S. Vilenskiy, V.A. Yershov, V.F. Skarzhinskiy – and according to the artist Ya. Romas, the station should look as shown in Fig. 1 [2]. The archi-

itects sought to visually highlight round and square caissons located on the ceiling of the station hall by setting the tectonics for a long and simple room from the standpoint of the architectural design. The specific emphasis was placed on the connecting passage stairway: the ceiling above was decorated with a ring-shaped hinged structure as if floating in the air due to an original lighting solution. The pictures of 1935 (Fig. 2a) show that architects could not implement their ideas in the station design; although its appearance was close to the original project, it still did not fully correspond to the project (Fig. 1). Today we observe even more differences from the design drafts in the station appearance (Fig. 2d). It is difficult to recognize the old station in the pictures of 2018 despite the fact that all constructive elements of the station (caissons, limestone-trimmed columns, wall tiles, passing zone ring-shaped ceiling) remained in almost perfect condition (Figs. 2, 3). It is obvious that all significant changes in the station appearance are associated with modernisation of illumination installations.

It is known that (60–150) W incandescent lamps (ILs) were widely used as a light source in typical LDs of the first Moscow Metro stations [2]. Two types of LDs were used to illuminate the platform hall at Krasnoselskaya station; their main specifications are presented in Table 1. It was decided to replace round dome lamps with hanging balls in the 1950s; IL LDs were replaced with fluorescent lamp (FL) LDs later in the 1970s. As a result, the plat-

Table 1. Main Specification of Historical Luminaries of 1935

No.	Luminaire name	Luminaire draft	IL quantity and power (pieces × W)	Efficiency (%)
1	Dome lamp $D = 720$ mm		6 × 100 6 × 150	55
2	Hanging cylinder		6 × 60	67
3	Passing zone luminaire		1 × 150	65

form hall has changed out of all recognition: FL luminaries were installed in a line between columns that significantly increased illuminance on the floor of the platform hall but completely distorted its appearance.

According to the original project (Fig. 3), ILs were installed along the contour line of the ring-shaped awning behind the opal plates in the connecting passage; column capitals in the connecting passage were decorated in the same way (Fig. 4a). This design solution allowed creating the effect of light coming out of nowhere and the feeling that the ceiling and columns were floating in the air; however, such a decision was refused due to energy savings after lighting modernisation in the 1970s.

Only 2 luminaries that illuminate the passing zone survived from all first LDs described above; they operate as emergency lighting at the modern station (Fig. 4b); other survivors are several opal plates installed in the upper part of a column (Fig. 4a). All other LDs were lost.

2. METHODS

Krasnoselskaya station was modelled in *Dialux 4.13* based on these data [3]; lighting specifications were calculated for the LI of 1935; all results are shown in Fig. 5. The luminous intensity curve (LIC) of an authentic 60 W IL LD was used to calculate illuminance values [4]. The calculation showed that horizontal illuminance values on the floor surface in the platform hall and in the connecting passage fully correspond to the standards given in Table 2 [2].

In addition to values presented in Table 2, the unified glare rating (UGR) (Table 3) was determined at 4 key points with the most uncomfortable visual conditions, the values of which indicate that LD used in 1935 brought some visual discomfort to passengers and drivers [2]. It should also be noted that the total power consumption of the LI in 1935 was almost 46 kW.

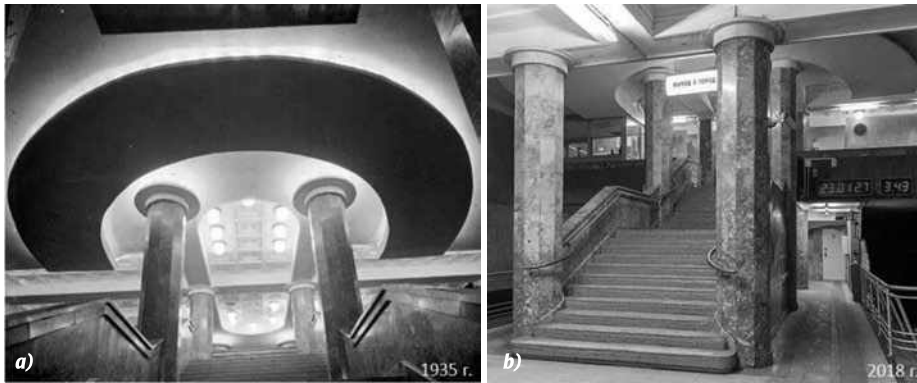


Fig. 3. Appearance of the connecting passage stairway at Krasnoselskaya station: (a) 1935, (b) 2018

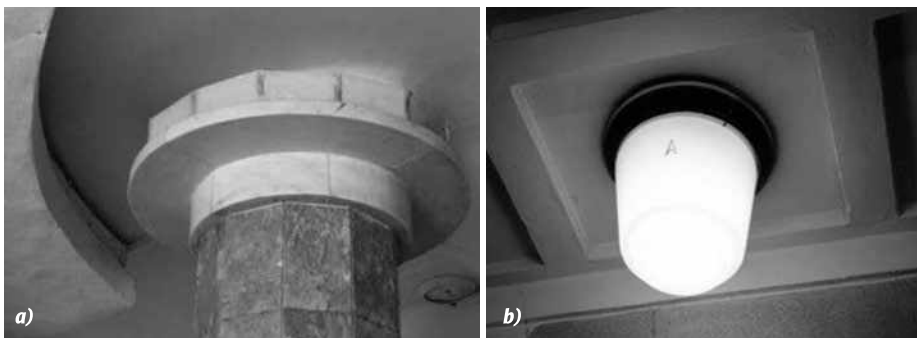


Fig. 4. First LDs of Krasnoselskaya station that survived to date: (a) opal plates used for lighting decoration of the stair flight, (b) luminaries of the connecting passage

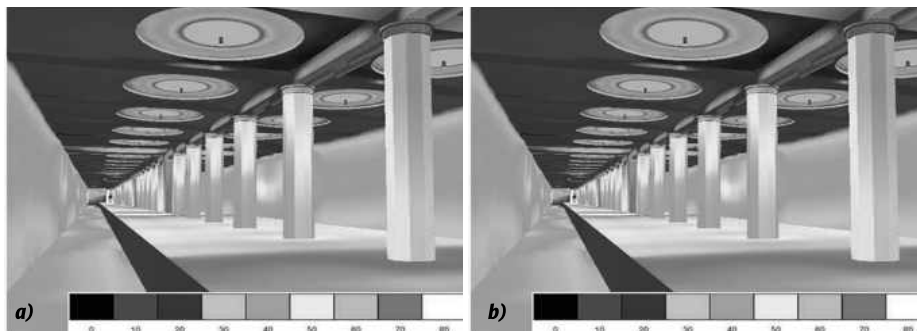


Fig. 5. Results of lighting calculation for the LI in 1935: (a) platform hall, (b) connecting passage

The same calculation was performed for the current LI at Krasnoselskaya Station, where *Osram* 58 W FL luminaries, which are installed by 3 pieces in a line, were used with the correlated colour temperature of 2 700 and 4 000 K, the length of 1 500 mm, and the luminous flux of 5 000 lm. The luminous intensity curve given on the company’s website was used to calculate illuminance values [5].

The calculation and measurement results show that the illuminance regulations are met only in the centre of the platform under luminaries. The illuminance rate falls down to 120 lx with more distance from the centre (Fig. 6), which does not comply with the current industry standards of metro lighting (Table 2) [6]. The illuminance calculation and measurements in the connecting passage showed that the illuminance regulations were met in this part of the station. Meanwhile, the values of the

unified glare rating given in Table 3 do not exceed the regulations by more than 20 % and therefore meet the standard norms. The total power consumption of LDs of the current LI is 11 330 W, which indicates that the efficiency of the new LI is almost 4 times higher than the original illumination installation efficiency.

The given analysis shows that, in the case of reconstruction of the LI at Krasnoselskaya station, the following difficult problems should be resolved:

- Safe illuminance levels in all station zones;
- Elimination of discomfort created by LDs according to the current industry regulations;
- Identification of main architectural elements of the station platform hall (round and square caissons);
- Return of lost lighting decoration of the stairway in the passing zone;

Table 2. Specified and Calculated Lighting Values in Different Zones at Krasnoselskaya Station

Zone	Platform halls			Connecting passages between stations			Escalator combs and stair flights		
	1935 II	2018 II	Proposed II	1935 II	2018 II	Proposed II	1935 II	2018 II	Proposed II
Rate-setting surface	Floor surface			Floor surface			Step level		
Specified value of horizontal illuminance (lx)	50	200		60	100		–	100	
Calculated value of horizontal illuminance (lx)	60	190	200	60	125	100	37	90	120

Table 3. Specified and Calculated UGR Values at 4 points under the Most Uncomfortable Vision Conditions for Passengers and Drivers

Position in space	Specified UGR value	Calculated UGR value		
		1935 II	2018 II	New II
View field of a passenger standing on the floor of the platform hall	20 (excess is allowed by 20 %, i.e. at most 24)	26	22	23
View field of a passenger standing on the stairs of the platform hall		26	23	22
View field of a passenger standing in the connecting passage		22	22	22
View field of a driver entering the station		26	24	22

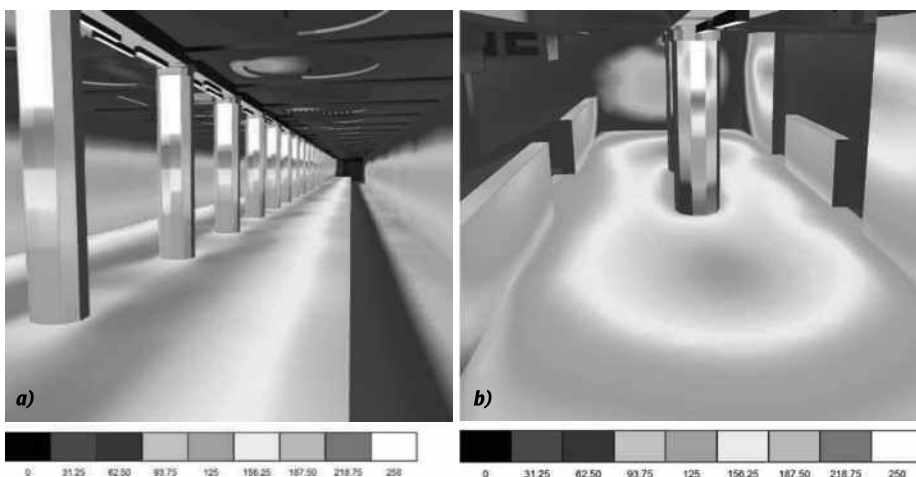


Fig. 6. Results of lighting calculation for the LI in 2018: (a) platform hall, (b) connecting passage

- Ensuring visual compliance of new LDs with lost luminaries as per the project of the 1930s.

Since illuminance of the platform hall needs to be increased by almost 4 times in comparison with the illumination installation of 1935, it is

obvious that a simple increase in the luminous flux of the light source would lead to a higher luminance of LDs and to a higher unified glare rating. Therefore, the solution of the above tasks would require significant structural changes in LDs.

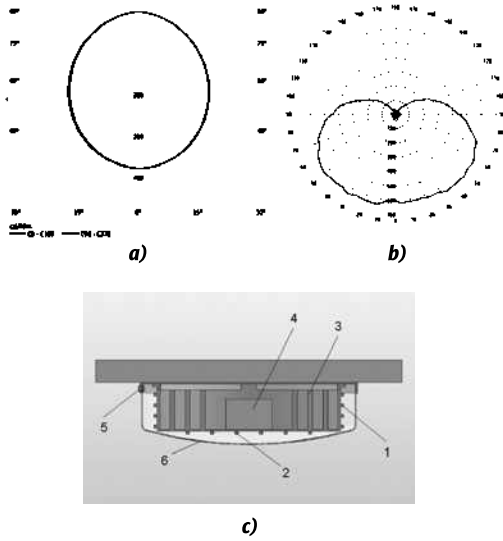


Fig. 7. Redistribution of the luminous flux on the ceiling of the station hall: (a) historical luminaire LIC, (b) proposed luminaire LIC, (c) dome lamp diagram (profile drawing by vertical projection plane) where 1 – Cree XP-L LED, 2 – Cree JK3030 3-V LED, 3 – heat radiator, 4 – LED control device, 5 – hydrophobic filter, 6 – opal diffuser

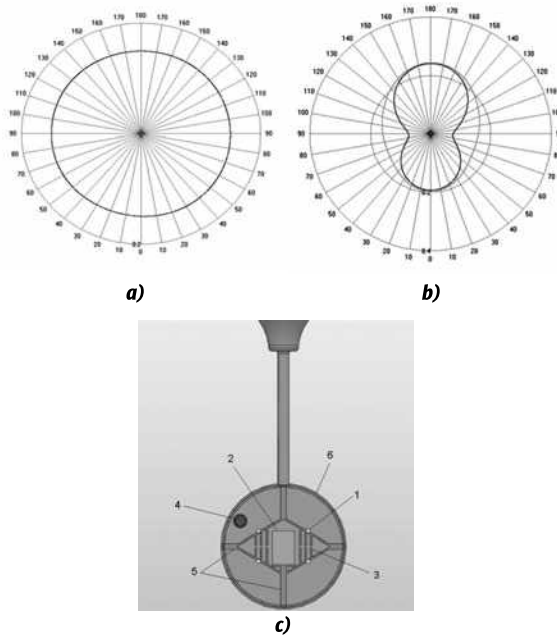


Fig. 8. Redistribution of the luminous flux for a cylindrical luminaire in the station hall: (a) historical luminaire LIC, (b) proposed luminaire LIC, (c) luminaire diagram (profile drawing by vertical projection plane) where 1 – Cree JK3030 3-V LED, 2 – LED control device, 3 – heat radiator, 4 – hydrophobic filter, 5 – holder block, 6 – opal diffuser

The analysis of round dome lamps located along the platform (Fig. 2a) showed that it is necessary to redistribute the flux from the light source to reduce the glare of these dome lamps. A little part of

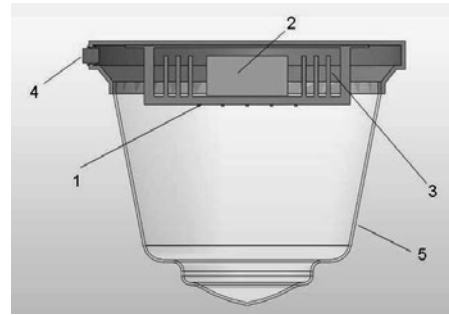


Fig. 9. Luminaire diagram for lighting of the connecting passage (profile drawing by vertical projection plane) where 1 – Cree JK3030 3-V LED, 2 – LED control device, 3 – heat radiator, 4 – hydrophobic filter, 5 – opal diffuser

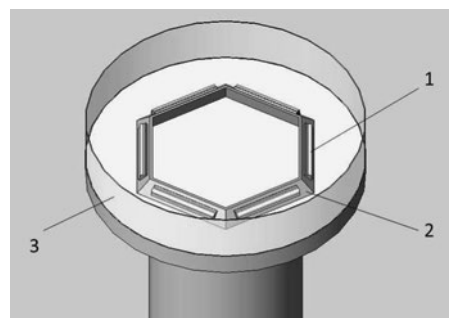


Fig. 10. Lighting decoration elements of column capitals: 1 – Lucendi LED lamps, 2 – brackets, 3 – opal diffuser

the flux should fall down, and a greater part of the flux should go to the upper hemisphere illuminating the platform floor with reflected light. For this purpose, a cylindrical LED module is installed in a dome lamp; the significant part of the luminous flux (90 %) comes from the Cree XP-L LED located on the cylinder forming surface; the remaining 10 % are emitted by the Cree JK3030 3-V LED mounted on the base of the cylindrical module (Fig. 7c). In this case, the surface and cavity of the cylinder serve as a radiator for convective transfer of excess heat generated by the LED; the total surface area of the radiator is 4355 cm². Besides, there is a room in the cylinder cavity for a control device installation. This solution allows to redistribute the flux in the necessary ratio in order to resolve the problem as shown in Fig. 7.

It is necessary to increase the luminous flux in the upper hemisphere and to reduce the luminous flux in the lower hemisphere for square caissons highlighting and for reduction of UGR in the case of cylindrical hanging lamps; it is easily achieved with the use of the Cree JK3030 3-V LED lines with different levels of current loads. To achieve this goal, the aluminium diamond-shaped construction is inserted into the lamp shell, which sides and cav-



Fig. 11. Visualisation of Krasnoselskaya station with the proposed LI: (a) platform hall, (b) stair flight of the connecting passage

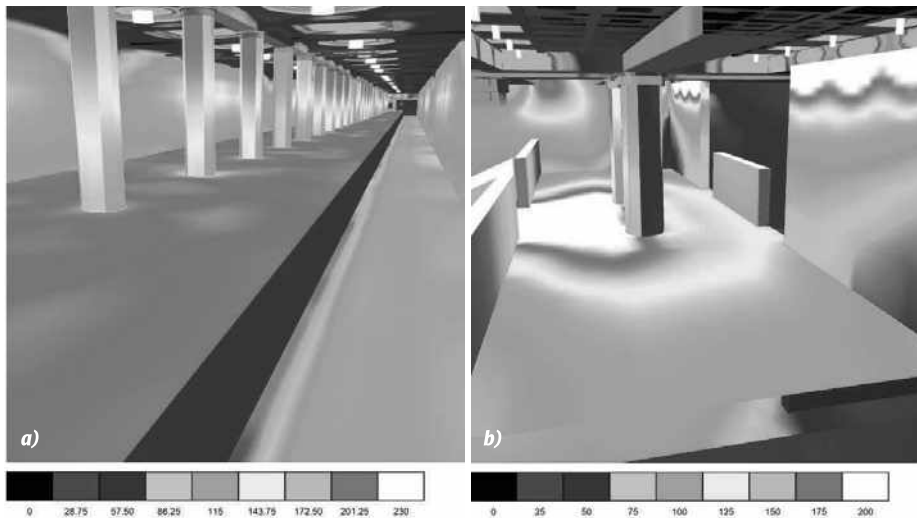


Fig. 12. Results of lighting calculation with the new LI: (a) platform hall, (b) stair flight of the connecting passage

ity are similar to surfaces of the cylindrical module described above; they represent a heat radiator with a surface area of 1220 cm². In addition, a LED power regulator is mounted in the inner cavity of the structure (Fig. 8).

It is assumed that the connecting passage would be illuminated with LDs that look like modern emergency lights (Fig. 4b); however, the *Cree JK3030 3-V* LED module will be used as a light source instead of 150 W IL (Fig. 9). As in the case

of luminaries described above, the control device and a heat radiator of 812 cm² will be placed at the top of the luminaire (Fig. 9).

It is assumed to use the technique included in the original project by the engineers of the *Russian National Electronic Technical Institute* (Moscow, Russia) in 1935 in order to restore the lost lighting decoration of the stairway in the connecting passage. 6 *Lucendi* LED lamps of 281 mm [7] forming a hexagon will be installed instead of ILs in the projected LI at the top of the column behind the opal diffuser (Fig. 10).

3. RESULTS

The above LDs were modelled in *Solidworks* [8]; *IES* files and luminous intensity curves (Figs. 8b, 9b) were obtained using the *Photopia* plug-in [9]. According to the results of lighting calculation carried out with regard to the properties of the proposed devices and based on result visualisation, it can be concluded that the station appearance with such lighting reconstruction becomes the original idea of the architects (Fig. 11). The new LI allows not only to identify the main architectural elements

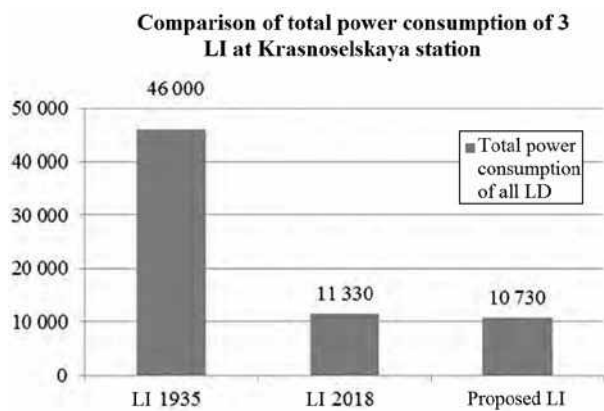


Fig. 13. Comparison diagram of total power consumption of 3 LI at Krasnoselskaya station

of the station, but fully meets modern standards for lighting and UGR (Table 3) (Fig. 12). Besides, the total power consumption of the proposed LI will be 10.7 kW, which is almost 0.6 kW lower than the power consumption of the existing LI (Fig. 13).

4. CONCLUSION

We should finally note that the lighting of many metro stations was modernised in the 1960s-1970s since the appearance of fluorescent lamps in the pursuit of efficiency. The first-priority Krasnoselskaya station is not the only one where modern lighting has radically changed its appearance. The appearance of powerful white LEDs radically changes the situation in the reconstruction of the LI of the Moscow Metro. Their relatively small size and high efficiency allow to solve a wide range of problems faced for restorers of cultural heritage; unification of their efforts with the efforts of lighting technicians allows us to expect that passengers will be able to see the first Moscow Metro stations as they were conceived by the architects and designers in the near future.

REFERENCES

1. Sanitarnye pravila ekspluatatsii metropolitenov. SP 2.5.1337-03 [Sanitary Regulations of Metro Operation. SP 2.5.1337-03] (as edited in Amendments No. 1 on 30 April 2010, No. 50).
2. Gorbachev N.V., Ratner, Ye.S. Osveshcheniye moskovskogo metro [Moscow Metro Lighting] // Svetotekhnika, 1935, No. 1, pp. 2-11.
3. <https://www.dial.de/de/dialux/>
4. Gutorov M.M. Osnovy svetotekhniki i istochniki sveta: Ucheb. posobiye dlya vuzov (2-e izd., dop. i pererab.) [Fundamentals of Lighting Engineering and Light Sources: Textbook for Universities (2nd ed., supplemented and revised)] // Energoatomizdat, Moscow, 1983.
5. <https://www.osram.com>
6. SP 32-105-2004. Metropoliteny. Svod pravil po proektirovaniyu i stroitelstvu [SP 32-105-2004. Metros. Specifications on Design and Construction]
7. <http://lucendi.ru/lynus>
8. <https://www.solidworks.com/>
9. <http://www.ltioptics.com/en/photopia-general-2017.html> Alexander Kotov.



Ksenia I. Nechaeva,

M. Sc. in Electronics and Nanoelectronics. She is a specialist in lighting engineering at ILEC “BL GROUP” LLC (Moscow, Russia)

COMPARISON OF LED AND HPS LUMINAIRES IN TERMS OF ENERGY SAVINGS AT TUNNEL ILLUMINATION

Behçet Kocaman and Sabir Rüstemli

Bitlis Eren University, Bitlis, Turkey
E-mail: bkocaman@beu.edu.tr; srustemli@beu.edu.tr

ABSTRACT

Energy demand is increasing day by day because of the step-up of population, rising living standards, rising energy prices, global warming and climate change, developments in industry and technology in developing countries. In order to meet this increasing energy demand, it is not possible to increase production only due to limited energy resources. Therefore existing energy sources need to be used in the most efficient way. One of the most important means of reaching this target is the efficient use of energy and its saving. Tunnel illumination is one of the areas of efficient and saving use of energy. In this study, high-pressure sodium (HPS) and light emitting diode (LED) luminaires usage are compared to Buzlupınar tunnel, which is a short tunnel in Bitlis province. It has also been found that illumination with LED luminaires is more efficient and economical in tunnel illumination instead of HPS.

Keywords: tunnel illumination, LED, HPS, energy saving

1. INTRODUCTION

Turkey is a country with limited resources in terms of energy resources. In other words, the country does not have adequate energy resources to meet the energy demand growth. It is a country that depends on outsiders, who can provide about a quarter of its energy needs from its own resources and the rest from external sources. Basic target should be to provide energy needs, adequate,

reliable and economical, to getting rid of external dependency.

Tunnels are constructed on the pedestrian road, railway, highway, canal, etc. in a situation, where it is technically impossible for the roads to pass through the earth or in order to pass underground a part of the way to arrange the traffic flow in the city or outside the city. It is necessary to illuminate the tunnels with artificial lighting during the day as well as at night using different designs and techniques. The main purpose of tunnel illumination is to provide the right comfort and safety while the driver is in the tunnel, passes inside the tunnel, and exits the tunnel.

These two points are of great importance in night illumination in the tunnels. Nowadays illumination and energy efficiency are gaining importance. As technology develops, the need for information on how illumination products are tested, with which methods and which standards are used, is increasing day by day. Levels of illumination in the tunnel begin to be revised from a lighting installation, which combines extensive research and existing technologies to develop a solution with visibility and security [1]. Luminaires are designed by taking into account the intensities of exhaust and other gases that pollute the air inside the tunnels. Stainless materials, especially steel and hardened glass lens materials, are durable to corrosion.

The distances between the luminaires are important, and illumination equipment needs to be positioned more tightly than if it is based on aesthetic considerations. Different types of electric lu-

minaires such as HPS, mercury vapour, and LED are used in tunnel illumination.

Generally, tunnel projects using long-life illumination elements are provided with more fluorescent luminaires and LED selections. The choice of illumination colours, suitable for improved traffic safety, must be specific to the architecture of the tunnel. Therefore illumination should be designed differently on the inside of the tunnel, differently towards the exit of the tunnel [2].

Tunnel in terms of illumination can be classified into two types like short and long tunnels. The short tunnels appear as “dark frames” in the field of view. In a flat tunnel, the observation area is approximately 20 meters when looking at an obstacle of 100 meters distance to 20 cm height. Considering the contributions of daylight at the entrance and exit, the length of the straight tunnel, which does not require daylighting, can be accepted as 50 meters. Short tunnels do not need illumination in the daytime. However, when the tunnel is bend or ramp or where traffic intensity is too much that is shorter than this length may also need illumination in daytime [3].

The model of a tunnel with two tubes is shown in Fig. 1. As shown in figure 1, the tunnel is divided into 4 zones such as access, entrance, interior, and exit.

The access zone is a part of the road immediately outside the tunnel, in which an approaching driver must be able to recognize a possible obstacle. Its length is equal to the stopping distance. In the entrance zone, luminance levels decrease slowly in order to allow the adaptation of the driver’s eyes to the lower lighting levels featuring the interior zone. The interior zone is a part located between the transition zone and the exit zone. Luminance levels

should guarantee a safe drive. The exit zone is a terminal part of the tunnel, where the visibility is influenced by the external luminance. In some cases, adaptive lighting can be required.

2. THE IMPORTANCE OF TUNNEL ILLUMINATION

Good illumination of the tunnels is extremely important in terms of the safety and comfort of the passengers. In addition, appropriate illumination solutions and used suitable luminaires for tunnel construction provide energy efficiency. Correct illumination provides not only luminous adaptation to the environment when the drivers enter the tunnel but also the driver’s confidence sense to travel in the tunnel.

A tunnel, which has inadequate illumination, leads to the impression of a “black hole” for an impending driver, and the driver suffers a loss of sight [4]. Tunnels need to be illuminated gradually in order to prevent drivers’ visibility loss in the tunnel. A tunnel road is a relatively enclosed space where the illumination suddenly alters from bright to dark (“black hole”) at the entrance of the tunnel and from dark to bright light (“bright hole”) at the exit of the tunnel as shown in Fig. 2.

Light sources used in tunnel illumination must have certain characteristics. These are the higher the efficiency factor, long life span and the luminaire can be used easily in it.

Light sources need to be used with suitable luminaires for a correct illumination. The luminaires to be used in the tunnel illumination must have the following characteristics [3]:

- Being economical;
- Must be installed easily and easy to maintain;

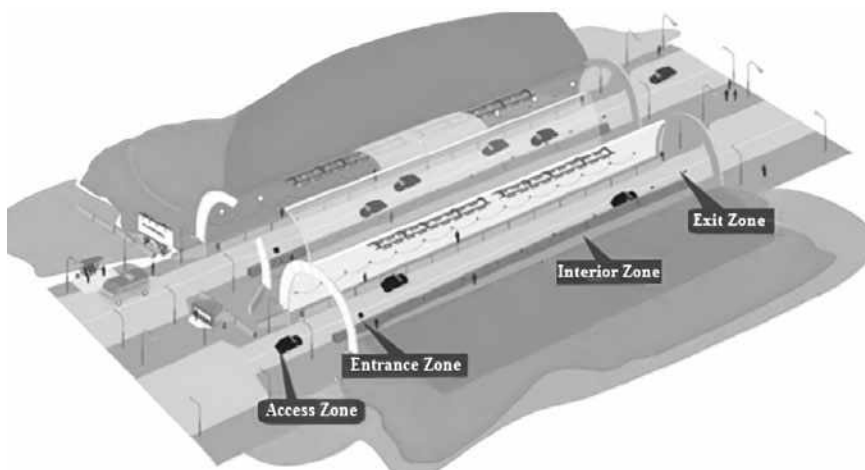


Fig. 1. The model of a tunnel with two tubes

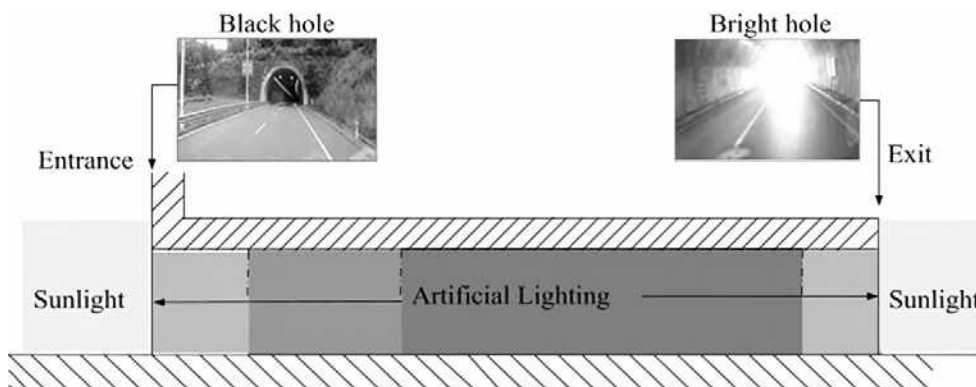


Fig. 2. A tunnel with black and bright hole

- Prevent glare;
- Waterproof against pressured water, durable to detergent and corrosion;
- Controlling the light distribution curve of the bare lamp and giving it the desired light distribution curve shape;
- Be adaptable to SCADA programs which are used with developing technology in tunnels;
- Providing visual guidance.

The luminous efficacy of the lamp chosen in the illumination is very important in terms of economic efficiency. The luminous efficacy is the rate of conversion of the electrical energy drawn from the network to the light.

2.1. Luminaires Used in Tunnel Illumination

Different types of electric luminaires are used in tunnel illumination such as fluorescent, low/high-pressure sodium vapour, mercury vapour, and LED luminaires. LEDs from these luminaires have begun to become more preferred in tunnel illumination in recent years, due to their efficiency and longer life span and easier maintenance than other luminaires. For this reason, it is important to replace the HPS luminaires with LED luminaires, which are used to minimize the energy consumption in the tunnels.

2.2. High-Pressure Sodium Luminaires

High-pressure sodium (HPS) luminaires, a member of the high-intensity discharge (HID) lamp family, are the most efficient white light source commercially available today. HPS luminaires feature highly energy efficient performance with a very long life by comparison to other conventional luminaires. HPS luminaire is one of the luminaires used in tunnel illumination. In these luminaires, the dis-

charge tube is placed in a hard glass balloon in the form of an evacuated tube.

The characteristic features of HPS luminaires are long-life span, provides high luminous efficacy, low maintenance costs, for outside and inside illumination use, universal operating position, resistant against changes in voltage, used together with assistant elements.

2.3. Light Emitting Diode (LED) Luminaires

The light in the LED luminaires is generated by electron movements in a semiconductor structure. When starting to design LED luminaires, firstly, the lighting criteria should be determined from the standards and proposals that must be provided in the lighting installations intended to be used with the luminaire. Then luminaire design objectives must be determined in suitable with these criteria. LED luminaires require different optical solutions for LED light sources and suitable luminaire designs due to small in size relative to conventional light sources. LED luminaires for a tunnel are available. Today, the usage areas and technical characteristics of LED luminaires are developing with technology every passing day [5]. It has the following advantages:

- Solid light source;
- No pollution, no ultraviolet;
- High colour rendering index;
- Continuous illumination control by adjusting the electric current and the control speed is fast, almost instantaneous;
- Through the design of a dedicated communication controller, each luminaire status, fault information, and the continuous adjustment of illumination are available [6].

In recent years, along with improvements in technology, control systems and the use of LED



Fig. 3. Two tube views of the Buzlupınar tunnel

luminaires have made great improvements in tunnel illumination. Today, however, most of the tunnels are illuminated by high-pressure sodium-vapour or mercury-vapour luminaires, which consume more energy [7]. For this reason, LED luminaires should be used to provide significant energy saving and efficient solutions for tunnel illumination.

LED luminaires should be preferred in the tunnels for the following reasons:

- Achieve high energy efficiency;
- At 25°C their luminous efficacy is at least 130 lm/W;
- Easy and diverse designs can easily be made thanks to the minimal size of an LED chip;
- They quickly enter the mode;
- They are easy to install and maintain as they are not made of fragile elements such as glass or filaments;
- Do not cause sound vibrations to be heard with the human ear because they work with DC current;
- They are environmentally safe, as they don't contain heavy metals such as mercury;
- It has flicker-free light features;
- They can be used safely because they are luminaires, which do not give very high heat like gas discharge luminaires;
- If any LED source fails in the luminaire, it is short-circuited. In this case, the luminaire continues to light. There is not a huge change in the homogeneity of the illumination until the number of broken LED sources reaches a certain amount;
- The improvements in LED optical design can easily be made symmetrical, asymmetrical;
- LED luminaires can detect objects in their true colour because of the Colour Rendering Index (CRI) values are about 70 [8].



Fig. 4. Illumination of the Buzlupınar tunnel using HPS luminaires

3. TUNNEL ILLUMINATION APPLICATION

The Buzlupınar tunnel is located on Bitlis-Diyarbakır highway, at the coordinates of 38°17'48" north and 41°59'52" east. Buzlupınar tunnel by General Directorate of Highways within the borders of Bitlis province. It is made of two tubes for two directions of traffic (Fig. 3).

However, this study was analysed using the right tube data. The total length of the right tube is 233 meters. This tunnel is one of Turkey's first highway tunnel illumination with LED luminaires. The energy quantities of HPS and LED luminaires when used were analysed in the tunnel illumination. Comparison of LED luminaire and HPS luminaire are given in Table 1.

In this study, the cost and energy savings will be analysed considering the costs of investment and the power consumption of the LED luminaires instead of the HPS luminaires using the same energy source. Moreover, comparison of LED and HPS luminaires in terms of energy saving in tunnel illumination was done for daily illumination. The number of HPS luminaires, lamp power, ballast power, and total power consumed in the Buzlupınar tunnel are given in Table 2.

According to the amount of light needed to enter the tunnel, HPS luminaires are phased in gradually. In total, there are 6 steps, which are: all of the luminaires are on, 75 % of the luminaires are on, 50 % of the luminaires are on, 25 % of the luminaires are on, night mode, and emergency illumination. Emergency illumination is only used in energy interruptions and is supplied by the uninterrupted power supply. The power, uptimes, and daily-consumed energy of the HPS luminaires used ac-

Table 1. Comparison of LED and HPS Luminaires

Characteristics	HPS Luminaires	LED Luminaires
Power (W)	100–500	43–170
Dimmability	Requires special ballast	Yes
Dimming limit	50 %	10 %
Luminous efficacy (lm/W)	80–140	114–160
Lifetime in hours ($\times 1000$)	10–24	100+
Mercury content	~ 6 mg/100 W	0
Warm up time (minutes)	2–15	Instant
Restrike time (minutes)	4–5	Instant
Operating temperature ($^{\circ}\text{C}$)	-30 to 65	-55 to 70

Table 2. Used HPS Luminaires Values

Power of HPS luminaires (W)	Number of luminaires used	Ballast Power (W)	Total Power (W)
70	168	13	13 944
150	28	26	4928
250	20	35	5700
400	120	50	54000
Total			78572

cording to their steps in the tunnel in one day are given in Table 3.

As shown in Table 3, uptimes of HPS luminaires are 2.75 h in step 1, 1.33 h in step 2, 1.50 h in step 3, 1.25 h in step 4, 17.17 h in step 5 in one day. The daily consumed energy of the HPS luminaires is 637,012.08 Wh (637.01 kWh).

Illumination of the Buzlupinar tunnel using HPS luminaires is given in Fig. 4.

The number of LED luminaires used in Buzlupinar tunnel, the luminaire power, the ballast power, and the total power consumed are given in Table 4.

LED luminaires are used in steps as they are in HPS luminaires. However, the emergency illumination step is not available in LED applications. For this reason, LED luminaires are used in 5 steps and in comparative 6th step calculations are not included.

The power, uptimes, and daily-consumed energy of the LED luminaires used according to their steps in the tunnel in one day are given in Table 5.

As shown in Table 5, uptimes of LED luminaires are 2.75 h in step 1, 1.33 h in step 2, 1.50 h in step 3, 1.25 h in step 4, 17.17 h in step 5 in one day.

Moreover as shown in Table 5, the daily-consumed energy of the LED luminaire is 380,230.50 Wh (380.23 kWh).

Illumination of the Buzlupinar tunnel using an LED luminaires are given in Fig. 5.

4. COMPARISON OF LED AND HPS LUMINAIRES AT TUNNEL ILLUMINATION

On average, the power spent on daily illumination with a day HPS luminaires is 637.01 kWh, while with a day LED luminaires is 380.23 kWh.

The advantages of the use of the LED luminaires instead of the HPS luminaires in the tunnel are:

- Daily average energy saving is $(637.01 - 380.23)$ kWh = 256.78 kWh/day;
- Monthly average energy saving is 256.78 kWh/day $\times 30$ day = 7703.4 kWh/month;
- Annual average energy saving is 7703.4 kWh/month $\times 12$ month = 92440.8 kWh/year.

According to the Republic of Turkey Energy Market Regulatory tariff, the general illumination applied since 01.04.2018 the unit price of elec-

Table 3. Daily Consumed Energy of HPS Luminaires

HPS	Power of HPS luminaire (W)	Number of luminaires used	Ballast Power (W)	Total Power (W)	Time (h)	Daily Consumed Energy (Wh)
Step 1	70	168	13	13944	2.75	38346.00
	150	28	26	4928	2.75	13552.00
	250	20	35	5700	2.75	15675.00
	400	120	50	54000	2.75	148500.00
Step 2	70	168	13	13944	1.33	18545.52
	150	16	26	2816	1.33	3745.28
	250	16	35	4560	1.33	6064.80
	400	88	50	39600	1.33	52668.00
Step 3	70	168	13	13944	1.50	20916.00
	150	4	26	704	1.50	1056.00
	250	8	35	2280	1.50	3420.00
	400	60	50	27000	1.50	40500.00
Step 4	70	168	13	13944	1.25	17430.00
	150	0	26	0	1.25	0.00
	250	4	35	1140	1.25	1425.00
	400	28	50	12600	1.25	15750.00
Step 5	70	168	13	13944	17.17	239418.48
	150	0	26	0	17.17	0.00
	250	0	35	0	17.17	0.00
	400	0	50	0	17.17	0.00
Step 6	Used only in emergencies (eg power interruption)					
Total Daily Consumed Energy (Wh)						637012.08

tric energy is 0.346747 TL / kWh. According to this, in the case of using the LED luminaire for daily illumination of the tunnel, one-year energy cost is saved: $92440.8 \text{ kWh} \times 0.346747 \text{ TL / kWh} = 32053.57 \text{ TL}$.



Fig. 5. Illumination of the Buzlupınar tunnel using LED luminaires

The prices of luminaires and ballasts used in tunnel illumination vary from mark to mark, while labour prices vary from company to company. From this point of view, an average value is determined from the firms in the internet, market research is carried out, and the cost account is given as in Tables 6–7.

The same workmanship is calculated for HPS and LED luminaires used in tunnel illumination. For this reason, montage workmanship did not participate in the account. According to the calculations made, the cost for HPS luminaires was 415,200 TL and 715,400 TL for LED luminaires. The investment made with LED luminaire is $(715,400 - 415,200) \text{ TL} = 300,200 \text{ TL}$ more in terms of initial installation cost. However, LED luminaires save 32053.57 TL per year.

According to these values, the LED illumination instead of HPS will pay off in 9.37 years

Table 4. Used LED Luminaire Values

Lamp type / LED driver	Number of luminaires used (Number)	Power of luminaires (W)	Total power (W)
96 LED500 mA	30	153	4590
96 LED700 mA	166	213	35358
Total			39948

Table 5. Daily Consumed Energy of LED Luminaires

LED	Power of LED luminaire (W)	Number of luminaires used	Total Power (W)	Uptime (h)	Daily Consumed Energy (Wh)
Step 1	153	30	4590	2.75	12622.50
	213	166	35358	2.75	97234.50
Step 2	153	8	1224	1.33	1627.92
	213	166	35358	1.33	47026.14
Step 3	153	8	1224	1.50	1836.00
	213	126	26838	1.50	40257.00
Step 4	153	8	1224	1.25	1530.00
	213	80	17040	1.25	21300.00
Step 5	153	4	612	17.17	10508.04
	213	40	8520	17.17	146288.40
Total Daily Consumed Energy (Wh)					380230.50

Table 6. Cost Accounting of HPS Luminaires

HPS luminaire Power (W)	Luminaire Unit Price (TL)	Ballast Unit Price (TL)	The number of Luminaire / Ballast	Total Price (TL)
70	930	80	168	169680
150	1200	65	28	35420
250	1250	75	20	26500
400	1400	130	120	183600
Total				415200

(300,200 TL / 32,053.57 TL), and it will be cheaper to use in the following years. This study was done for a 233-meter tunnel. However, in longer tunnels, this time will shorten.

5. CONCLUSION

The creation of efficient illumination systems in the tunnels requires good luminaire design and use of control systems. The luminaire design, which can be controlled from a centralized system with technological and low power consumption, should

be developed. In addition, in order to prevent darkness of the tunnels, it is necessary to consider an illumination circuit to be switched on in case of an emergency. Therefore, besides the network, it needs to be fed from a 3-phase generator, which will be switched on in case of necessity.

LED illumination is more advantageous since it does not require frequent maintenance and it is more energy-efficient than the conventional luminaires. These luminaires should be used to provide significant energy saving and efficient solutions for tunnel illumination. For this reason, it is important

Table 7. Cost accounting of LED Luminaires

LED Luminaire Type	Luminaire Unit Price (TL)	The number of Luminaire	Total Price (TL)
96 LED500 mA	3650	30	109500
96 LED700 mA	3650	166	605900
Generally Total			715400

to replace the HPS luminaires with LED luminaires, which are used to minimize the energy consumption in the tunnels.

Daily illumination of the Buzlupınar tunnel in Bitlis province was compared with HPS and LED luminaire usage. This study was done for daily illumination in it. When the tunnel is made with LED luminaire instead of HPS luminaire, energy saving of 256.78 kWh per day is achieved. This savings are calculated to provide 92440.8 kWh of energy savings on a yearly basis. This is why it is very advantageous for energy saving. In the calculation made, the LED luminaire will be amortized within 9.37 years, although the initial cost of the LED luminaire is higher than the HPS luminaire. This study was done for a 233 meters tunnel. The calculated time for amortization can be a little long. However, this time will shorten in longer tunnels. The maintenance of the luminaires used in the tunnel is a separate expenditure. LED luminaires have little maintenance cost compared to HPS luminaires. This is a major advantage of LED luminaires. In addition, LED luminaire lifespan is more than other luminaires. Therefore, care should be taken to make tunnels with less energy-consuming LED luminaires.

REFERENCES

1. Cengiz M.S., Rustemli S. The Relationship Between Height And Efficiency And Solution Offerings in Tunnel And Sub-Sea Tunnels // *Light & Engineering*, 2014, Vol. 22, # 2, pp. 76–83.
2. Yazıcıoğlu D.A. Tünel Ve Alt Geçitlerde Aydınlatma Tasarımı // *Lightworld Aydınlatma Dünyası Dergisi*, 2016, Vol. 38, pp. 52–566.
3. Akbulut A., Tünel Aydınlatması, Yıldız Teknik Üniversitesi, Fen Bilimleri Enstitüsü, Yüksek Lisans Tezi, İstanbul, 2006.
4. Qin L., Dong L.L., Xu W.H., Zhang L.D., and Leon A.S. An Intelligent Luminance Control Method for

Tunnel Lighting Based on Traffic Volume // *Sustainability*, 2017, Vol. 9, 12 p.

5. Yi H., Zheyang L., Aiogu W., Changbin L., and Shouzhong F. Research on Intelligent Control of Tunnel Lighting System Based on LED // *International Conference on Optoelectronics and Image Processing*, 2010.

6. He Y., Li C., Wu A., Feng S. LED Lighting Control System in Tunnel Based on Intelligent Illumination curve // *Fifth International Conference on Intelligent Computation Technology and Automation*, 2012, pp. 698–701.

7. <https://www.slideshare.net/FarukATLITRK/light-world-led-lighting-technology> (Access date:15.04.2018).

8. Peng F.Z. Application Issues of Active Power Filters // *IEEE Industry Applications Magazine*, 1998, Vol. 4, #5, pp. 21–30.



Behçet Kocaman,
Ph.D. in Electrical Engineering, Kocaeli University. Assistant Professor at department of Electrical and Electronic Engineering at Bitlis Eren University. His research areas are energy efficiency,

illumination, renewable energy sources, energy management and transmission and distribution technologies



Sabir Rüstemli,
Ph.D. in Electrical Engineering, Azerbaijan Scientific-Research Institute of Electric. He became Associate Professor in 1997 and Professor in 2005. Chairman of Electrical-Electronics

Engineering and also Vice Rector in Bitlis Eren University

THE RELATIONSHIP BETWEEN MAINTENANCE FACTOR AND LIGHTING LEVEL IN TUNEL LIGHTING

Mehmet Sait Cengiz

Bitlis Eren University, Biltis, Turkey
E-mail: msaitcengiz@gmail.com

ABSTRACT

Performance decreases in lighting equipment with a high level of contamination have been analysed in this study. Effect of decreases in luminous flux arising from abrasions and usage on tunnel illumination levels has been analysed and results of measurements in real environment and simulation environment have been compared. Calculations, which are complicated and difficult by traditional methods, have been visualized by a simulation program prepared in the computer environment. Results recorded at 60 points by measuring by a luxmeter, which was placed in the middle of 2.266 m² fields on the road surface into the tunnel, have been compared with simulation results. Thanks to the simulation program used, tunnel lighting measurements would not be necessary, which they take a long time in the physical environment by measurement devices and are carried out by stopping vehicle traffic. Tunnel lighting maintenances, which are complicated and take a long time, will be carried out in a short time and more accurately, and waste of resources could be prevented. It has been determined in the study that more accurate results could be obtained in ergonomic, economic, and using aspects.

Keywords: tunnel lighting, maintenance factor, illumination levels

1. INTRODUCTION

The main purpose of tunnel lighting is to ensure the safe flow of vehicles or traffic under day

and night conditions. Performance of tunnel lighting is evaluated depending on parameters such as illuminance of the road surface and walls, overall and longitudinal lighting uniformity, glare control, the formation of the contrast required to perceive the objects and flicker frequency [1, 2].

Efficient use of energy without any decrease in producing energy conservation, comfort and labour force is not to waste. People have been motivated to find new methods to save energy due to rapid and unconscious consumption of the energy resources used [2–4]. For that reason, it is critical to use luminaires of high productivity and efficiency in tunnel lighting systems, which are active continuously. Stopping distance is considered in calculations while tunnel lighting is designed. This distance is related to the time when driver sees the obstacle in front of him/her and reacts to. Stopping distance demonstrates that tunnel lighting is required as well as it constitutes the main foundation of lighting design. It is critical in terms of traffic safety that drivers could enter the tunnel safely and without disturbance throughout the tunnel, go ahead throughout the tunnel, and continue to drive at the tunnel exit. It is required to calculate illumination levels accurately so that drivers could realize an object into the tunnel [3–5].

It is difficult to determine the average life for tunnel lighting systems and determine the rate of losses of light intensity in lighting equipment. It is also complicated to evaluate the working performance of the system and determine maintenance time. Illuminance measurements have been carried out to determine maintenance time for tun-

nel lighting in this study. In other words, measurements were carried out with a measuring instrument at many points into the tunnel in order to determine, if there is any loss of lighting equipment. However, it is difficult and time-consuming to do so for each tunnel lighting. A study that would take a long time was necessary in order to determine maintenance of lighting system, lifecycle of the system, and losses of lighting equipment in a luxury aspect even though the study was carried out for only one tunnel.

2. PERFORMANCE LOSSES OF LIGHTING SYSTEMS

Lighting, in the simplest term, is to supply the required illuminance for an operation. The most important objective to design lighting systems is to obtain sufficient light without supplying excessive lighting and increasing energy cost [6]. For that reason, it is important to know about factors, which have a direct effect on proper illumination level in an environment. Attenuation of the luminous flux values of the lighting equipment used in tunnels might occur over time. Performance loss of the luminaires, which occurs depending on operating time, affects directly the performance of the system. The most important reason why luminaires lose their performance is that light transmittance decreases since the luminaires are contaminated by environmental reasons. Another reason for performance loss is that light source efficiency depends on operating time and the light source expires earlier. Since luminaires lose performance depending on the time, the performance of the lighting system will be identified for the time period specified. The time period may include maintenance works, which would recover performances of the luminaires such as cleaning the glass of luminaires or replacing lamps of the luminaires as well as replacing all the luminaires at the expiration date. A lighting system can supply minimum required lighting even at the end of the period when it has the lowest performance, if the estimated decrease in performance is included in the system performance at design phase [7–9]. Deficiencies in lighting because of the decrease in illumination levels of the lamps and lacks of maintenance would affect visual conditions adversely. Lighting simulation programs to be used at this phase will provide great convenience at the first installation. However, it is still a compli-



Fig. 1. Tunnel lighting with double suspensions

cated problem: how to assess the sufficiency of an existing lighting system with a lighting technique. It is required to measure illumination levels in tunnel lighting, at first, in order to evaluate the conformity of illumination levels in the environment. Lighting equipment is maintained at periodic intervals in order to prevent performance loss happened to the lighting equipment.

3. MAINTENANCE FACTOR IN TUNNEL LIGHTING

A lighting instrument should supply the minimum illumination level during the operating time. Contamination on lighting instrument causes loss of luminous flux in the luminaire and structural defects on the surface of the optical equipment. Loss of lighting performance makes the maintenance of lighting instruments necessary. This effect, which is formed by the mutual effect of several parameters and applied at periodic intervals, is Maintenance Factor (MF). MF varies by type of lighting system, environmental conditions, and features of luminaires. MF should be calculated accurately so that tunnel lighting systems can be implemented in accordance with the objectives and they can sustain the performance to meet the expectations even at the end of maintenance period or lifecycle of the system. MF has an important place in the total cost of a lighting system, since it affects directly energy consumption. For luminaires, MF is defined as the proportion of total light coming from a luminaire at the end of the maintenance period to total light of the luminaire during the primary use. In accordance with standards associated with the use of MF

in lighting, lighting system is specified by the chosen lighting equipment, environmental conditions, and the maintenance factor calculated for a specified period of maintenance CIE154:2003. According to CIE154:2003, lighting performance should not drop below minimum levels specified in the standards [10–12]. *MF* consists of Lamp Lumen Maintenance Factor (*LLMF*), which is the proportion of performance loss in the lamp, the luminous flux at the end of the specified period, to the initial luminous flux. *LLMF* value is reached by the catalogue of the manufacturer. Lamp Survival Factor (*LSF*) is the percentage of lamp survival ratio for maintenance factor. *LSF* value is reached by the catalogue of the lamp.

Luminaire Maintenance Factor (*LMF*) is the proportion of luminous flux, which decreases at the end of the described/specified period as a result of a structural feature of the luminaire and also environmental factors, to the initial luminous flux. *LMF* depends on protection class of luminaire against contamination (IP) and environmental pollution. It is specified by the designer according to the contamination condition of the environment during the maintenance period or the relevant specification is consulted. *MF* is calculated according to Equation 1:

$$MF = LLMF \cdot LSF \cdot LMF . \tag{1}$$

In the standard concerning the calculation of lighting performances, *MF* is formed by the product of luminous flux *MF* and luminaire *MF*. Equation 2 demonstrates the relationship between *MF* and Lighting Level [1, 13].

$$E = \frac{I \cdot \cos^3 \varepsilon \cdot \Phi \cdot MF}{h^2}, \tag{2}$$

where *I* is the given luminous intensity value (cd/lm), Φ is the luminous flux (lm), *MF* is the maintenance factor, *h* is the height of the luminaire from the ground (m), ε is the angle between the light coming from the luminaire to the surface and the normal of the surface.

4. APPLICATION IN TUNNEL LIGHTING

Various design tools or physical measurements are used in order to determine the illumination levels of certain points selected in lighting systems. These are physical measurements carried out by models, numerical equations, and computer programs or by luxmeter in the real environment. In this study, HPS100 W luminaires inserted dually 6 m high are used in the tunnel. Maintenance factor for high-pressure sodium vapour (HPS) luminaires is specified by the product of three main factors described above (Equation 1). Determination of maintenance factor for a 100 W HPS luminaire with protection class IP65 is calculated during simulation. Fig. 1 illustrates a sample of tunnel lighting with double suspensions [11, 12, 14].

4.1. Physical Measurements

Measurements of illuminance levels have been carried out in an active tunnel used in daily life. Measurements have been carried out at night and in the interior zone of the tunnel in order to avoid sunlight. High-pressure sodium vapour lamps (HPS) 100 W were used in the interior lighting of the tunnel. The road in the tunnel was divided into 60 areas of $(1.70 \times 1.333) = 2.266 \text{ m}^2$, and measurements were carried out separately in each of these areas (Fig. 2).

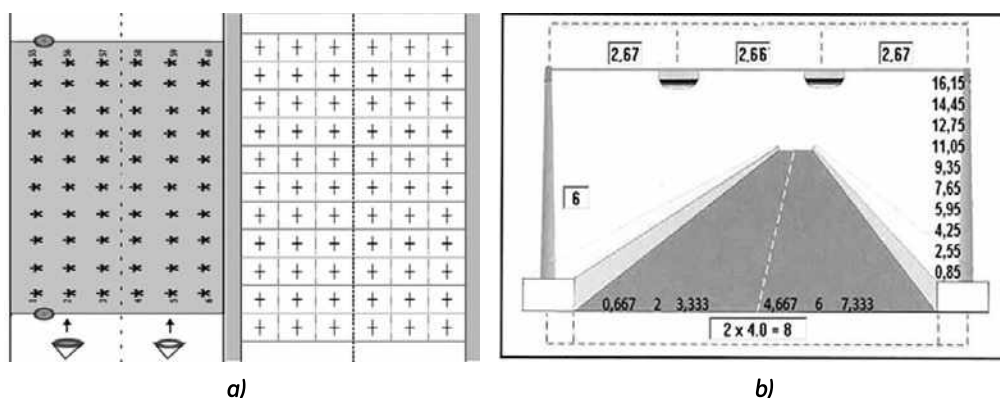


Fig. 2. a – chart of the fields measured in a two-lane tunnel; b – section of the road measured

Table 1. The Tunnel Road and Lighting Parameters

Tunnel Road Parameters		Tunnel Lighting Parameters	
Double luminaire, transverse arrangement			
Road class	R3	Luminaire height	6 m
Number of lanes	2	Boom angle	0
Strip width	4 m	IP protection	IP65
Road width	8 m	Pollution category	High
Q_0	0.07	Annual clear period (year)	2
Road lighting class	M2	Distance between luminaires	17 m

4.2. Simulation Design and Planning Process

Various choices are available for the road parameters in the simulation program. For the road parameters, the lighting system (bilateral, displaced, divided road, tunnel road with single luminaire, tunnel road with two luminaires, etc.), road class (R1, R2, R3, R4, N1, N2, N3, N4, etc.), number of lanes, lane width, refuge width, and road lighting class (M1, M2, M3, M4, M5, M6, etc.) can be chosen. For the lighting parameters, features such as distance between the luminaires, the height of the luminaire, distance of the luminaire from the road, boom angle, IP protection class, pollution rate, cleaning period, and maintenance factor are chosen for post or hanger lighting installations. For the luminaire parameters, the name, angle of the luminaire (angle relative to the road), power of the lamp used, lifetime, luminous flux, ballast power, and

new lamps can be added into this simulation under the Database process at any time. As a result, it is possible to add any kind of lamp into the simulation [15–18]. An easy and accurate calculation is achieved in the simulation results for the lighting system in which data is entered. Fig. 3 shows the algorithm of the simulation program and the data entered [17].

Table 1 illustrates the road and lighting parameters belonging to the tunnel measured.

Table 2 illustrates type styles luminaire maintenance factor by protection class of luminaire and category of environmental pollution [10–12].

The display of the luminaire parameters in the simulation program are illustrated in Fig. 4.

In this study, the lighting system of a tunnel, which still operates actively and has parameters illustrated in Table 1, has been analysed at first. Parameters in Table 1 has been transmitted to the

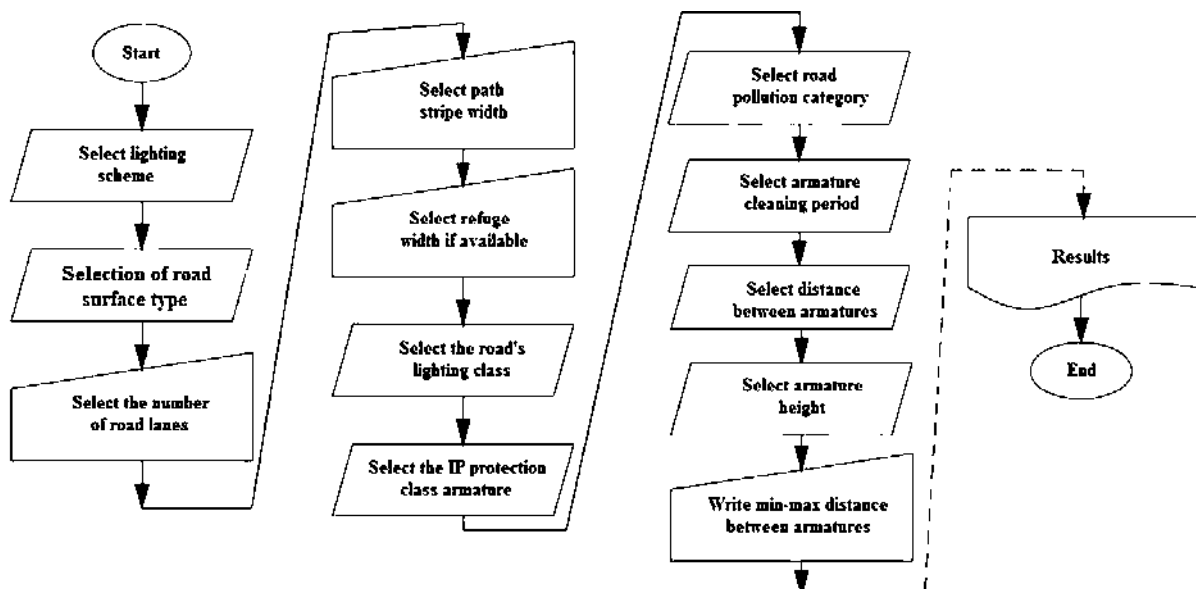


Fig. 3. The algorithm of the simulation program and data entered [17]

Table 2. Type Styles Luminaire Maintenance Factor by Protection Class of Luminaire and Category of Environmental Pollution [11]

Optical Compartment IP Rating	Pollution Category	Exposure time (Years)				
		1	1.5	2	2.5	3
IP2X	High	0.53	0.48	0.45	0.43	0.42
	Medium	0.62	0.58	0.56	0.54	0.53
	Low	0.82	0.80	0.79	0.78	0.78
IP5X	High	0.89	0.87	0.84	0.80	0.76
	Medium	0.90	0.88	0.86	0.84	0.82
	Low	0.92	0.91	0.90	0.89	0.88
IP6X	High	0.91	0.90	0.88	0.85	0.83
	Medium	0.92	0.92	0.89	0.88	0.87
	Low	0.93	0.93	0.91	0.90	0.90

Table 3. Results of Simulation (E Values)
 $MF=0.88$; $E_{min}=37.54$ lx; $E_{max}=83.65$ lx; $E_{average}=60.53$ lx

1 time in 2 year	0.8	2.5	4.2	5.9	7.6	9.3	11.0	12.7	14.4	16.1
0.7	68.73	58.92	47.32	38.69	37.54	37.55	38.72	47.36	58.99	68.83
20	83.54	77.59	62.83	52.8	52.12	52.13	52.83	62.87	77.66	83.64
3.3	68.57	69.32	63.25	59.75	66.55	66.56	59.78	63.3	69.39	68.67
4.7	68.57	69.32	63.25	59.75	66.55	66.56	59.78	63.3	69.39	68.67
6.0	83.54	77.59	62.83	52.8	52.12	52.13	52.83	62.87	77.66	83.64
7.3	68.73	58.92	47.32	38.69	37.54	37.55	38.72	47.36	58.99	68.83

simulation designed in Visual Basic Program. The surface of luminaires is cleaned by carrying out maintenance for the luminaires in this tunnel once a year. In addition, lamps, which break down for whatever reason, are replaced. However, they are replaced regardless of the tunnel, road conditions, weather conditions, traffic density or MF . 60 measurements have been performed at the points chosen previously by a luxmeter into the tunnel at night when traffic was not busy.

As for the simulation used for this tunnel, numerical results are generated and recorded for MF , E_{min} , E_{max} , E_{avr} belonging to tunnel and E values belonging to 60 points. Then the results of the measurement and results produced by the simulation were compared and percentage deviations were calculated for 60 points chosen. Road and lighting parameters used in the simulation were obtained from Table 1 and MF value was obtained from Table 2.

Table 3 has been obtained as a result of these parameters entered into the simulation. E values belonging to 60 points chosen in the simulation could be seen provided that maintenance would be carried out once a year.

Table 4 illustrates E values formed as a result of measurement performed at 60 points chosen in a tunnel for which maintenance is carried out once a year.

Table 5 illustrates the percentage difference E between the physical measurements performed in the tunnel and simulation.

Depending on Table 5, possible performance loss in this tunnel in case of maintenance several times in a year and once every three years will be estimated roughly. Table 6 illustrates simulation results belonging to this tunnel if maintenance is performed once a year. Table 7 is created using Table 5 by determining the amount of the deviation for the

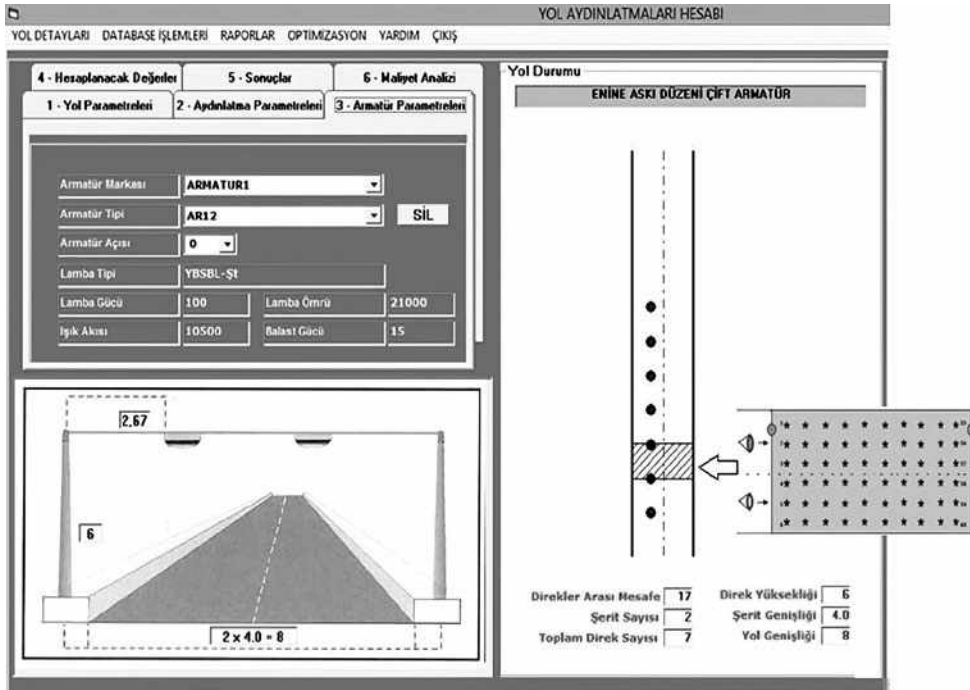


Fig. 4. Luminaire parameters in the simulation program

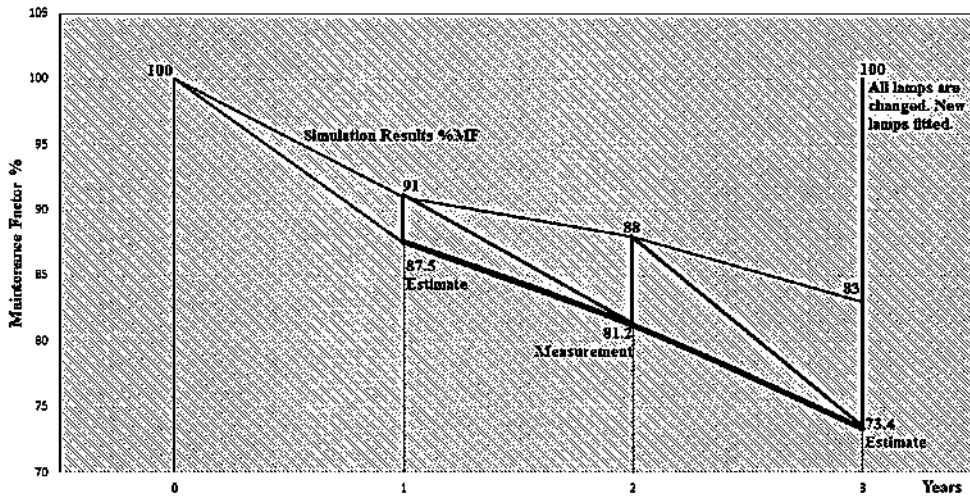


Fig. 5. Optical performance variation with HPS luminaires 100 W

1-year period. If amounts of deviation in Table 7 are applied to Table 6, one can obtain *E* values and *MF* value in Table 8. Table 9 illustrates simulation results belonging to this tunnel if maintenance is performed once every three years. Table 10 is created using Table 5 by determining the amount of the deviation for the 3-year period. If amounts of deviation in Table 10 are applied to Table 9, one can obtain *E* values and *MF* value in Table 11.

Optical performance variation with HPS luminaires 100 W is illustrated in Fig. 5.

When Fig. 5 is examined:

- While *MF* decreases to 84.68 % at the end of the 1st year, *MF* increases to 91 % by cleaning glasses of the luminaires;

- While *MF* decreases to 80.26 % at the end of the 2nd year, *MF* increases to 88 % by cleaning glasses of the luminaires;

- While *MF* reduces to 73.4 % after three years, it increases up to 83 % as a result of the cleaning glasses of the luminaires.

However, all lamps should be replaced since cleaning the glass of luminaires fails to satisfy. Decrease in illuminance levels would not be tolerated because of the decrease in luminous flux of the lamps after 3 years. All lamps used for 3 years should be replaced even though they operate instead of replacing the broken or dead lamps. When examining catalogue of the manufacturer, it is seen that HPS lamps 100 W cannot be used after approx-

Table 4. Results of Measurements (*E* Values)
Measurements: $MF=0.812$; $E_{min}=32.11$ lx; $E_{max}=79.92$ lx; $E_{average}=55.87$ lx

1 time in 2 year	0.8	2.5	4.2	5.9	7.6	9.3	11.0	12.7	14.4	16.1
0.7	65.73	53.05	40.99	35.33	32.92	33.17	35.81	45.21	53.87	65.32
2.0	77.56	69.98	57.68	48.65	46.86	48.59	46.09	57.94	72.04	79.55
3.3	63.51	59.96	58.13	56.32	60.98	59.93	56.66	58.94	65.52	65.97
4.7	64.09	60.95	56.47	56.01	60.96	60.99	56.08	58.72	65.55	66.09
6.0	77.01	73.12	57.27	48.84	47.93	47.91	47.54	56.86	74.73	79.92
7.3	64.11	53.43	42.07	36.31	32.11	33.72	35.95	42.33	56.42	66.61

Table 5. Percentage Difference *E* between the Measurements and Simulation

Deflection	0.8	2.5	4.2	5.9	7.6	9.3	11.0	12.7	14.4	16.1
0.7	4.37 %	9.97 %	13.38 %	8.70 %	12.31 %	11.67 %	7.53 %	4.55 %	8.68 %	5.10 %
2.0	7.17 %	9.81 %	8.20 %	7.87 %	10.11 %	6.80 %	12.76 %	7.85 %	7.24 %	4.90 %
3.3	7.39 %	13.51 %	8.10 %	5.75 %	8.38 %	9.97 %	5.23 %	6.89 %	5.59 %	3.94 %
4.7	6.54 %	12.08 %	10.72 %	6.27 %	8.41 %	8.38 %	6.20 %	7.24 %	5.55 %	3.77 %
6.0	7.83 %	5.76 %	8.85 %	7.51 %	8.05 %	8.11 %	10.02 %	9.57 %	3.77 %	4.46 %
7.3	6.73 %	9.33 %	11.10 %	6.17 %	14.47 %	10.20 %	7.16 %	10.63 %	4.36 %	3.23 %

Table 6. Results of Simulation (*E* Values) Provided that Maintenance Would Be Carried out Once a Year
 $MF=0.91$; $E_{min}=38.82$ lx; $E_{max}=86.50$ lx; $E_{average}=62.59$ lx

1 time in 1 year	0.8	2.5	4.2	5.9	7.6	9.3	11.0	12.7	14.4	16.1
0.6	71.07	60.93	48.93	40.01	38.82	38.83	40.04	48.98	61.00	71.17
2.0	86.39	80.23	64.97	54.60	53.90	53.91	54.63	65.02	80.30	86.49
3.3	70.91	71.69	65.40	61.79	68.82	68.83	61.82	65.45	71.76	71.01
4.7	70.91	71.69	65.40	61.79	68.82	68.83	61.82	65.45	71.76	71.01
6.0	86.39	80.23	64.97	54.60	53.90	53.91	54.63	65.02	80.30	86.49
7.3	71.07	60.93	48.93	40.01	38.82	38.83	40.04	48.98	61.00	71.17

imately 26000 hours (it corresponds to 3-year study for tunnel lighting) because of the decrease in luminous flux. For that reason, all lamps should be replaced.

As seen in Fig 5, while *MF* difference is 6.3 % for 1–2 years (for 365 days), *MF* difference increases up to 7.8 % for 2 or 3 years (for 365 days). As it is understood in this aspect, E_{avr} reduces rapidly since the lamps and other equipment used wear off. Results from simulation and prediction promote this thought.

5. RESULTS

As a result of these estimates, it will be easier to make improvements by responding on time after determining, if lighting elements expire and if they have sufficient luminous flux, and thus to prevent waste of electrical energy, which does not turn into light. Since simulation study makes easier to determine contamination time of lighting equipment, it increases the chance to find a solution by estimating workforce gain and losses of energy oc-

Table 7. Percentage Difference E between the Estimate Performed in the Tunnel and Simulation

Deflection	0.8	2.5	4.2	5.9	7.6	9.3	11.0	12.7	14.4	16.1
0.7	2.19 %	4.99 %	6.69 %	4.35 %	6.16 %	5.83 %	3.76 %	2.28 %	4.34 %	2.55 %
2.0	3.58 %	4.90 %	4.10 %	3.93 %	5.05 %	3.40 %	6.38 %	3.93 %	3.62 %	2.45 %
3.3	3.69 %	6.76 %	4.05 %	2.88 %	4.19 %	4.99 %	2.62 %	3.44 %	2.79 %	1.97 %
4.7	3.27 %	6.04 %	5.36 %	3.14 %	4.21 %	4.19 %	3.10 %	3.62 %	2.77 %	1.88 %
6.0	3.91 %	2.88 %	4.42 %	3.75 %	4.03 %	4.05 %	5.01 %	4.79 %	1.89 %	2.23 %
7.3	3.37 %	4.66 %	5.55 %	3.08 %	7.23 %	5.10 %	3.58 %	5.32 %	2.18 %	1.61 %

Table 8. Results of Estimation (E Values) Provided that Maintenance Would Be Carried out Once a Year

1 time in 1 year	0.8	2.5	4.2	5.9	7.6	9.3	11.0	12.7	14.4	16.1
0.7	69.51	57.89	45.66	38.27	36.43	36.57	38.53	47.86	58.35	69.36
2.0	83.30	76.30	62.31	52.45	51.18	52.08	51.14	62.46	77.39	84.37
3.3	68.29	66.84	62.75	60.01	65.94	65.40	60.20	63.20	69.76	69.61
4.7	68.59	67.36	61.89	59.85	65.92	65.95	59.90	63.08	69.77	69.68
6.0	83.01	77.92	62.10	52.55	51.73	51.73	51.89	61.91	78.78	84.56
7.3	68.67	58.09	46.21	38.78	36.01	36.85	38.61	46.37	59.67	70.02

Table 9. Results of Simulation (E Values) Provided that Maintenance Would Be Carried out Once Every Three Years
 $MF=0.83$; $E_{min}=35.41$ lx; $E_{max}=78.89$ lx; $E_{average}=57.09$ lx

1 time in 3 year	0.8	2.5	4.2	5.9	7.6	9.3	11.0	12.7	14.4	16.1
0.7	64.83	55.57	44.63	36.49	35.40	35.41	36.52	44.67	55.64	64.91
2.0	78.80	73.18	59.26	49.80	49.16	49.17	49.83	59.30	73.24	78.89
3.3	64.67	65.38	59.65	56.36	62.77	62.78	56.39	59.70	65.45	64.77
4.7	64.67	65.38	59.65	56.36	62.77	62.78	56.39	59.70	65.45	64.77
6.0	78.80	73.18	59.26	49.80	49.16	49.17	49.83	59.30	73.24	78.89
7.3	64.83	55.57	44.63	36.49	35.40	35.41	36.52	44.67	55.64	64.91

Table 10. Percentage Difference E between the Estimate Performed in the Tunnel and Simulation

Deflection	0.8	2.5	4.2	5.9	7.6	9.3	11.0	12.7	14.4	16.1
0.7	6.56 %	14.96 %	20.07 %	13.05 %	18.47 %	17.50 %	11.29 %	6.83 %	13.02 %	7.65 %
2.0	10.75 %	14.71 %	12.30 %	11.80 %	15.16 %	10.20 %	19.14 %	11.78 %	10.86 %	7.35 %
3.3	11.08 %	20.27 %	12.15 %	8.63 %	12.57 %	14.96 %	7.85 %	10.33 %	8.38 %	5.91 %
4.7	9.81 %	18.12 %	16.08 %	9.41 %	12.62 %	12.57 %	9.30 %	10.85 %	8.32 %	5.65 %
6.0	11.74 %	8.64 %	13.27 %	11.26 %	12.08 %	12.16 %	15.03 %	14.36 %	5.66 %	6.69 %
7.3	10.10 %	13.99 %	16.64 %	9.25 %	21.70 %	15.30 %	10.75 %	15.95 %	6.54 %	4.84 %

Table 11. Results of Estimation (E Values) Provided that Maintenance Would Be Carried out Once Every Three Years
 $MF=0.734$; $E_{min}=27.72$ lx; $E_{max}=73.62$ lx; $E_{average}=50.50$ lx

1 time in 3 year	0.8	2.5	4.2	5.9	7.6	9.3	11.0	12.7	14.4	16.1
0.7	60.57	47.26	35.67	31.73	28.86	29.21	32.40	41.62	48.39	59.95
2.0	70.32	62.41	51.97	43.92	41.71	44.15	40.29	52.31	65.29	73.09
3.3	57.51	52.13	52.41	51.49	54.88	53.39	51.96	53.53	59.96	60.94
4.7	58.33	53.53	50.06	51.06	54.85	54.89	51.14	53.22	60.01	61.11
6.0	69.54	66.85	51.39	44.19	43.22	43.19	42.34	50.79	69.10	73.62
7.3	58.28	47.80	37.20	33.12	27.72	29.99	32.59	37.54	52.00	61.77

curing over time. Energy consumption that does not turn into light because of performance losses with the lighting equipment can be thus prevented.

This study analyzes the importance of designs for lighting systems, which are an essential part of indoor areas such as tunnels, and effects of time-dependent losses of lighting equipment in these environments on lighting systems. Effect of MF on tunnel lighting has been analysed by comparing the simulation results with the real measurement results. Predictions on the tunnels, maintenance of which is carried out at 1-year and 3-year intervals, have been made according to the results from measurements, which were performed at 60 points into a tunnel, maintenance period of which is once a year. It is thus found that more accurate results may be obtained by the tunnels having 1-year and 3-year MF , physical measurements of which are not performed. Losses formed by the scenarios that tunnel lighting maintenance is performed once a year and once every three years may be determined based on the difference of% between simulation environment and physical measurement.

6. CONCLUSION

It is concluded that it is a successful method in estimating MF of the tunnels to use simulation results and real measurements together in tunnel lighting systems, which have similar environmental conditions (contamination, climate, temperature, moisture, wind, vehicle density, etc.). Estimates based on scientific data in simulation environment will offer easier and quicker solutions since it is a difficult and time-consuming process to stop traf-

fic and make physical measurement in the tunnels where traffic is busy.

It is critical to calculate properly MF in order to install lighting systems of road pursuant to the purposes and maintain the performance to meet the expectations even at the end of maintenance period or operating time of the system.

MF takes an important part in the total cost of a lighting system since it affects directly energy consumption. It is required to determine which one of these options are more economical depending on energy consumption, cost of lamps and changing lamps.

Start-up costs and maintenance costs of the systems should be considered to compare energy efficiency.

Increasing the maintenance factor used as a multiplier in performance calculations increases the energy efficiency by decreasing the energy consumed.

REFERENCES

1. Özkaya M. Aydınlatma Tekniği // Birsen Yayinevi, İstanbul, 1994, 384 p.
2. Tetri, E., Chenani, S.B., Rasanen R.S. Advancement in Road Lighting // Light & Engineering, 2018, Vol. 26, #1, pp. 99–109.
3. Barua P., Mazumdar S., Chakraborty S., Bhat-tacharjee S. Road Classification Based Energy Efficient Design and its Validation for Indian Roads // Light & Engineering, 2018, Vol. 26, #2, pp. 110–121.
4. Iacomussi P., Rossi G., Soardo P. Energy Saving and Environmental Compatibility in Road Lighting // Light & Engineering, 2012, Vol. 20, #4, pp. 55–63.

5. Van Bommel W., Van Den Beld, G., Van Ooyen M. Industrial Light and Productivity // Light & Engineering, 2003, Vol. 11, #1, pp. 14–21.
6. Güler Ö., Onaygil S. The effect of luminance uniformity on visibility level in road lighting // Lighting Research Technology, 2002, Vol. 35, pp. 199–215.
7. Jantzen R. Flimmerwirkung der Verkehrsbeleuchtung // Lichttechnik, 1960, Vol. 12.
8. Schreuder D.A. The lighting of vehicular traffic tunnels. Thesis, University of Technology Eindhoven, 1964.
9. Walthert R. Tunnel lighting systems // International Light Review, 1977, Vol. 4, P. 112.
10. CIE Technical Report, CIE-88–2004. Guide for the Lighting of Road Tunnels and Underpasses, 2004.
11. CIE Technical Report, CIE-154–2003. The Maintenance of Outdoor Lighting Systems, 2003.
12. CIE Technical Report, CIE-194–2011. On Site Measurement of the Photometric Properties of Road and Tunnel Lighting, 2011
13. TSE standard: TS EN13201–2, Road lighting – Part 2: Performance requirements, 2016.
14. Master Son-T Apia PlusXtra, HPS-100, 2018. URL: https://www.assets.lighting.philips.com/is/content/PhilipsLighting/fp928483300095-pss-tr_tr
15. Onaygil S. TEDAŞ Genel Müdürlüğü Meslek İçi Eğitim Semineri-Gölbaşı Eğitim Tesisleri, Yol aydınlatma Semineri 23–24 Ocak 2007.
16. Onaygil S. TEDAŞ Genel Müdürlüğü Meslek İçi Eğitim Semineri, TEDAŞ Basımevi, Ankara.
17. Cengiz M.S. A Simulation and Design Study for Interior Zone Luminance In Tunnel Lighting // Light & Engineering, 2019, Vol. 27, #2.
18. Onaygil, S. Yol aydınlatma projelerinde yol sınıfının belirlenmesinin önemi // Kaynak Elektrik Dergisi, 1998, Vol. 12, pp. 125–132.



Mehmet Sait Cengiz,

Ph.D. in Electrical and Electronics Engineering, 2016, Inonu University. Works in the field of applied lighting. He is currently working at Bitlis Eren University. Director of Research and Development, 2000–2010, in Turkey Electricity Distribution Company

A REVIEW OF DIMENSIONALITY REDUCTION TECHNIQUES FOR PROCESSING HYPER-SPECTRAL OPTICAL SIGNAL

Ana del Águila, Dmitry S. Efremenko, and Thomas Trautmann

*Deutsches Zentrum für Luft- und Raumfahrt (DLR), Institut für Methodik
der Fernerkundung (IMF), 82234 Oberpfaffenhofen, Germany
E-mail: dmitry.efremenko@dlr.de*

ABSTRACT

Hyper-spectral sensors take measurements in the narrow contiguous bands across the electromagnetic spectrum. Usually, the goal is to detect a certain object or a component of the medium with unique spectral signatures. In particular, the hyper-spectral measurements are used in atmospheric remote sensing to detect trace gases. To improve the efficiency of hyper-spectral processing algorithms, data reduction methods are applied. This paper outlines the dimensionality reduction techniques in the context of hyper-spectral remote sensing of the atmosphere. The dimensionality reduction excludes redundant information from the data and currently is the integral part of high-performance radiation transfer models. In this survey, it is shown how the principal component analysis can be applied for spectral radiance modelling and retrieval of atmospheric constituents, thereby speeding up the data processing by orders of magnitude. The discussed techniques are generic and can be readily applied for solving atmospheric as well as material science problems.

Keywords: passive remote sensing, hyper-spectral data, principal component analysis, full-physics machine learning, trace gas retrieval

1. INTRODUCTION

Hyper-spectral sensors record the transmitted or reflected radiance in the narrow contiguous bands across the electromagnetic spectrum. The goal is to detect a certain object or a component of the

medium, which has a unique spectral signature, i.e. a fingerprint. Hyper-spectral imaging has emerged as one of the most powerful technologies in various fields including astronomy, mineralogy, agriculture, medicine and chemistry. For instance, hyper-spectral data (sometimes referred to as hypercube data or as an image cube) are used in astronomy and Earth remote sensing to create a spatially-resolved spectral image allowing more accurate recognition and classification of the objects in the instrument field of view. At the same time, significant data storage and computational power are required to process the hyper-spectral information and to retrieve a certain parameter of the scattering medium.

In this survey we are focused on hyper-spectral remote sensing of the atmosphere. The passive atmospheric composition sensors (ACS) detect and record the radiance reflected by the Earth atmosphere in the ultraviolet (UV), visible (VIS), and thermal infrared (IR) regions. The information about the atmosphere is then retrieved from the spectral data by using the so called atmospheric processors, i.e. codes which are specifically designed to invert ACS measurements [1]. Extracting the information about geophysical parameters (level-2 data) from spectral radiance distributions (level-1 data) turns out to be a major computational challenge and requires high performance computing (HPC) [2].

The recent developments in optics, sensor design and measurement techniques significantly improve the characteristics of hyper-spectral ACS, such as the spatial resolution and the signal-to-noise

Table. Characteristics of Atmospheric Composition Sensors

Instrument	GOME	GOME-2	TROPOMI
Platform	ERS-2	MetOp (A, B, C)	Sentinel 5 Precursor
Spatial resolution (km ²)	320x40	80x40	7x3.5
Amount of level-1 data (TB per year)	0.8	4.2	240
Operational	1995–2011	2006–present	2017–present

ratio. Table shows a comparison between previous generation instruments like the Global Ozone Monitoring Experiment (GOME and GOME-2) and the newest, the TROPOspheric Monitoring Instrument (TROPOMI) [3] on board of the Copernicus Sentinel 5 Precursor (S5P) satellite. The spatial resolution of TROPOMI is two orders of magnitude higher, providing 21 million level-1B spectra per day, i.e. almost 8 milliards spectral points, while the signal-to-noise ratio in the UV/VIS channels reaches the values of about 1500. Fig. 1 shows the example of a retrieved map of tropospheric nitrogen dioxide (NO₂) from S5P measurements (the data is freely available at <https://s5phub.copernicus.eu/dhus>). Observe that air pollution emitted by big cities and shipping lanes is clearly visible. With the high resolution data it is possible to detect air pollution over individual cities as well as to locate where pollutants are being emitted, and so, identifying pollution hotspots. Such high resolution satellite remote sensing observations are extremely useful for diagnosing the impact of atmospheric constituents on a global scale, in particular, allowing detection of small-scale sources, and increasing the fraction of

cloud-free observations. However, the high spatial resolution of the state-of-the-art ACS results in very challenging data volumes to be processed – 240 TB (terabyte) per year of level-1 data.

In fact, the amount of satellite data increases faster than the computational power [4]. The remote sensing data is recognized as Big Data [5] since it satisfies Doug Laney's 3V criterion: significant growth in the volume, velocity and variety. New efficient techniques have to be developed for next generation atmospheric processors to cope with these high efficiency requirements.

The radiative transfer modelling (RTM) is the key component and the major performance bottle-neck in the atmospheric processors. Furthermore, the hyper-spectral RTMs involve a hierarchy of nested computational loops [6] as shown in the pseudo-code in Fig. 2. Recent surveys such as those provided by V. Natraj [7] and D. Efremenko et al. [8, 9] showed that a significant performance enhancement can be achieved by optimizing the framework in which the radiative transfer solver is called rather than accelerating the RTM solver itself. In fact, the efficiency of monochromatic radiative transfer solvers hardly

can be further improved [10]. Several attempts have been made to optimize loops over ground pixels and geometry (see, e.g., [11, 12, 13, 14] and references therein). Currently the loop over wavelengths (which expresses the hyper-spectral processing) remains the most computationally demanding part.

The essential part of the Big Data analysis is the dimensionality reduc-

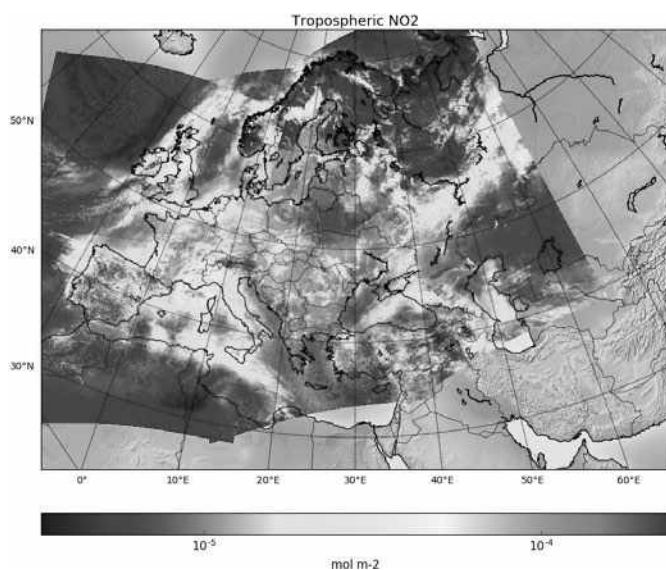


Fig. 1. Example of Sentinel-5P tropospheric nitrogen dioxide (NO₂) measurements on 1.04.2019 (data is freely available at <https://s5phub.copernicus.eu/dhus>)


```

for each ground pixel:
  for each wavelength: #<--loop for hyper-spectral processing
    for each geometry:
      call Radiative_transfer_solver;

```

Fig. 2. Hierarchy of computational loops, in which the radiative transfer solver is called

tion procedures which are related in the context of RTMs to the loop over wavelengths. The principal component analysis (PCA) is one of the famous representatives of them. PCA was proposed in 1901 by K. Pearson [15] and today has become an integral part of hyper-spectral RTMs.

In this regard, many efforts have been made to develop hyper-spectral RTMs which explicitly take into account the interdependency and statistical relations between level-1 and level-2 data [16]. The motivation of this survey is to present basic concepts of dimensionality reduction for design of atmospheric processors in a systematic way and to put in one context recent developments in this field.

2. DIMENSIONALITY REDUCTION

2.1. Heritage from the k -Distribution Technique

The techniques of dimensionality reduction in atmospheric science and astrophysics were preceded by methods which exploit a strong interdependency in the hyper-spectral data, although do not use PCA explicitly. Ambartsumian [17] noted that the transmission within a spectral interval does not depend on the line-by-line (LBL) variation of the absorption coefficient k with respect to wavelength λ , but rather on the distribution of absorption coefficient within the spectral interval. Such concept is called the k -distribution approach. It is based on the cumulative frequency distribution of k , namely, $G(k)$; as a matter of fact, the inverse distribution $k(G)$ is the k -distribution function. Since $G(k)$ is a smooth function and $k(\lambda)$ has a strong variation with respect to λ , it is beneficial from the numerical point of view to replace the integration in λ -space by that in G -space (less number of quadrature points for numerical integration is required). This method was extended by Goody et al. [18] to the cases of inhomogeneous atmosphere assuming that there is a correlation between k -distributions at different pressure levels, and that is the correlated- k distribution method. Other techniques (e.g. exponential sum fitting [19], spectral map-

ping [20], k -binning approach [21], opacity sampling method [22], multi-dimensional k -distribution method [23], and fast k -distribution models [24, 25]) use similar ideas although based on a more elaborative mathematical basis. In [26], a modification of the k -distribution technique was considered, in which the integration is performed in the original λ -space. In [27], an empirical procedure based on uniform spectral grids was proposed for choosing the most representative spectral points in LBL computations. Together, the studies related to the k -distribution function outline that the hyper-spectral radiances can be modelled by much fewer number of monochromatic computations than required by the LBL-framework, thereby providing a basis to dimensionality reduction of the problem.

2.2. Basic Concept of Dimensionality Reduction

In simple words, dimensionality reduction means representing the initial data set with less number of parameters than it is initially represented. It can be considered as one of the lossy data compression paradigms [28]. Dimensionality reduction is crucial for stable and high-performance processing of spectral measurements. It excludes redundant information from the initial dataset, reduces the number of independent parameters and improves the efficiency of machine learning.

There is a distinction between linear and non-linear techniques for dimensionality reduction. A more detailed review can be found in [29, 30, 31, 32] and references therein. Linear and non-linear techniques have been inter-compared in [33]. Results of these numerical experiments reveal that non-linear techniques perform well on selected artificial tasks. However, they hardly outperform PCA on real-world tasks. Similar conclusions were reported in [34], where several methods for dimensionality reduction were inter-compared in the context of accelerating radiative transfer performance. Bearing in mind that no obviously superior method has emerged in the benchmarking studies (increasingly time-consuming and sophisticated dimensionality

reduction techniques lead to more accurate results, and vice versa) our analysis will be limited with the classical PCA.

2.3. Principal Component Analysis

Although the dimensionality reduction techniques are well-known and covered by many statistical libraries (e.g., scikit-learn [35] for Python), we make a short mathematical exposition to put the above considerations in a proper context. For clarity, we specify sizes of matrices using the notation $\in \mathbb{R}^{\text{rows} \times \text{columns}}$. Let $\mathbf{y} = (y(\lambda_1), y(\lambda_2), \dots, y(\lambda_W))$, $\mathbf{y} \in R^{1 \times W}$, be a row-vector of atmospheric radiances at W wavelengths $\{\lambda_w\}_{w=1, \dots, W}$. A set of S spectra are assembled into a matrix $\mathbf{Y} \in R^{S \times W}$ whose i -th row is \mathbf{y}_i . Then, \mathbf{y}_i can be represented in a new basis system as follows:

$$\mathbf{y}_i = \bar{\mathbf{y}} + \sum_{k=1}^W t_{ik} \mathbf{f}_k.$$

Here, $\bar{\mathbf{y}} = \sum_{i=1}^S \mathbf{y}_i / S$, $\bar{\mathbf{y}} \in R^{1 \times W}$ is the sample mean of the spectra (the average spectrum), t_{ik} is the k^{th} coordinate of the vector \mathbf{y}_i in the new basis system and $\mathbf{f}_k = (f_k(\lambda_1), f_k(\lambda_2), \dots, f_k(\lambda_W)) \in R^{1 \times W}$ is the k^{th} basis vector. Noting that high-dimensional real data are often situated on or near a lower-dimensional manifold, the spectrum \mathbf{y}_i can be projected onto the K -dimensional subspace ($K < W$) as follows:

$$\mathbf{y}_i \approx \bar{\mathbf{y}} + \sum_{k=1}^K t_{ik} \mathbf{f}_k, \quad (1)$$

or in matrix form for the initial dataset:

$$\mathbf{Y} \approx \bar{\mathbf{Y}} + \mathbf{T}\mathbf{F},$$

where $\bar{\mathbf{Y}} = \{\bar{\mathbf{y}}, \dots, \bar{\mathbf{y}}\} \in R^{S \times W}$,

$\mathbf{F} = \{\mathbf{f}_1, \mathbf{f}_2, \dots, \mathbf{f}_K\}^T \in R^{K \times W}$, $\mathbf{T} \in R^{S \times K}$ is the matrix

whose entries are $\{t_{ik}\}_{i=1, \dots, S}^{k=1, \dots, K}$. Hereinafter the super-

script T stands for ‘‘transpose’’. The transformation (1) can be done using dimensionality reduc-

tion techniques, such as PCA [15]. In the latter, basic vectors \mathbf{f}_k in (1) are referred to as ‘‘principal components’’ (PCs) or empirical orthogonal functions (EOFs) and are taken as K eigenvectors related to the K most significant eigenvalues of the

covariance matrix $\text{cov}(\mathbf{Y}, \mathbf{Y}) \in R^{W \times W}$. The coordinates t_{ik} in the new coordinates system and the corresponding matrix \mathbf{T} are called ‘‘principal component scores’’.

3. PRINCIPAL COMPONENT-BASED RADIATIVE TRANSFER MODEL FOR HYPER-SPECTRAL SIGNALS

The most conceptually simple approach uses the training data set of spectra in order to establish a set of EOFs by using PCA and then to restore hyper-spectral signal in W spectral points by using K monochromatic radiances. Naturally, we have $K < W$.

The theory of PCA briefly discussed in the previous section reveals a linear relationship between PC scores and monochromatic radiances:

$$\mathbf{y}(\lambda) = \bar{\mathbf{y}}(\lambda) + t_1 \mathbf{f}_1(\lambda) + \dots + t_K \mathbf{f}_K(\lambda). \quad (2)$$

Hence, for a given set of K EOFs and K spectral points it is possible to obtain a closed linear system of K equations:

$$\begin{cases} \mathbf{y}(\lambda_1) = \bar{\mathbf{y}}(\lambda) + t_1 \mathbf{f}_1(\lambda_1) + \dots + t_K \mathbf{f}_K(\lambda_1), \\ \mathbf{y}(\lambda_2) = \bar{\mathbf{y}}(\lambda) + t_1 \mathbf{f}_1(\lambda_2) + \dots + t_K \mathbf{f}_K(\lambda_2), \\ \dots \\ \mathbf{y}(\lambda_K) = \bar{\mathbf{y}}(\lambda) + t_1 \mathbf{f}_1(\lambda_K) + \dots + t_K \mathbf{f}_K(\lambda_K). \end{cases} \quad (3)$$

The key point here is that the radiance values in K spectral points are represented through the same EOFs. Then, by solving (3) we obtain PC scores t_1, \dots, t_K , and, by using (2), the full spectrum in W spectral points can be readily restored.

This approach requires a set of precomputed EOFs which is derived from a training data set of simulated or measured spectra. Fig. 3 shows the example of the PCA applied to the dataset of spectra computed in the Hartley-Huggins band used for ozone retrieval. The data set consists of 10^5 spectra. The following parameters are varied for the generation of reflectance spectra: the solar zenith angle, the viewing zenith angle, the relative azimuthally

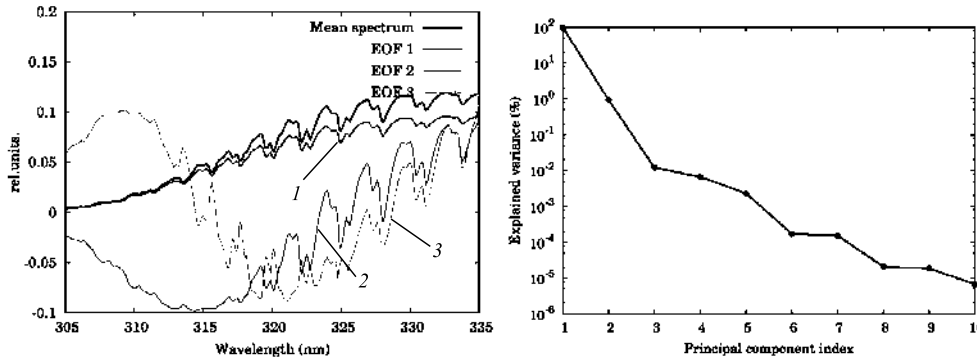


Fig. 3. (Left) Mean spectrum and first three empirical orthogonal functions computed in the Huggins band; (right) explained variance in percentage as a function of the principal component index

angle, the surface albedo, the ozone total column, the surface height, and the temperature. The right plot in Fig. 3 shows that almost 99.9 % of the variance in the data can be explained just with 5 principal components.

To obtain best efficiency, the parameters of this scheme, such as K and a set of chosen wavelengths, have to be tuned empirically. The number K depends on the desired level of variance to be captured by the principal components. Several semi-empirical rules have been proposed for the optimal number of principal components (e.g. the broken stick model [36]). However, there is no universal rule for the selection of K ; the choice is application-specific.

Regarding the choice of wavelengths, in [37] a method is proposed for selecting the location of monochromatic wavelengths by using a correlation function. In particular, this method involves the following steps:

- The correlation coefficients are computed for the radiance values and then converted to vector angles by an arccosine function;
- The spectral data is rearranged according to the magnitudes of the correlation coefficients;
- The monochromatic radiances are selected by choosing predictors with equal distances in the values of the correlation coefficients.

The schematic representation of the principal component-based hyper-spectral radiative transfer model is shown in Fig. 4. For the input data set containing optical parameters of the atmosphere for a set of wavelengths, the monochromatic radiative transfer solver is called. To obtain the most representative dataset, the smart sampling method [38] is recommended based on Halton sequences [39]. That produces a data set of spectra, which is divided into training data set and validation data set. By applying PCA and the correlation analysis to the training set, the system of EOFs is computed and a sub-

set of spectral points is chosen (spectral sampling), respectively. These two outputs are stored and used for computing PC scores for the validation data set. The spectra in the full wavelength range are restored using Eq. (2) and the error of this reconstruction can be estimated. If the error is larger than required, the number of generated spectra and the number of principal components) are increased. The main output of the training phase are empirical orthogonal functions and spectral sampling (marked with red in Fig. 4), which allow to process new data in the online phase (as shown in Fig. 5).

In [37], it was noted that the slit function convolution operator and the PCA are linear. Therefore the PC scores of the *convolved* spectra are linear functions of monochromatic radiances. Then at the training stage, the corresponding weighting factors of linear dependency are stored together with the system of EOFs and spectral sampling. Authors claim that for an infrared spectrum ranging from 650 cm^{-1} to 3000 cm^{-1} this representation for convolved spectra reduces the number of monochromatic computations from a few thousands to a few hundreds.

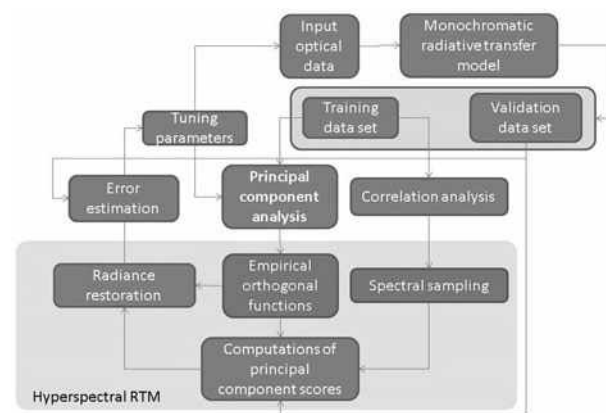


Fig. 4. Schematic representation of the PCA-based radiative transfer model with precomputed empirical orthogonal functions – offline phase



Fig. 5 The same as in Fig. 4, but online phase

The presented approach proved to be efficient and implemented in several packages (e.g. PCTRM [37], RTTOV [40] and others [41, 42]). The main drawback is that it requires time consuming computations of the training data set.

4. PRINCIPAL COMPONENT ANALYSIS IN THE FRAMEWORK OF DIFFERENTIAL OPTICAL ABSORPTION SPECTROSCOPY

In this section we consider the application of the PCA in the framework of the differential optical absorption spectroscopy (DOAS) [43]. DOAS is widely used to retrieve the trace gas content. The main advantages of this technique are the simplicity and robustness as it is able to filter out the influence of factors, which are not taken into account properly in the RTM. The main idea of DOAS consists in the fact that the absorption caused by gases leads to a strong spectral signatures in the spectral radiances, while the influence of multiple scattering and other factors is usually smooth in the wavelength space. Following [44], the radiance reflected by the atmosphere consisting of N_g gas species with absorption coefficients $\sigma_{abs,g}$ is represented using the weak absorption Beer-Lambert law as

$$\ln y(\lambda) = -\sum_{g=1}^{N_g} S_g \sigma_{abs,g}(\lambda) - P(\lambda) - RRS(\lambda), \quad (4)$$

where S_g is the number density of gas g along the optical path (also referred to as the slant column density), $P(\lambda)$ is the polynomial term which represents the impact of Rayleigh and aerosol/cloud scattering as well as the surface reflectance, while RRS is a term representing the rotational Raman scattering [45, 46]. In the conventional DOAS, S_g is retrieved through least squares fitting that minimizes the residual between the measured (left part of Eq. (4)) and simulated (right part of Eq. (4)) radiance spectra. Then S_g is converted into the vertical column density (Ω_g) through the air mass factor (AMF). The latter is computed at a single wavelength as-

suming a prescribed vertical profile of gas g [47, 48].

In [49] the modification of the DOAS approach was proposed for retrieving the SO_2 total column. The PCA is applied for the measured spectra in regions with no significant SO_2 , e.g. the equatorial Pacific:

$$\ln y(\lambda) = \overline{\ln y}(\lambda) + \sum_{i=1}^K t_i \mathbf{f}_i(\lambda). \quad (5)$$

In this way, the EOFs capture the variability of the data caused by physical processes (i.e. Rayleigh and Raman scattering and ozone absorption). In addition, the features of the instrument (e.g. the instrumental degradation, the slit function and measurement artefacts) are implicitly accounted for by EOFs. That is the training phase. Then, for polluted regions with SO_2 , representation (5) will produce a residual which is associated with SO_2 content. Thus,

$$\ln y(\lambda) = \overline{\ln y}(\lambda) + \sum_{i=1}^K t_i \mathbf{f}_i(\lambda) + \Omega_{SO_2} \frac{\partial \ln y(\lambda)}{\partial \Omega_{SO_2}}, \quad (6)$$

where Ω_{SO_2} is the SO_2 vertical column density. The derivative in the last term can be estimated either by finite differences or by using linearized radiative transfer models [50, 51]. Then Ω_{SO_2} can be readily retrieved from Eq. (6).

This method has been applied to the Ozone Monitoring Instrument (OMI) [52] data in the spectral range (310–340) nm. As the high order principal components represent the noise rather than a useful signal, the truncation over the principal components also acts as a filter. To reconstruct the spectral radiances, at least 20–30 principal components were required while in the presence of relatively strong SO_2 signals that number could be reduced to 8. Authors claim that the noise in the data was decreased by factor of 2 thereby providing greater sensitivity to anthropogenic sources of SO_2 .

So far, there are no reports of applying the similar approach to other trace gases. One reason for that is the difficulty of obtaining the system of EOFs for regions without a certain trace gas. The second reason is that, strictly speaking, representation (6) is approximate. For SO_2 it works correctly and the residual is associated with the SO_2 signal. For other trace gases representation (6) might be not valid and more elaborated approach is required.

5. DIMENSIONALITY REDUCTION IN RTMS WITH MACHINE LEARNING

5.1. General Consideration

Following [53], the inverse problem is solved by reducing it to an exercise in optimization. The main idea behind this method is to find the state vector that minimizes the residual between simulated data and measurements. A non-linear inverse problem is solved iteratively [54, 55]. Assuming an *a priori* state vector \mathbf{x} , a non-linear forward model is linearized about \mathbf{x} . Then, the linearized model can be easily inverted and a new estimation for the state vector can be found. This iterative approach is widely used for trace gases retrieval as well as for estimating aerosol and cloud properties [56]. However this inversion method is very time-consuming, due to repeated calls to complex radiative transfer forward models that simulate radiances and Jacobians (i.e. matrices of the first-order partial derivatives of spectral radiances with respect to \mathbf{x}), and subsequent inversion of relatively large matrices. These considerations motivate the development of alternative inversion techniques for remote sensing real-time applications, which are based on machine learning and therefore sometimes referred to as full-physics inverse learning machines (FP-ILM) [57].

5.2. The Concept of Learning Machines for Atmospheric Retrievals

Machine learning algorithms do not consider the optimization problem explicitly. Rather, they *learn* from a given dataset and make predictions regarding parameters of interest. Conceptually, the machine learning algorithm consists of a training phase, wherein the inversion operator is obtained using synthetic data generated by the radiative transfer model, which expresses the “full-physics” component, and an operational phase, in which the inversion operator is applied to real measurements. Here the main advantage over the classical optimization approach is that the time-consuming training phase involving complex radiative transfer modeling is performed off-line; the inverse operator itself is robust and computationally simple.

Fig. 6 is a schematic representation of the possible implementation of the learning machine. During the training phase, a training dataset is computed using a full-physics forward model, which

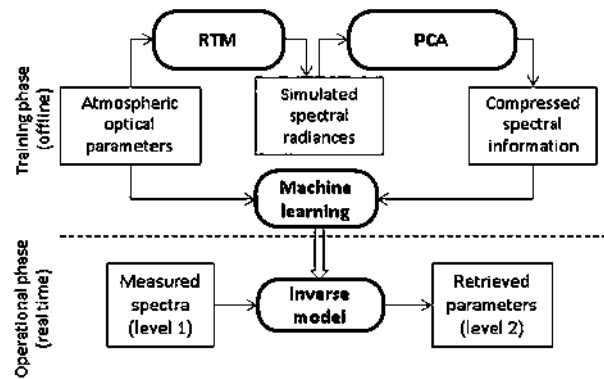


Fig. 6. Schematic representation of the machine learning retrieval algorithm which exploits the dimensionality reduction of the spectral radiances

in our case is the radiative transfer model. In order to capture the essential features of the simulated data and to avoid “over-dimensionality” (the so-called Hughes effect [58]), the simulated spectral data are compressed using an appropriate dimensionality-reduction technique. The mapping between the dimensionality-reduced spectral simulations and the parameter of interest is captured via machine learning.

5.3. Machine Learning Based on the Linear Regression Schemes

In the retrieval algorithms based on linear regression, the following representation for the retrieved parameter x is exploited:

$$x = c + \sum_{w=1}^W l_w y(\lambda_w),$$

where c is the linear offset and l_w are the regression coefficients. The principal component regression (PCR) method employs the linear regression model between x and the principal component scores of the spectral radiance:

$$x = c + \sum_{k=1}^K l_k t_k;$$

As $K \ll W$, the dimension of the linear regression model (and the corresponding inverse problem) is reduced. Moreover, since the instrument noise does not affect PC scores of low order, the whole inversion scheme is more stable.

For noisy data, the set of eigenvectors \mathbf{F} must be computed for the matrix $\mathbf{C}_Y + \mathbf{C}_e$, rather than for \mathbf{C}_Y , where \mathbf{C}_e is the noise covariance matrix. In this case, the PC scores for the noisy data are cor-

related and are therefore called “projected principal components” [59]. If the statistics of the noise is unknown, the noise covariance matrix can be estimated by making some assumptions (e.g., Gaussian noise) or by using the following approximation $\mathbf{C}_e \approx \alpha \mathbf{I}$, where \mathbf{I} is the identity matrix and α is the regularization parameter. This procedure reduces the impact of high-order principal components.

The kernel ridge regression (KRR) algorithm [60] generalizes the PCR method; KRR has been used for predicting atmospheric profiles from the IASI (the infrared atmospheric sounding interferometer) instrument [61]. One drawback of the PCR and KRR models is that the basis vectors \mathbf{F} characterize the measurements \mathbf{Y} , while information contained in \mathbf{X} is not taken into account. An alternative model that gets round this drawback is the partial least squares regression (PLSR) [62]. In [62, 64], it was shown that PLSR leads to model-fitting with fewer PCs than required with PCR. In its turn, the PLSR approach can be generalized to the case when we are retrieving a set of correlated parameters (e.g., the temperature profile) rather than a single variable x . The corresponding method is then referred to as canonical correlations [65]. The use of canonical correlations in atmospheric sciences applications is summarized in [66].

The approach based on the PCR has been successfully applied for solving the problems of volcanic plume-height retrieval from GOME-2 [67] and TROPOMI measurements [68], as well as CO₂ retrieval from GOSAT measurements [69, 70].

6. DIMENSIONALITY REDUCTION OF INPUT OPTICAL DATA

6.1. Spectra Simulation

An efficient technique using the dimensionality reduction of the optical data has been proposed in [71]. This method relies on the local linearization of the radiative transfer model with respect to input parameters using finite differences. To reduce the number of radiative transfer model calls for estimating finite difference values, the linearization is done in the reduced data space. The method can be summarized as follows. We introduce a correction function as follows:

$$Q(\lambda_w) = \ln[y(\lambda_w)/y_a(\lambda_w)]. \quad (7)$$

Here y is the radiance computed with a full radiative transfer model, while y_a is the radiance computed with an approximate model (e.g., the two-stream model). Then, for the atmosphere consisting of L layers, we consider a state vector $\mathbf{x}_w \in R^{2L+1}$ containing optical parameters for all layers, i.e.,

$$\mathbf{x}_w^T = \begin{bmatrix} \sigma_{\text{abs},1}(\lambda_w), \dots, \sigma_{\text{abs},L}(\lambda_w), \\ \sigma_{\text{sct},1}(\lambda_w), \dots, \sigma_{\text{sct},L}(\lambda_w), \rho(\lambda_w) \end{bmatrix},$$

where $\sigma_{\text{sct},i}$ and $\sigma_{\text{abs},i}$ are the scattering coefficient and the absorption coefficient in the i^{th} layer, respectively, while ρ is the surface albedo. Thus, the wavelength variability of the optical parameters, representing the radiative transfer code input parameters, is encapsulated in the vector \mathbf{x}_w . Note, that the phase function is assumed to be constant within a given spectral interval and therefore not included in the vector \mathbf{x}_w . By applying the PCA to $\{\mathbf{x}_w\}_{w=1}^W$, we obtain

$$\mathbf{x}_w \approx \bar{\mathbf{x}} + \sum_{k=1}^K t_{wk} \mathbf{f}_k, \quad \bar{\mathbf{x}} = (1/W) \sum_{w=1}^W \mathbf{x}_w.$$

Fig. 7 shows the results of PCA for input optical data in the Huggins band (315–335 nm) and O2A band (755–775 nm). Optical data is taken from [72]. Note that four principal components are sufficient to capture 99.9 % variability of the datasets.

Now, let us assume that $Q(\mathbf{x}_w)$ can be approximated sufficiently well by its Taylor expansion around $\bar{\mathbf{x}}$, that is,

$$\begin{aligned} Q(\mathbf{x}_w) &\approx Q(\bar{\mathbf{x}} + \Delta \mathbf{x}_w) \approx \\ &\approx Q(\bar{\mathbf{x}}) + \Delta \mathbf{x}_w^T \nabla Q(\bar{\mathbf{x}}) + \frac{1}{2} \Delta \mathbf{x}_w^T \nabla^2 Q(\bar{\mathbf{x}}) \Delta \mathbf{x}_w, \end{aligned} \quad (8)$$

where ∇Q and $\nabla^2 Q$ are the gradient and the Hessian of Q , respectively. By using central differences to approximate the first and the second-order directional derivatives in (8), we obtain

$$\begin{aligned} Q(\mathbf{x}_w) &\approx Q(\bar{\mathbf{x}}) + \frac{1}{2} \sum_{k=1}^K \left[Q(\bar{\mathbf{x}} + \mathbf{f}_k) - Q(\bar{\mathbf{x}} - \mathbf{f}_k) \right] t_{wk} \\ &\quad + \frac{1}{2} \sum_{k=1}^K \left[Q(\bar{\mathbf{x}} + \mathbf{f}_k) - 2Q(\bar{\mathbf{x}}) + Q(\bar{\mathbf{x}} - \mathbf{f}_k) \right] t_{wk}^2. \end{aligned} \quad (9)$$

From (9) and (7) it is apparent that the computation of the correction factor requires $2K + 1$ calls of the full- and two-stream models. Note that if we estimated the correction function using finite differences in the initial data space, that would require $2L + 1$ calls of the full- and two-stream models. As a result and taking into account that usually $K \ll L$, we are led to a substantial reduction of the computational time.

This approach has been applied for simulating the spectra in the O2A band [71], the Huggins band [34], and CO₂ bands [73, 74]. Kopparla et al [75] applied the similar approach for modelling the radiances in the UV/Vis/NIR spectral range (0.3–3000) nm. In all cases authors reported that the root mean square errors of the computed radiances are of order 0.01 %, yet achieving almost a 10-fold increase in speed. The big advantage of this method is that unlike previously considered techniques, this one does not require precomputed databases of spectra.

In [76], the efficiency of input and output space dimensionality reduction techniques was analyzed for simulating the Hartley-Huggins band. The hybrid usage of these techniques was proposed. The output space reduction and the spectral sampling methods are applied to the two-stream solution by using corresponding lookup tables, while multi-stream solution computations are performed within the input data reduction framework, described in this Section. It was found that the combined use of these techniques yields accuracy better than 0.05 % while the speedup factor is about 20.

6.2. Retrieval in the Reduced Input Data Space

Since the atmospheric retrieval problem is severely ill-posed, a physically correct result can be obtained only by using a regularization procedure. The latter takes into account some *a priori* information. In this context, dimensionality reduction of the input data space can be regarded as a special type of regularization, i.e. the retrieved parameters should obey a certain dependency reproduced by a chosen set of EOFs.

Timofeyev et al. [77] applied the dimensionality reduction technique to parameterize the aerosol extinction coefficient for incorporation into the inversion algorithm, in which the corresponding PC scores rather than aerosol extinction dependence were retrieved. The system of EOFs was defined for

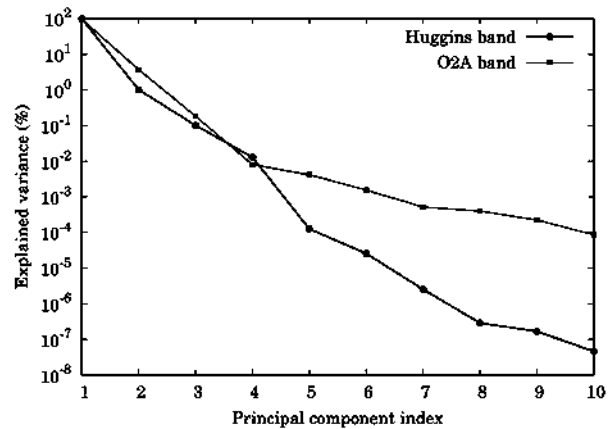


Fig. 7. The explained variance in percentage as a function of the principal component index in the Huggins band and the O2A band

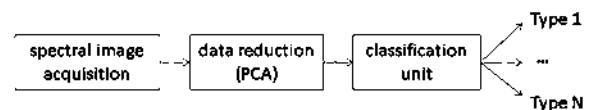


Fig. 8. A schematic representation of the PCA-based classification algorithms applied to the hyperspectral data

a dataset of aerosol extinction coefficients computed on the base of Mie theory [78] and algorithms for particle ensembles. Finally, in [79] the dimensionality reduction is performed in the input (temperature and humidity profiles) and output spaces (spectral radiances), while artificial neural networks are used to establish the interdependency between PC scores. Since the number of independent parameters is reduced, such scheme is more robust and efficient than the conventional one.

7. DIMENSIONALITY REDUCTION OF HYPER-SPECTRAL DATA IN CLASSIFICATION PROBLEMS

Dimensionality reduction plays an important role in classification algorithms applied to the hyper-spectral data. On-line anomaly detection and object recognition in remote sensing imagery is extremely important for forest fire and volcanic activity monitoring. In such kind of applications we are confronted with the classification problem. In a reduced data space, the number of variables used in classification is smaller, yet their value is higher than that in the original space. Therefore, the classification algorithms (e.g. K -nearest neighbour) are more robust and efficient [80, 81]. PCA can be used to visualize the hyper-spectral

data on a 2D plane, thereby identifying regions with certain features. The concept of combined usage of PCA with classifiers is illustrated in Fig. 8. Such an approach is used not only in space-borne data processing, but also in other fields, such as material science [82, 83], tobacco industry [84] and food production [85].

8. CONCLUSIONS

In this review, several techniques of hyper-spectral data processing have been considered. They are all based on the dimensionality reduction procedure. It has been shown that the principal component analysis can be utilized in several ways for hyper-spectral modelling. Therefore it seems that the nomenclature “PCA-based radiative transfer model” is not appropriate since it does not characterize the specific features of the algorithm (e.g., papers [40, 49, 75] present absolutely different models, although all of them are “PCA-based”).

It has been shown that the concept of dimensionality reduction gives the framework for formulating hyper-spectral RTM that directly takes into account a strong interdependency in the hyper-spectral data. Further research needs to examine more closely how to combine techniques outlined in this review. For instance in [86], a hybrid approach comprising the correlated- k method and the dimensionality reduction of the input data has been described. Such models are extremely important for processing remote sensing Big Data in the current missions, and becoming a mainstream in the development of next generation atmospheric processors.

The discussed principles of data reduction of hyper-spectral data are generic and can be applied in various applications, including material science and electron spectroscopy due to the similar methodologies adopted in these fields [87]. In addition, PCA is a perspective tool for analysing hyper-spectral optical data in medicine. In particular, recent studies have shown that the dimensionality reduction of data cubes can improve the recognition and classification algorithms, which would be extremely important for optical early disease diagnostics [88].

ACKNOWLEDGEMENTS

The authors are grateful to the Editor-in-Chief of the journal “Light and Engineering” professor

Vladimir P. Budak for inviting to write this survey, as well as to the anonymous reviewer for careful reading of the manuscript and valuable suggestions.

REFERENCES

1. D.G. Loyola, S. Gimeno Garcia, R. Lutz, A. Argyrouli, F. Romahn, R.J.D. Spurr, M. Pedernana, A. Doicu, V. Molina Garcá, and O. Schüssler. The operational cloud retrieval algorithms from TROPOMI on board Sentinel-5 precursor. *Atmospheric Measurement Techniques*, 2018,11(1), pp.409–427.
2. C.A. Lee, S.D. Gasster, A. Plaza, C. Chang, and B. Huang. Recent developments in high performance computing for remote sensing: A review. *IEEE Journal of Selected Topics in Applied Earth Observations and Remote Sensing*, 20114(3), pp.508–527.
3. J.P. Veefkind, I. Aben, K. McMullan, H. Forster, J. de Vries, G. Otter, J. Claas, H.J. Eskes, J.F. de Haan, Q. Kleipool, and et al. TROPOMI on the ESA Sentinel-5 Precursor: A GMES mission for global observations of the atmospheric composition for climate, air quality and ozone layer applications. *Remote Sensing of Environment*, 2012, 120, pp.70–83.
4. Y. Ma, H. Wu, L. Wang, B. Huang, R. Ranjan, A. Zomaya, and W. Jie. Remote sensing big data computing: Challenges and opportunities. *Future Generation Computer Systems*, 2015, 51, pp.47–60.
5. P. Liu. A survey of remote-sensing big data. *Frontiers in Environmental Science*, 2015, 3, 45p.
6. V.M. Roozendael, R. Spurr, D. Loyola, C. Lerot, D. Balis, J.C. Lambert, W. Zimmer, J. Gent, J. Van Geffen, M.E. Koukouli, J. Granville, A. Doicu, C. Fayt, and C. Zehner. Sixteen years of GOME/ERS2 total ozone data: the new direct-fitting GOME Data Processor (GDP) Version 5: I. algorithm description. *J Geophys Res: Atmospheres*, 2012,117: D03305, pp.1–18.
7. V. Natraj. A review of fast radiative transfer techniques. In A.A. Kokhanovsky, editor, *Light scattering reviews*, volume 8, pages 475–504. Springer Berlin Heidelberg, 2013.
8. D. Efremenko, A. Doicu, D. Loyola, and T. Trautmann. Acceleration techniques for the discrete ordinate method. *J Quant Spectrosc Radiat Transfer*, 2013,114, pp.73–81.
9. D.S. Efremenko, D. Loyola, A. Doicu, and T. Trautmann. Data-intensive computing in radiative transfer modelling. In P. Soille and P.G. Marchetti, editors, *Proc. of the 2016 conference on Big Data from Space (BiDS16)*, Santa Cruz de Tenerife, Spain, 2016, pp. 188–191.

10. V.P. Budak, G.A. Kaloshin, O.V. Shagalov, and V.S. Zheltov. Numerical modeling of the radiative transfer in a turbid medium using the synthetic iteration. *Opt. Express*, 23(15): A829, 2015.
11. D.S. Efremenko, D.G. Loyola, A. Doicu, and R.J.D. Spurr. Multi-core-CPU and GPU-accelerated radiative transfer models based on the discrete ordinate method. *Computer Physics Communications*, 2014, 185(12), pp.3079–3089.
12. D.S. Efremenko, D. Loyola, R.J.D. Spurr, and A. Doicu. Acceleration of radiative transfer model calculations for the retrieval of trace gases under cloudy conditions. *J Quant Spectrosc Radiat Transfer*, 2014,135, pp.58–65.
13. R.J.D. Spurr. VLIDORT: A linearized pseudo-spherical vector discrete ordinate radiative transfer code for forward model and retrieval studies in multilayer multiple scattering media. *J Quant Spectrosc Radiat Transfer*, 2006, 102(2), pp.316–342.
14. R.J.D. Spurr, T.P. Kurosu, and K.V. Chance. A linearized discrete ordinate radiative transfer model for atmospheric remote-sensing retrieval. *J Quant Spectrosc Radiat Transfer*, 2001, 68(6), pp.689–735.
15. K. Pearson. On lines and planes of closest fit to systems of points in space. *Phil Mag*, 19012, 6, pp.559–572.
16. R. D. Morris, A. Kottas, M. Taddy, R. Furfaro, and B.D. Ganapol. A statistical framework for the sensitivity analysis of radiative transfer models. *IEEE Transactions on Geoscience and Remote Sensing*, 2008,46(12), pp.4062–4074.
17. V.A. Ambartzumyan. The effect of the absorption lines on the radiative equilibrium of the outer layers of the stars. *Publ. Obs. Astron. Univ. Leningrad*, 1936, 6, pp.7–18.
18. R.M. Goody, R. West, L. Chen, and D. Crisp. The correlated k-method for radiation calculations in nonhomogeneous atmosphere. *J Quant Spectrosc Radiat Transfer*, 1989, 42, 6, pp.539–550.
19. W.J. Wiscombe and J.W. Evans. Exponential-sum fitting of radiative transmission functions. *J Comput Phys*, 1997, 24, 4, pp.416–444.
20. R. West, D. Crisp, and L. Chen. Mapping transformations for broadband atmospheric radiation calculation. *J Quant Spectrosc Radiat Transfer*, 1990, 43,3, pp.191–199.
21. E. Boesche, P. Stammes, R. Preusker, R. Benartz, W. Knap, and J. Fischer. Polarization of skylight in the O2A band: effects of aerosol properties. *Applied Optics*, 2008, 47, 19, p. 3467.
22. Christiane Helling and Uffe Grae Jorgensen. Optimizing the opacity sampling method. *Astronomy and Astrophysics*, 1998, 337, pp.477–486.
23. Frédéric André, Longfeng Hou, Maxime Roger, and Rodolphe Vaillon. The multispectral gas radiation modeling: A new theoretical framework based on a multidimensional approach to k-distribution methods. *Journal of Quantitative Spectroscopy and Radiative Transfer*, 2014,147, pp.178–195.
24. Boris A. Fomin. A k-distribution technique for radiative transfer simulation in inhomogeneous atmosphere: 1. FKDM, fast k-distribution model for the longwave. *Journal of Geophysical Research*, 109(D2), 2004.
25. Boris Fomin. A k-distribution technique for radiative transfer simulation in inhomogeneous atmosphere: 2. FKDM, fast k-distribution model for the shortwave. *Journal of Geophysical Research*, 110(D2), 2005.
26. V. A. Falaleeva and B.A. Fomin. Overcoming spectroscopic challenges in direct problems of satellite sounding of the atmosphere. *Atmospheric and Oceanic Optics*, 2017, 30(1), pp.1–6.
27. B.A. Fomin. Effective interpolation technique for line-by-line calculations of radiation absorption in gases. *Journal of Quantitative Spectroscopy and Radiative Transfer*, 1995, 53(6), pp.663–669.
28. S. Najmabadi, P. Offenhäuser, M. Hamann, G. Jajnabalkya, F. Hempert, C. Glass, and S. Simon. Analyzing the effect and performance of lossy compression on aeroacoustic simulation of gas injector. *Computation*, 2017, 5(4):24.
29. S.T. Roweis and L.K. Saul. Nonlinear dimensionality reduction by locally linear embedding. *Science*, 2000, 290(22), pp.2323–2326.
30. M.A. Kramer. Nonlinear principal component analysis using autoassociative neural networks. *AIChE Journal*, 1991, 37(2), pp.233–243.
31. A.N. Gorban, B. Kégl, D.C. Wunsch, and A.Y. Zinovyev, editors. *Principal Manifolds for Data Visualization and Dimension Reduction*. Springer Berlin Heidelberg, 2008.
32. I.K. Fodor. *A Survey of Dimension Reduction Techniques*. Office of Scientific and Technical Information (OSTI), 2002.
33. L.J.P. van der Maaten, E.O. Postma, and H.J. van den Herik. *Dimensionality Reduction: A Comparative Review*. Tilburg University Technical Report, TiCC-TR2009–005, 2009.
34. D.S. Efremenko, A. Doicu, D. Loyola, and T. Trautmann. Optical property dimensionality reduction techniques for accelerated radiative transfer performance: Application to remote sensing total ozone re-

- trievals. *J Quant Spectrosc Radiat Transfer*, 2014, 133, pp.128–135.
35. F. Pedregosa, G. Varoquaux, A. Gramfort, V. Michel, B. Thirion, O. Grisel, M. Blondel, P. Prettenhofer, R. Weiss, V. Dubourg, J. Vanderplas, A. Passos, D. Cournapeau, M. Brucher, M. Perrot, and E. Duchesnay. Scikit-learn: Machine learning in Python. *Journal of Machine Learning Research*, 2011,12, pp.2825–2830.
36. Robert H. MacArthur. On the relative abundance of bird species. *Proc Natl Acad Sci USA*, 1957, 43(3), pp.293–295.
37. X Liu, W.L. Smith, D.K. Zhou, and A. Larar. Principal component-based radiative transfer model for hyperspectral sensors: theoretical concept. *Applied Optics*, 2006, 45(1), pp.201–208.
38. D. G. Loyola, M. Pedernana, and S. Gimeno Garcia. Smart sampling and incremental function learning for very large high dimensional data. *Neural Networks*, 2016, 78, pp.75–87.
39. J. H. Halton. Algorithm 247: Radical-inverse quasi-random point sequence. *Commun ACM*, 1964, 7(12), pp.701–702.
40. M. Matricardi. A principal component based version of the RTTOV fast radiative transfer model. *Quarterly Journal of the Royal Meteorological Society*, 2010, 136, pp.1823–1835.
41. P. D. Hurley, S. Oliver, D. Farrah, L. Wang, and A. Efstathiou. Principal component analysis and radiative transfer modelling of Spitzer Infrared spectrograph spectra of ultraluminous infrared galaxies. *Monthly Notices of the Royal Astronomical Society*, 2012, 424(3), pp.2069–2078.
42. A. Hollstein and R. Lindstrot. Fast reconstruction of hyperspectral radiative transfer simulations by using small spectral subsets: application to the oxygen A band. *Atmospheric Measurement Techniques*, 2014, 7(2), pp.599–607.
43. U. Platt. Differential optical absorption spectroscopy (DOAS). *Chem Anal Series*, 1994, 127, pp.27–83.
44. U. Platt and J. Stutz. *Differential Optical Absorption Spectroscopy: Principles and Applications*. Springer-Verlag, Berlin, Heidelberg, 2008.
45. G.W. Kattawar, A.T. Young, and T.J. Humphreys. Inelastic scattering in planetary atmospheres. I. The Ring effect, without aerosols. *Astrophys J*, 1981, 243, pp.1049–1057.
46. M. Vountas, V.V. Rozanov, and J.P. Burrows. Ring effect: Impact of rotational Raman scattering on radiative transfer in earth's atmosphere. *J Quant Spectrosc Radiat Transfer*, 1998, 60(6), pp.943–961.
47. James Slusser, Kyle Hammond, Arve Kylling, Knut Stamnes, Lori Perliski, Arne Dahlback, Donald Anderson, and Robert DeMajistre. Comparison of air mass computations. *Journal of Geophysical Research: Atmospheres*, 1996,101(D5), pp. 9315–9321.
48. Lori M. Perliski and Susan Solomon. On the evaluation of air mass factors for atmospheric near-ultraviolet and visible absorption spectroscopy. *Journal of Geophysical Research*, 1993, 98(D6), p.10363.
49. Can Li, Joanna Joiner, Nickolay A. Krotkov, and Pawan K. Bhartia. A fast and sensitive new satellite SO₂ retrieval algorithm based on principal component analysis: Application to the ozone monitoring instrument. *Geophysical Research Letters*, 2013, 40(23), pp. 6314–6318.
50. R.J.D. Spurr. LIDORT and VLIDORT. Linearized pseudo-spherical scalar and vector discrete ordinate radiative transfer models for use in remote sensing retrieval problems. In A.A. Kokhanovsky, editor, *Light scattering reviews*, 2008, V. 3, pp. 229–275.
51. A. Doicu and T. Trautmann. Two linearization methods for atmospheric remote sensing. *J Quant Spectrosc Radiat Transfer*, 2009, 110(8), pp. 477–490.
52. P.F. Levelt, G.H.J. van den Oord, M.R. Dobber, A. Malkki, Huib Visser, Johan de Vries, P. Stammes, J.O.V. Lundell, and H. Saari. The ozone monitoring instrument. *IEEE Transactions on Geoscience and Remote Sensing*, 2006, 44(5), pp.1093–1101.
53. A.N. Tikhonov and V.Y. Arsenin. *Solution of Ill-Posed Problems*. Winston, 1977.
54. C.D. Rodgers. *Inverse methods for atmospheric sounding: Theory and Practice*. World Scientific Publishing, 2000.
55. A. Doicu, T. Trautmann, and F. Schreier. *Numerical Regularization for Atmospheric Inverse Problems*. Springer, 2010.
56. D. S. Efremenko, O. Schüssler, A. Doicu, and D. Loyola. A stochastic cloud model for cloud and ozone retrievals from UV measurements. *J Quant Spectrosc Radiat Transfer*, November 2016,184, pp.167–179.
57. J. Xu, O. Schussler, D.G. Loyola Rodriguez, F. Romahn, and A. Doicu. A novel ozone profile shape retrieval using full-physics inverse learning machine (FP-ILM). *IEEE Journal of Selected Topics in Applied Earth Observations and Remote Sensing*, 2017, 10(12), pp.5442–5457.
58. G. Hughes. On the mean accuracy of statistical pattern recognizers. *IEEE Trans. Inform. Theory*, 1968, 14(1), pp.55–63.
59. W.J. Blackwell and F.W. Chen. *Neural Networks in Atmospheric Remote Sensing*. Lexington, 2009.

60. John Shawe-Taylor and Nello Cristianini. *Kernel Methods for Pattern Analysis*. Cambridge University Press, New York, NY, USA, 2004.
61. G. Camps-Valls, J. Munoz-Mari, L. Gomez-Chova, L. Guanter, and X. Calbet. Nonlinear statistical retrieval of atmospheric profiles from MetOp-IASI and MTG-IRS infrared sounding data. *IEEE Transactions on Geoscience and Remote Sensing*, May 2012 50(5), pp.1759–1769.
62. Roman Rosipal and Nicole Krämer. Overview and recent advances in partial least squares. In *Subspace, Latent Structure and Feature Selection*, pages 34–51. Springer Science + Business Media, 2006.
63. Peter D. Wentzell and Lorenzo Vega Montoto. Comparison of principal components regression and partial least squares regression through generic simulations of complex mixtures. *Chemometrics and Intelligent Laboratory Systems*, 2003, 65(2), pp.257–279.
64. Saikat Maitra and Jun Yan. Principal component analysis and partial least squares: Two dimension reduction techniques for regression. In *Discussion Papers: 2008 Discussion Paper Program – Applying Multivariate Statistical Models*, 2008, pp.79–90, Casualty actuarial society.
65. H. Hotelling. The most predictable criterion. *Journal of Educational Psychology*, 1935, 26, pp.139–142.
66. D. Wilks. *Statistical Methods in the Atmospheric Sciences, 3rd Edition*. New York: Elsevier, 2011.
67. D.S. Efremenko, D.G. Loyola R., P. Hedelt, and R.J.D. Spurr. Volcanic SO₂ plume height retrieval from UV sensors using a full-physics inverse learning machine algorithm. *International Journal of Remote Sensing*, 2017, 38(sup1), pp.1–27.
68. Pascal Hedelt, Dmitry S. Efremenko, Diego G. Loyola, Robert Spurr, and Lieven Clarisse. SO₂ layer height retrieval from Sentinel-5 Precursor/TROPOMI using FP_ILM. *Atmospheric Measurement Techniques Discussions*, Feb. 2019, pp.1–23.
69. M.Yu. Kataev, A.K. Lukyanov, and A.A. Bekerov. Modification of the empirical orthogonal functions method for solving the inverse task of retrieving of the CO₂ total content from satellite data. *Journal of Siberian Federal University. Engineering & Technologies*, 2018,11(1), pp.77–85.
70. M.Y. Kataev and A.K. Lukyanov. Empirical orthogonal functions and its modification in the task of retrieving of the total amount CO₂ and CH₄ with help of satellite Fourier transform spectrometer GOSAT (TANSO-FTS). In G.G. Matvienko and O.A. Romanovskii, editors, *22nd International Symposium on Atmospheric and Ocean Optics: Atmospheric Physics*. SPIE-Intl Soc Optical Eng, 2016.
71. V. Natraj, X. Jiang, R.L. Shia, X. Huang, J.S. Margolis, and Y.L. Yung. Application of the principal component analysis to high spectral resolution radiative transfer: A case study of the O₂A-band. *J Quant Spectrosc Radiat Transfer*, 2005, 95(4), pp.539–556.
72. I.E. Gordon, L.S. Rothman, C. Hill, R.V. Kochanov, Y. Tan, P.F. Bernath, M. Birk, V. Boudon, A. Campargue, K.V. Chance, B.J. Drouin, J.-M. Flaud, R.R. Gamache, J.T. Hodges, D. Jacquemart, V.I. Perevalov, A. Perrin, K.P. Shine, M.-A.H. Smith, J. Tennyson, G.C. Toon, H. Tran, V.G. Tyuterev, A. Barbe, A.G. Császár, V.M. Devi, T. Furtenbacher, J.J. Harrison, J.-M. Hartmann, A. Jolly, T.J. Johnson, T. Karman, I. Kleiner, A.A. Kyuberis, J. Loos, O.M. Lyulin, S.T. Massie, S.N. Mikhailenko, N. Moazzen-Ahmadi, H.S.P. Müller, O.V. Naumenko, A.V. Nikitin, O.L. Polyansky, M. Rey, M. Rotger, S.W. Sharpe, K. Sung, E. Starikova, S.A. Tashkun, J. Vander Auwera, G. Wagner, J. Wilzewski, P. Wcislo, S. Yu, and E.J. Zak. The HITRAN2016 molecular spectroscopic database. *Journal of Quantitative Spectroscopy and Radiative Transfer*, 2017, 203, pp.3–69.
73. P. Somkuti, H. Boesch, V. Natraj, and P. Koppa. Application of a PCA-based fast radiative transfer model to XCO₂ retrievals in the shortwave infrared. *Journal of Geophysical Research: Atmospheres*, 122(19), pp.10,477–10,496.
74. V. Natraj, R.L. Shia, and Y.L. Yung. On the use of principal component analysis to speed up radiative transfer calculations. *J Quant Spectrosc Radiat Transfer*, 2010, 111(5), pp.810–816.
75. P. Koppa, V. Natraj, R. Spurr, R. Shia, D. Crisp, and Y.L. Yung. A fast and accurate PCA based radiative transfer model: Extension to the broadband shortwave region. *Journal of Quantitative Spectroscopy and Radiative Transfer*, 2016, 173, pp. 65–71.
76. Ana del Águila, Dmitry Efremenko, Víctor Molina García, and Jian Xu. Analysis of two dimensionality reduction techniques for fast simulation of the spectral radiances in the Hartley-Huggins band. *Atmosphere*, Mar. 2019,10(3), p.142.
77. Y. Timofeyev, A. Polyakov, H. Steele, and M. Newchurch. Optimal eigenanalysis for the treatment of aerosols in the retrieval of atmospheric composition from transmission measurements. *Appl. Opt.*, July 2003,42 (15), p.2635.
78. G. Mie. Beitrage zur optik trueber medien, speziell kolloidaler metalloesungen. *Annalen der Physik*, 1908, 330(3), pp.377–445.

79. A. V. Polyakov, Yu.M. Timofeev, and Ya.A. Viro-lainen. Using artificial neural networks in the temperature and humidity sounding of the atmosphere. *Izvestiya, Atmospheric and Oceanic Physics*, 2014, 50(3), pp.330–336.
80. Michael T. Eismann, Joseph Meola, and Rus-sell C. Hardie. Hyperspectral change detection in the presence of diurnal and seasonal variations. *IEEE Transactions on Geoscience and Remote Sensing*, 2008, 46(1), pp. 237–249.
81. Dandan Ma, Yuan Yuan, and Qi Wang. Hyper-spectral anomaly detection via discriminative feature learning with multiple-dictionary sparse representation. *Remote Sensing*, May 2018,10(5), p.745.
82. David B Brough, Daniel Wheeler, and Surya R. Kalidindi. Materials knowledge systems in python – a data science framework for accelerated development of hierarchical materials. *Integrating Mate-rials and Manufacturing Innovation*, Mar.2017, 6(1), pp. 36–53.
83. Sai Kiranmayee Samudrala, Prasanna Venkatara-man Balachandran, Jaroslaw Zola, Krishna Rajan, and Baskar Ganapathysubramanian. A software framework for data dimensionality reduction: application to chemical crystallography. *Integrating Materials and Manufacturing Innovation*, 3(1), Jun. 2014.
84. Pilar B. Garcá-Allende, Olga M. Conde, Ana M. Cubillas, César Jáuregui, and José M. López-Higuera. New raw material discrimination system based on a spatial optical spectroscopy technique. *Sensors and Actuators A: Physical*, Apr. 2007, 135(2), pp. 605–612.
85. Juan Xing, Cédric Bravo, Pál T. Jancsó, Herman Ramon, and Josse De Baerdemaeker. Detecting bruises on ‘golden delicious’ apples using hyperspectral imaging with multiple wavebands. *Biosystems Engineering*, Jan 2005, 90(1), pp.27–36.
86. V. Molina García, S. Sasi, D.S. Efremenko, A. Doicu, and D. Loyola. Radiative transfer models for retrieval of cloud parameters from EPIC/DSCOVR measurements. *Journal of Quantitative Spectroscopy and Ra-diative Transfer*, 2018, 213, pp. 228–240.
87. V.P. Afanas’ev, V.P. Budak, D.S. Efremenko, and P.S. Kaplya. Application of the photometric theory of the radiance field in the problems of electron scattering. *Light & Engineering*, 2019, 27(2), pp. 88–96.
88. F. Vasefi, N. MacKinnon, and D.L. Farkas. Hyper-spectral and multispectral imaging in dermatology. In *Imaging in Dermatology*, Elsevier, 2016, pp. 187–201.



Ana del Águila

graduated in Physics from the Granada University (UGR) in 2015. From 2016-2018 she worked as an early-stage researcher at the National Institute for Aerospace Technology (INTA) in Spain. At present, she is doing the Ph.D. in the German Aerospace Centre (DLR) with a DAAD/DLR scholarship. Her scientific interests are in-situ atmospheric aerosols, lidar systems, remote sensing, radiate transfer and Big Data analysis



Dmitry S. Efremenko

graduated from the Moscow Power Engineering institute (MPEI) in 2009. He received his Ph.D. degree from the Moscow State University in 2011 and the habilitation degree from MPEI in 2017. Since 2011 he works as a research scientist at the German Aerospace Centre (DLR). His scientific interests include radiate transfer, remote sensing, and Big Data analysis



Thomas Trautmann,

Prof., Dr., graduated with a diploma in meteorology at the Johannes Gutenberg University at Mainz (JGU) in 1985. From the JGU he received a Ph.D. degree in 1989, a habilitation degree in 1997, and in 2003 he was appointed as applicant Prof. at the University of Leipzig. Since 2003 he works as head of department Atmospheric Processors at the German Aerospace Center (DLR). His scientific interests include radiate transfer, electromagnetic scattering and atmospheric remote sensing

HYPER SPECTROMETER BASED ON AN ACOUSTO-OPTIC TUNABLE FILTERS FOR UAVS

Vitold E. Pozhar^{1,2}, Alexander S. Machikhin^{1,3}, Maxim I. Gaponov², Sergei V. Shirokov¹,
Mikhail M. Mazur⁴ and Alexei E. Sheryshev⁵

¹*Scientific and Technological Centre of Unique Instrumentation of the Russian Academy of Sciences;*

²*Bauman Moscow State Technical University;*

³*Moscow Power Engineering Institute;*

⁴*VNIIFTRI (Russian Research Institute of Physical Technical and Radio Engineering Measurements)*

⁵*MAI (Moscow Aviation Institute)*

E-mail: vitold@ntcup.ru

ABSTRACT

The problem of creating a hyper spectral opto-electronic system for observing natural and artificial objects by means of unmanned aerial vehicles (UAV) is considered. The structure and composition of the system that solves this problem are described. It is based on acousto-optic filters. The results of laboratory testing of the hyper spectrometer are presented.

Keywords: hyper spectral imaging, tuneable acousto-optic filters, remote sensing

Hyper spectral systems (HS), providing synchronous registration of spectral data and its spatial distribution, have a high potential for application in the field of earth surface monitoring, natural resources and economic activity [1–2]. Systems and methods that can provide optical information from a particular location at a particular time are now becoming increasingly valuable. The location of the recording system on the aircraft is most effective for regular and operational monitoring of land plots. The use of compact UAVs for hyper spectrometer basing increases the mobility of the system and allows obtaining data more quickly [3–4].

To date, a variety of schemes and designs of hyper spectral imaging systems have been developed.

According to the principle of spectral selection they can be divided into two large classes:

- Systems with spatial decomposition of the spectrum;
- Systems that have an optical filter (monochromator) that is tuneable by wavelength.

However, the developed systems don't yet adequately meet all the requirements for UAV devices. These requirements can be conditionally divided into several groups, such as physical (image registration in a wide spectral range with a large number of spatially solvable elements in the frame at two coordinates with a minimum level of aberrations), structural (sufficiently small overall dimensions and energy consumption, resistance to external influences), and methodical (the possibility of obtaining information about the objects under study in real time).

The approach based on the spatial decomposition of the spectrum is difficult to realize on the UAV platform, since it requires uniform rectilinear motion. Therefore, for such devices a tuneable monochromator is preferable capable of registering spectrally contrasting images of objects. Methods of rapid analysis of incoming optical information are necessary for the operational decision on the further actions of the system, in particular, on the trajectory of the UAV. Selective spectral data recording tools

can be particularly effective. They can be implemented on the basis of tuneable acousto-optic (AO) filters [5], providing fast and arbitrary spectral access, which allow flexible selection of the spectrum of the recorded information.

The composition and structure of a HS, the features and characteristics of its key element (AO filter), the principles of its operation and the results of laboratory testing are described below.

SYSTEM STRUCTURE

A double compact AO monochromator is used in the developed hyper spectrometer as a spectral element [6]. It consists of two identical AO cells, deployed by 180° , which provides compensation for the majority of spatial-spectral distortions [7]. In each of these cells the incoming luminous flux is polarized by reflecting it from one of the faces of the anisotropic TeO_2 crystal. This scheme without a polarizer makes the design of the monochromator simpler and allows reducing light losses during the passage of polarizer.

The optical scheme of the developed AO hyper spectrometer is presented in Fig. 1. The radiation from the object under study 1 is directed by means of the telephoto lens 2 to the input of the AO monochromator. The beam splitter 3, which remove 10 % of the radiation to the colour video camera 5, is installed in front of it. The monochromator consists of two identical non-collinear rotated 180° cells 6 and 8 and the polarizer 7 located between them.

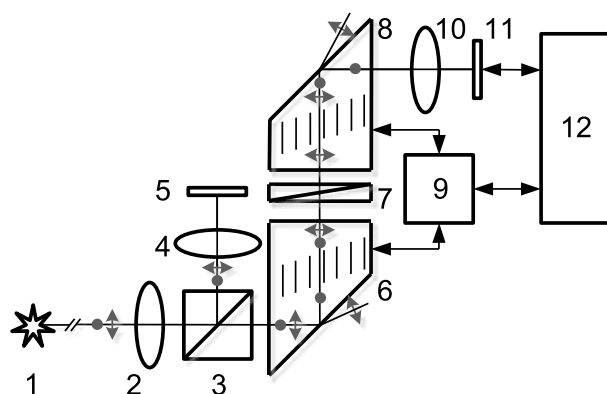


Fig. 1. Block diagram of the AO hyper spectrometer: 1 – object under study; 2 – input lens; 3 – light splitter; 4, 10 – lenses; 5 – colour video camera; 6, 8 – AO cells; 7 – polarizer; 9 – control unit (generator); 11 – monochrome video camera; 12 – computer; light polarization is indicated on the rays, and ultrasonic diffraction gratings are depicted in AO cells

tween them. On the oblique face of cell 6 the input stream is divided by polarization. Further, the optical radiation, whose wavelength corresponds with the exact fulfilment of synchronism conditions, diffracts on the lattice created by the acoustic wave. As a result, the polarization of the radiation changes the orientation. The radiation of other wavelengths passes through the AO cell without changes and is cut off by the polarizer 7. Similarly, in the AO cell 8 the light diffraction repeats with the polarization change, which provides additional radiation filtration. The selection of the filtered radiation takes place on the oblique face of the cell 8. Then it is focused by the lens 10 on the sensor of the monochrome video camera 11. It is possible to reconstruct the diffraction gratings period and to obtain an image of the object at an arbitrarily given wavelength by changing the frequency of acoustic waves using a high-frequency generator located in the control unit 9. The signal from the video camera 11 enters the computer, where it is processed with the help of specialized software and archived for further analysis by other methods.

The main elements of the hyper spectral system are shown in Fig. 2. They have the following characteristics: the spectral range is (450–850) nm; the bandwidth is $\Delta\lambda = 5$ nm at the wavelength $\lambda = 633$ nm, which corresponds to the transmission window at optical frequencies 100 cm^{-1} and approximately 100 wavelength-resolvable channels; the transmittance is 60 % (at the wavelength 633 nm); the entrance pupil is 8 mm; the field of view is $3^\circ \times 3^\circ$; the spatial resolution is 600×500 elements; the power consumption is not more than 5 W; the weight of the system operating part (with optics but without the

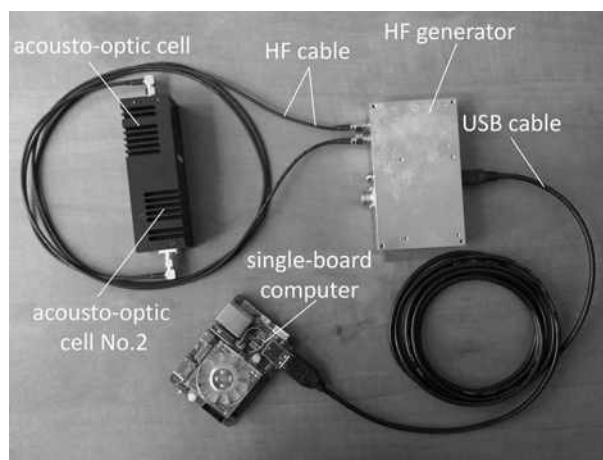


Fig. 2. Basic elements of the hyper spectrometer model

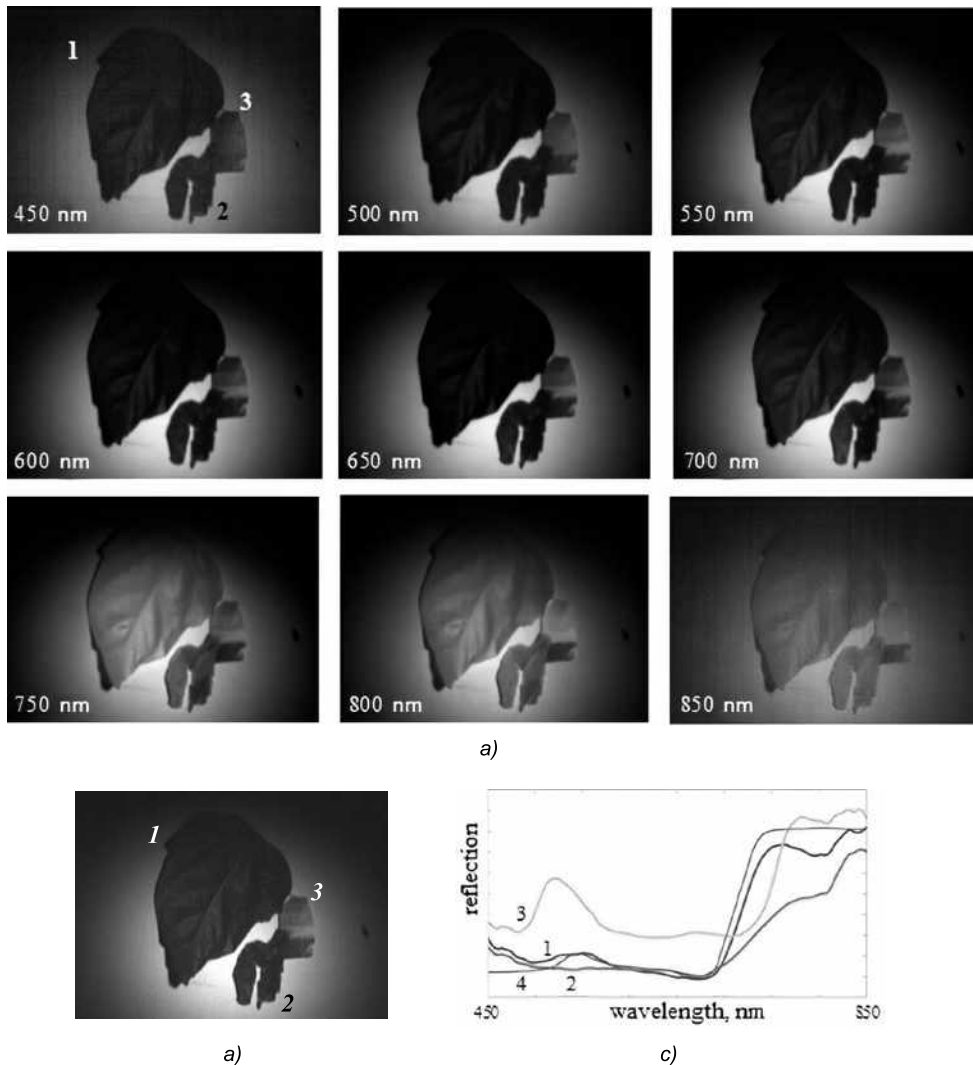


Fig. 3. Registered images of objects: green geranium leaf (1), kelp (2), green cardboard (3): spectral (a) and black-and-white (b) images, as well as reflection spectra (b) determined from spectral images in comparison with poplar leaf (4), [16]

computer) is 1.2 kg; the length is 20 cm; the control is performed by USB2.0.

The characteristics of the system are generally not worse than those of other systems of a similar purpose based on the diffraction grating [8–9], including using prisms [10], based on a Fabry-Perot interferometer [11], based on a Fourier-transform spectrometer [12] and on a multispectral (“multi-aperture”) matrix detector [13]. Such systems have the following characteristics: the spectral range is $I_{\max}/I_{\min}=1.5\text{--}2.5$; the number of spectral channels is from several tens to several hundreds and the number of solvable elements by angle (space) is 100–1000. At the same time, their mass and power consumption are not lower than those of the AO system: (1–10) kg and (10–20) W. Some systems have a wide operating range, for example, HYDICE and AVIRIS have $(0.4\text{--}2.5)\ \mu\text{m}$, and substantially

include a set of devices having a total mass more than 300 kg and power consumption more than 100 W [14, 15]. Thus, the hyper spectrometer based on the AO filter is one of the most effective technical solutions suitable for UAVs.

TESTING

Two plant objects (fresh leaf of tree and dried kelp) and one artificial (a piece of painted cardboard) were chosen for comparison. The things had a close colour shade – green. Registration of spectral images of these objects and determination of their spectral characteristics were made to illustrate the performance of the hyper spectrometer model. Fig. 3 shows the spectral images of these objects in the wavelength range from 450 nm to 850 nm in 50 nm steps with a halogen lamp illumination.

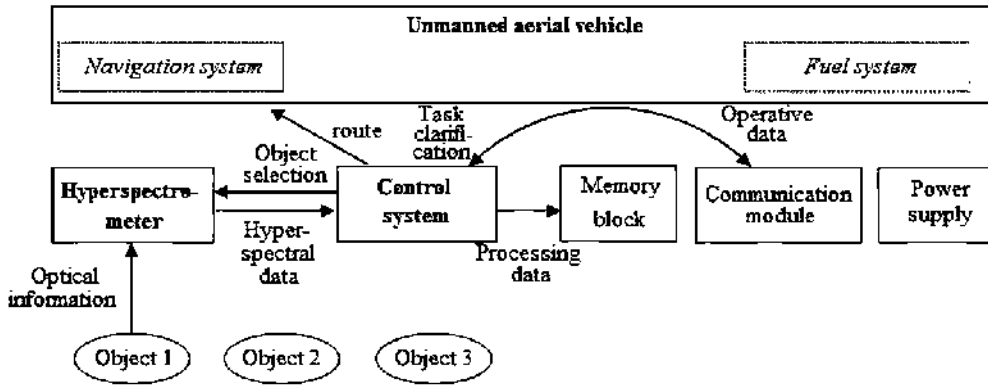


Fig. 4. Control scheme for a UAV with a hyper spectrometer

The mutual contrast of the object elements at different wavelengths varies significantly. For comparison, Fig. 3, b shows the image obtained by the same monochrome camera without the AO filter (wide-band image). The obtained hyper spectral data made it possible to identify reflection spectra (Fig. 3c), the general form of which is consistent with the reference data [16–17].

SYSTEM OPERATION PRINCIPLES

The main task of the system is the implementation of personalized hyper spectral monitoring. This means that the object under study and the type of task are determined directly by the user of the system and can be changed considerably from case to case. To do this, it is necessary to provide the possibility of clarifying or even changing the task directly during the flight. Accordingly, all elements of the system must be manageable and customizable. Such a system can contain the following three main modules: 1) a platform that provides its movement and positioning in space; 2) a hyper spectrometer that collects optical information; 3) the control device that forms the task execution algorithm in accordance with the given goal, and also taking into account the received information and the current situation. In addition, the system can have additional modules, for example, a communication module, an information storage unit and other devices that perform specialized functions. However, when the system is based on the UAV, neither the amount of available memory and computing resources, nor the bandwidth of the communication channel allow to completely process the flow of spectral information that the hyper spectrometer can provide, and therefore it is necessary to ensure the effective selection of useful information for obtaining real-time monitoring results.

The main principles on which the described system should be built, designed to solve various tasks based on the hyper spectral imaging, are the following: flexibility, manageability, the ability to quickly perform the analysis of recorded data, the ability to work in an autonomous mode and quickly reorient to other tasks. In the future, the system can be made adaptive, that is, quickly and independently reacting to the situation change.

To realize this concept, the carrier must be compact and easily manageable and allow various types of motion. The hyper spectrometer and control device must consume a minimum amount of resources.

This corresponds to a technical solution in the form of a compact multicopter and an image spectrometer based on controlled AO filters.

The multicopter is able to provide movement at various (even sufficiently low) speed, as well as modes of hovering and controlling the height of observation. The hyper spectrometer based on AO filters allows to implement an arbitrary spectral imaging algorithm: with any step in the spectrum, any sequence of wavelengths, varying exposure and varying spatial resolution, determined by observation height, angular field of view and the number of solvable positions.

The main tasks that the hyper spectrometer should solve: objects detection, their selection, identification, state control. For this purpose, however, effective methods of spectral-spatial distribution analysis should be developed and implemented in the form of software modules. One of the key approaches is the reduction of the full array of hyper-spectral data, which requires both a long recording time and large computing powers, to a minimally necessary set of data, namely, a set of spectral images obtained at the most informative wavelengths from the point of view of the problem being solved. Such an approach realizes the method of fragmen-

tary spectral registration, formulated and substantiated earlier for problems of this type [18].

The control device can be implemented on the basis of a compact computer that performs several hierarchically ordered functions: from controlling the AO monochromator and processing of hyperspectral data to analyzing the situation and making decisions, including those relating to the trajectory and flight mode. Control commands must be transferred to all elements of the system, including a separate independent flight management tool. The entire task must be divided by the control device into stages, each of which contains a description of the movement type, the measurement (observation) mode, the task of analysis and possible reactions of the system. When going to the next stage, all information received at the current moment should be taken into account, and therefore the task can be executed in different scenarios (branching algorithm).

The scheme of data exchange between the main components of the developed HS is shown in Fig. 4.

CONCLUSION

The developed hyper spectral device has physical and technical properties that make it possible to use it effectively on UAVs: compact size, low power consumption, the possibility of simultaneously obtaining spectral and colour images in a wide enough range of wavelengths (450–850) nm with high spectral (~5 nm) and spatial (600–500 elements) resolution, as well as compensation of chromatic aberrations. It enables recognition of images, both in spectrum and in the form of elements in the mode of their spectral contrast. In the future, it is planned to test it on site and implement real-time object recognition algorithms.

ACKNOWLEDGEMENT

This work was supported by the RFBR grant No. 16–29–11802 ofi_m. The equipment of the Scientific and Technological Centre of Unique Instrumentation of RAS was used in the work.

REFERENCES

1. Chang C.. Hyperspectral imaging: Techniques for spectral detection and classification // Springer Science & Business Media, 2003. 370 p.
2. Shaw G.A., Burke H.K. Spectral imaging for remote sensing // Lincoln Laboratory Journal. 2003, V. 14(1), pp. 3–26.
3. Bubion L., Miller P., Hayden A.. Comparison of AOTF, grating, and FTS imaging spectrometers for hyperspectral remote sensing applications // Proc. SPIE, 2000. V. 4049. № 239.
4. Gaponov M., Machikhin A., Pozhar V., Shurygin A.. Acousto-optical imaging spectrometer for unmanned aerial vehicles // Proc. SPIE, 2017. V. 10466. № 104661V.
5. Mazur M.M., Pozhar V.E. Spektrometry na akustoopticheskikh fil'trah [Spectrometers based on acousto-optic filters] // Measurement techniques. 2015, № 9. pp. 29–33.
6. Mazur M.M., Mazur L.I., Pustovojt V.I., Sudenok U.A., Shorin V.N. Svetosil'nyj dvuhkristal'nyj akustoopticheskij monohromator [High-transmission two-crystal acousto-optic monochromator] // Pis'ma v zhurnal tekhnicheskoy fiziki, 2017, T. 87, V. 9, pp. 1399–1402.
7. Machikhin A.C., Pozhar V.E. Prostranstvenno-spektral'nye iskazheniya izobrazheniya pri difrakcii obyknovenno polyarizovannogo svetovogo puchka na ul'trazvukovoj volne [Spatial-spectral image distortions in the diffraction of an ordinarily polarized light beam on an ultrasonic wave] // Kvantovaya Elektronika, 2015, T. 45, № 2, pp. 161–165.
8. Wu H., Haibach F.G., Bergles E., Qian J., Zhang Ch., Yang W.. Miniaturized handheld hyperspectral imager // Proc. SPIE, 2014. V. 9101, 91010W.
9. Rodionov I., Rodionov A., Vedeshin A., Vinogradov A., Egorov V., Kalinin A.. Bortovye giperspektral'nye sistemy dlya resheniya zadach distancionnogo zondirovaniya [Onboard hyperspectral systems for solving remote sensing problems] // Issledovanie Zemli iz Kosmosa. 2013, № 6, pp. 81–93.
10. Hu P., Lu Q., Shu R., Wang J.. An airborne pushbroom hyperspectral imager with wide field of view // Chinese optics letters, 2005, V. 3, № 12, pp. 689–691.
11. Saari H., Pölonen I., Salo H., et al.. Miniaturized hyperspectral imager calibration and UAV flight campaigns // 2013, Proc. SPIE. V. 8889, 88891O.
12. Lucey P.G., Akagi J.T., Hinrichs J.L., Crites S.T., Wright R.. A long-wave infrared hyperspectral sensor for Shadow class UAVs // Proc. SPIE, 2013. V. 8713, 87130D.
13. Downing J., Harvey A.R.. Multi-aperture hyperspectral imaging // OSA Technical Digest (online) (Optical Society of America, 2013) <https://doi.org/10.1364/AIO.2013.JW2B.2>

14. Mitchell P.A. Hyperspectral digital imagery collection experiment HYDICE // Proc. SPIE.1995, V. 2587, pp. 70–95.

15. <https://aviris.jpl.nasa.gov/aviris> (2018).

16. Gates D.M., Keegan H.J., Schleter J.C., Weidner V.R.. Spectral Properties of Plants // Applied Optics. 1965, V. 4(1), p. 11.

17. Uhl F., Bartsch I., Oppelt N.. Submerged Kelp Detection with Hyperspectral Data // Remote Sensing. 2016, V. 8(6), p. 487.

18. Fadeyev A.V., Pozhar V.E., Pustovoit V.I. The principle of fragmentary spectrum registration for acousto-optical spectrometers based on differential optical absorption spectroscopy // Proc. SPIE, 2013. V. 8890, 88900H.



Vitold E. Pozhar,
Prof., Dr. of phys.-math. sciences, graduated from the Moscow Institute of Physics and Technology (MIPT, Dolgoprudny, Moscow region) in 1981. He is the head of the Department of the

Scientific and Technological Centre of Unique Instrumentation of the Russian Academy of Sciences, a Professor at the Bauman Moscow State Technical University and at National Research Nuclear University



Sergei V. Shirokov,
graduated from the Department of Oceanography of the Kant Baltic Federal University, worked at the Baltic fleet hydrography branch, Southern Federal University (SFU), Papanin

Institute for Biology of Inland Waters of RAS, Krasnodarberegozashchita. At present time, he is a science secretary assistant in SFU and scientific researcher at the Scientific and Technological Centre of Unique Instrumentation of the Russian Academy of Sciences



Alexander S. Machikhin
Ph.D. of phys.-math. sciences, graduated from the Bauman Moscow State Technical University in 2007. He is the leading researcher of Scientific and Technological Centre

of Unique Instrumentation of the Russian Academy of Sciences and an Assistant Professor at the National Research University “Moscow Power Engineering Institute”



Mikhail M. Mazur
Dr. of phys.-math. sciences, graduated from the Moscow Institute of Physics and Technology (MIPT, Dolgoprudny, Moscow region) in 1970. At present time, he is the Head of a laboratory

in the Institute of Physical Technical and Radio Engineering Measurements (Mendeleevo, Moscow region)



Maksim I. Gaponov,
bachelor, graduated from the Bauman Moscow State Technical University in 2016. At present time, he is working on his master thesis at the Bauman Moscow State Technical University



Alexei E. Sheryshev
Ph.D. of technical science, graduated from the Tsiolkovskii Moscow State Aviation Technological University. At present time, he is a Professor at the Moscow State Technical University

of Civil Aviation and an Associate Professor at the National Research University “MAI”

DOUBLE BEAM SPECTROPHOTOMETER FOR SIMULTANEOUS MEASUREMENT OF THE UPWELLING SEA RADIANCE AND THE INCIDENT SEA IRRADIANCE

Michael Young-gon Lee and Sergei V. Fedorov

Marine Hydrophysical Institute of the Russian Academy of Science, Sevastopol
Email: michael.lee.mhi@gmail.com

ABSTRACT

The article describes the structure and the operation principle of the spectrophotometer developed on the basis of a compact rapid monochromator with one input port and two output ports and a radiometric unit where upwelling radiation radiance and sea surface irradiance channels are located. A new approach to measurements of spectral characteristics of upwelling radiation of sea based on combination of advantages of a double beam photometer with a photomultiplier and a direct-reading photometer with a high-stability silicon photodiode for its absolute adjustment in energy units is implemented.

Keywords: marine desk spectrophotometer, instrumental measurements, spectral radiance factor

1. INTRODUCTION

The main parameter of water quality monitoring from outer space is spectral radiance factor of water layer $R_{rs}(\lambda)$ (SRFWL) determined by spectral radiance concentration (SRC) of upwelling radiation at upper boundary of the atmosphere measured by spectral radiometers of ocean colour satellite scanners. SRC is a secondary optical characteristic of waters and depends on features of marine water and irradiation of water surface [1]:

$$R_{rs}(\lambda) = \frac{L_w(\lambda, 0^+)}{E_d(\lambda, 0^+)}, \quad (1)$$

$$L_{wN}(\lambda) = R_{rs}(\lambda) \cdot F_0(\lambda), \quad (2)$$

where $L_w(\lambda, 0^+)$ is the SRC of upwelling water layer; $E_d(\lambda, 0^+)$ is the spectral irradiance concentration (SIC) on the sea surface; 0^+ shows that the parameter is measured directly above the sea surface; $L_{wN}(\lambda)$ is the normalised SRC of upwelling water layer; $F_0(\lambda)$ is the SIC from the Sun on the outer boundary of Earth atmosphere (at average distance between the Earth and the Sun).

Using SRF values, both primary optical characteristics of water and content of optically active components (phytoplankton pigments, dissolved organic matter and mineral particles) can be defined. This became possible due to development of semi-analytical and empirical algorithms which establish relation between one or several bio-optical characteristics and SRF or normalised SRC of upwelling sea water. Enhancement of these algorithms, in turn, is related to performance of field measurement requiring application of highly precise spectrophotometers.

In-situ measurements are required also for validation of upwelling water layers values SRC obtained on the basis of satellite data. The procedure of concordance of the latter with the values obtained in actual conditions is an important and mandatory element of remote sensing of ocean from space [2, 3], which requires large-scale sub-satellite measurements.

The sea truth (sub-satellite) measurements are performed using stationary platforms, buoy stations

and vessels [4–9]. The measurements performed using stationary platforms are capable to provide long dynamic series of data for one area, usually in waters with optical properties varying insufficiently, which is important for compensational adjustment of satellite data. The vessel measurements, on the contrary, are required for short-term measurements in the waters of seas and oceans with optical properties varying significantly. That is why they are extremely important for development of bio-optical algorithms.

The existing contact methods are based on measurements of SRC upwelling water layers (UWL) directly above or under the sea surface [4–10]. Each of them has its own advantages and disadvantages. The vessel spectrophotometers most often apply the method of measurement of UWL SRC directly above the sea surface. The total sea SRC $L_{tot}(\lambda)$ measured in this case is a sum of UWL SRC ($L_w(\lambda, 0^+)$) and spectral concentration (SC) of the sky radiation reflected by the sea. To separate these components, the device should contain two relevant optical channels and the third one for measurement of SIC on the sea surface [7–10].

In foreign practice, three identical spectrophotometers simultaneously measuring the total SRC of the sea, the SRC of sky radiation and SIC of the sea surface are used for vessel measurements [7–9]. In this case, there is a disadvantage due to necessity of absolute calibration of each optical channel which is hard to be performed with high precision both in conditions of expedition and in stationary metrology laboratories due non-availability of relevant spectral radiation standards.

Russian practice applies vessel photometers measuring total SRC of the sea, SRC of sky radiation and sea surface SIC alternately (with high frequency) by means of one photo detector (PMT) via different optical channels [11]. The disadvantage of this method is low precision of absolute measurements of the said values in wide ranges of their magnitudes. This is caused by the fact that, first, the signals of radiance and irradiance channels differ from each other by one or two orders of magnitude, and second, depending on the illuminance conditions (clouds, sunny day), these signals may be changed by several orders of magnitude, and these changes may occur simultaneously and several times in the course of measurement. So, high precision absolute measurement of two spectral magnitudes by the PMT, highly depending on illumination conditions,

is difficult because of necessity to maintain continuity of PMT sensitivity for a long period of time. Moreover, definition of absolute values requires separate calibration of each optical channel and, as mentioned above, impossibility to obtain more precise calibration in conditions of expedition, which lowers precision of measurements.

Application of a differential photometer [12] measuring SRFWL allows to increase precision of measurements significantly since it does not require absolute optical channels calibration and provides optimal conditions for operation of PMT. But in order to validate SRC upwelling sea water layer, which is defined by using satellite data, and for a number of application tasks, it is also important to know absolute values of SRC for upwelling sea layer and SIC for sea surface apart from SRFWL.

This article proposes a new approach to measurements of spectral characteristics of upwelling radiation of sea based on combination of advantages of a double beam differential photometer with a photomultiplier as a photo detector [12] and a direct-reading photometer with a high-stability silicon photodiode for its absolute calibration in energy units. The structure of a marine desk multifunctional spectrophotometer (MDMS) based on the proposed approach allowing measurements both SRFWL and absolute values of sea surface SIC, which are used for recovery of absolute values of upwelling sea water layers SRC, is described.

2. THE STRUCTURE OF THE MARINE SHIP-BASED MULTIFUNCTIONAL SPECTROPHOTOMETER

MDMS (Fig. 1) contains a photometric unit installed on the slit of the M150 monochromator and a photoelectric module (Fig. 2).

The photometric unit (Fig. 2) contains two optical channels for measurement of upwelling sea water layers SRC and sea surface SIC respectively. The first one is made in the form of an optical head 4 consisting of a lens 3 and a mirror 5 deflecting radiation beam by 90° . The focal distance of the lens 3 is 180 mm and it is determined by the selected structure of the photometric unit; the lens is made of KV fused quartz glass with high transparency within the whole set spectral range of (350–800) nm. The diameter of the lens, 54 mm, is calculated with consideration of necessity of concordance be-

tween the angle of view of the sea radiance channel and the monochromator relative aperture. For the purpose of mounting convenience, the mirror 5 is made in the form of an ellipse with axial dimensions of 52×74.5 mm and of fused quartz glass too. The optical head 4 is capable to be rotated so that it provides SRC measurements of upwelling water layer and sky radiation SRC between nadir and zenith. For this purpose, the optical head is mounted on the cover 8 of the body of the photometric unit by means of a rotary joint 6 with a waterproof gasket 7. The rotating structure of the optical head also allows it to select the area of sea surface free of sun glares in the course of measurements.

The SIC sea surface measurements channel (Fig. 2) consists of a flat cosine collector 2 and of a glare shield 13. Without taking additional measures, at high radiation angles of incidence (exceeding 60°), due to relation between the reflectance factor of the flat surface of the collector and this angle, distortion of cosine distribution of the measured signal occurs. Due to this fact, the relevant recommendations of [13] were taken into account in design of the cosine collector (Fig. 3). The mounting seat for the cosine collector is a socket on the body of the photometric unit, which forms the required angle of view equal to 85° and provides the height of the collector above the body equal to 2 mm. The cosine collector itself is a disk with diameter of 38 mm and thickness of 3 mm made of MS-13 frosted glass glued together with a disk made of KV fused quartz with diameter of 40 mm and thickness of 3 mm. By means of this disk, the collector is mounted to the body of the photometric unit leak-proof. Such structure of the collector provides formation of spatial characteristic with inaccuracy not exceeding 8% [13].

By means of the rotating modulator 10 three beams get into the monochromator from the SRC of upwelling water layers and SIC of sea surface channels by turns at high speed: one from the SRC channel and two others from the SIC channel (Fig. 2). The modulator 10 is a disk with gaps and sectors made of dark polished glass 16. Reflective coating is applied to surfaces of the polished sectors. This makes the radiation from the irradiance collector reflect in the form of two beams with one of them reflecting from the polish surface of the sector and the other one reflecting from the reflective coating, which multiplies intensity of the second beam by many times. The modulator 10 is rotated by micro



Fig. 1. Exterior of the marine desk-based multifunctional spectrophotometer (MDMS)

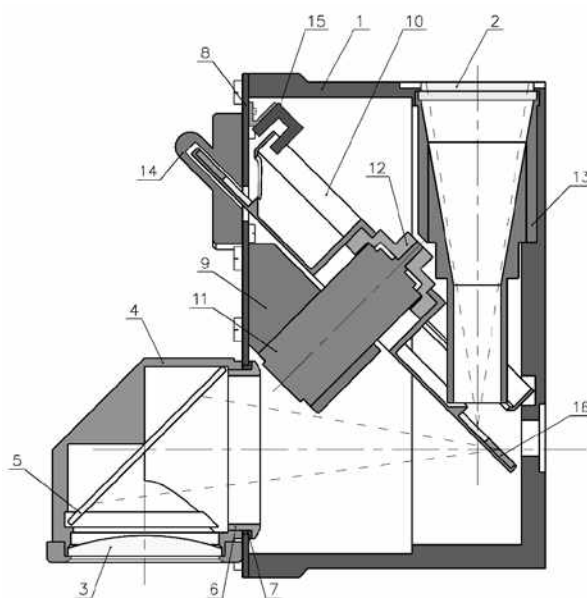


Fig. 2. Structure of the radiometric unit of MDMS

electric motor 11 (DC hollow anchor collector motor DPR-42-F1-03 type and motor speed 4500 rotations/min). This motor has an important distinction for marine field devices, as it is designed for continuous operation and has a long service life. On the inside of the body cover 8, there is a photon-coupled pair 15, which generates synchronous impulses at the moment each beam gets into the input port of M150 monochromator. Outside the cover part of the modulator 10 is protected by a waterproof casing 14.

For elimination of background illumination, the case 1 of the photometric unit and all plastic parts are made of black graphite-filled caprolon and the modulator 11 and all other parts made of duralumin are blacking by galvanizing.

The photometric unit is mounted on the input port of the universal compact M150 monochromator-spectrograph manufactured by SOLAR LS

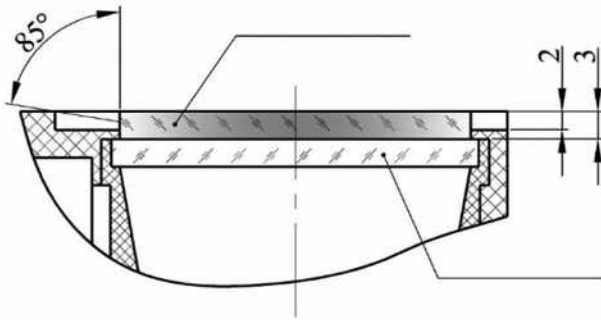


Fig. 3. Structure of the flat cosine collector of MDMS

[14]. M150 contains one input port and two output ports. The entrance slit is automatic, blades opening width is controlled by means of the device software. Both exit slits are equipped with precision focusing devices and superfine adjustment of the width of exit slits is performed manually by means of micro screws.

As shown in Fig. 4, both direct sun radiation and radiation diffused by sky get into the cosine collector 1 of the sea surface SIC channel. Inside the body of the photometric module, the radiation from the cosine collector 1 moves along the glare shield (item 13 in Fig. 2) and gets on the mirror sector 5 via the relevant slit of the modulator 4. The upwelling radiation from the sea gets on the plano-convex lens 2 of the radiance channel. The optical head of the radiance channel is capable to rotate around the body of the photometric module, which allows directing it to the area of sea surface free of sun glares. The radiation beam from the plano-convex lens 2 (shown by three arrows) is redirected by an elliptical flat mirror 3 and, after passing the relevant slit of the modulator 4, is focused in the relevant part of the entrance slit of the monochromator 7.

The modulator 4 inclined at angle of 45° alternately directs the radiation beams through the gaps in the 90° sector from the said optical channels to the entrance slit of the monochromator 7. The photon-coupled pair (item 15 in Fig. 2) generates synchronous impulses at the moment each beam gets into the slit. Opposite to the modulator slit, through which the beam from the SIC sea surface channel goes, there is a reflective sector 5 (made of dark glass) divided into two parts: the upper one with frontal reflective coating and with reflectance 98 % and the lower one without coating and with reflectance about 5 %. The radiation beam from the SIC channel is divided into two beams after being reflected from the reflective sector: the upper

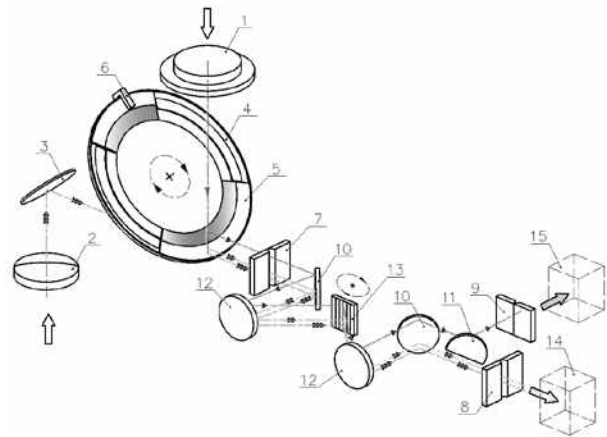


Fig. 4. Optical scheme of MSMS

one, more intensive (shown with one arrow) and the lower one, with intensity less by order of magnitude (shown with two arrows) each of which is redirected to the relevant part of the entrance slit of the monochromator 7. Additionally, in order to divide the beams from the SIC channel into the upper one and the lower one, there is a thin light-dividing plate (not shown) opposite the entrance slit of the monochromator 7.

The lower beam from the SIC channel is aligned with the optical axis of the beam from the SRC channel by the lower part of the reflective sector 5 (for convenience, these beams are dislocated in relation to each other in Fig. 4). These beams are alternately directed to the exit slit 8 of the monochromator where they get into the photoelectronic unit with PMT 10 thus implementing the scheme of the double beam photometer with one photo detector. After PMT, the signals from the SRC and SIC channels (lower beam of radiation) get into the recorder and then into the analogue unit (not shown) for SRFWL determination by finding ratio between these signals. With ratio between the signals of two channels measurements, it is not necessary to maintain continuous sensitivity of PMT, which is necessary in case of absolute measurements of SRC and SIC. By means of feedback from the recorder, the PMT splitter is supplied with slowly changing high voltage which adjusts sensitivity of PMT proportionately with average value of signals thus providing optimal operation conditions for the photo detector of the double beam spectrophotometer.

In the monochromator, the spectrum of the upper beam of radiation from the SIC channel is scanned and the beam is reflected by the mirror 11 to the second slit of monochromator 9 where it gets into the

photoelectric unit with a high-stability silicon photodiode 12 thus implementing the scheme of the direct-reading photometer for absolute measurements of sea surface SIC.

As a result of measurements, the electronic unit obtains voltages equal to absolute values of SIC and SRFWL which allow us to recover absolute values of upwelling sea water SRC at the stage of digital processing.

For absolute measurements of sea surface SIC, a high-stability photodiode for precision measurements is used. The signal from the photodiode is amplified and transferred to a computer via a communication line for its digitalisation, visualisation and further registration. Development of the electric diagram of the SIC channel is currently at the stage of optimisation with consideration of opportunity to apply required components by various manufacturers.

3. CONCLUSION

A new approach to measurements of spectral characteristics of upwelling radiation of sea based on combination of a double beam photometer with a photomultiplier (as a photo detector) and a direct-reading photometer with a high-stability silicon photodiode for its absolute adjustment in energy units is proposed. First, this approach significantly increases precision of measurements since it does not require absolute calibration of optical channels and provides optimal conditions for PMT operation; second, it allows absolute values of SIC and SRFWL to measure simultaneously and uses them further for determination of absolute values of upwelling sea water SRC at the stage of digital processing.

MDMS applying the proposed method may be used for measurement of spectral characteristics of radiation upwelling from the sea layer in field expedition studies both on a vessel moving and on hydrological stations.

ACKNOWLEDGMENT

The project is implemented as part of the State Project No. 0827–2018–0002 “Development of methods of operative oceanology on the basis of interdisciplinary studies of the processes of formation and evolution of sea environment and mathe-

tical simulation with application of distance and contact measurements”.

REFERENCES

1. Mobley C.D. Estimation of the remote-sensing reflectance from above-surface measurements // *Applied Optics*. 1999, Vol. 38, No. 36, pp. 7442–7455.
2. IOCCG Report #13. Mission Requirements for Future Ocean-Colour Sensors. Ed. Ch.R. McClain and G. Meister, 2012, 106 p.
3. Drinkwater M.R., Rebhan H. Sentinel-3: mission requirements document. EOP-SMO/1151/MD-md. 2007, Issue 2, Rev. 0, 67 p.
4. Zibordi G., Holben B., Slutsker I., Giles D., D’Alimonte D., Melin F., Berthon J.F., Vandemark D., Feng H., Schuster G. et al. Aeronet-OC: A network for the validation of ocean colour primary products // *J. Atmospheric and Oceanic Technology*. 2009, Vol. 26, pp. 1634–1651.
5. Zibordi G., Melin F., Hooker S.B., D’Alimonte D., Holbert B. An autonomous above-water system for the validation of ocean colour radiance data // *IEEE Transactions on Geoscience and Remote Sensing*. 2004, Vol. 42, No. 2, pp. 401–415.
6. Bailey S.W., Hooker S.B., Antoine D., Franz B.A., Werdell P.J. Sources and assumptions for the vicarious calibration of ocean colour satellite observations // *Applied Optics*. 2008, Vol. 47, No. 12, pp. 2035–2045.
7. Ruddick K., De Cauwer V., Park Y., Moore G. Seaborne measurements of near infrared water-leaving reflectance – the similarity spectrum for turbid waters // *Limnology and Oceanography*. 2006, Vol. 51, No. 2, pp. 1167–1179.
8. Brando V.E., Lovell J.L., King E.A., Boadle D., Scott R., Schroeder T. The Potential of Autonomous Ship-Borne Hyperspectral Radiometers for the Validation of Ocean Colour Radiometry Data // *Remote Sensing*. 2016, 8, 150, 18 p. doi:10.3390/rs8020150.
9. Garaba S.P., Voss D., Wollschlager J., Zielinski O. Modern approaches to shipborne ocean colour remote sensing // *Applied Optics*. 2015, Vol. 54, No. 12, pp. 3602–3612.
10. Zibordi G., Ruddick K., Ansko I., Moore G., Kratzer S., Icely J., Reinart A. In situ determination of the remote sensing reflectance: An inter-comparison // *Ocean Science*. 2012, No. 8, pp. 567–586.
11. *Oceanic Optics* / Edited by A.S. Monin. Vol. 1. Physical Optics of the Ocean. Moscow: Nauka, 1983, 240 p.

11. Optika okeana / Pod. red. A.S. Monina. T.1: Fizicheskaia optika okeana. M.: Nauka, 1983, 240 p.

12. Lee M.E., Martynov O.V. Spectral Radiance Factor Measurement Device for Under Satellite Measurement of Bio-Optical Parameters of Sea Waters // Environmental Protection of Coastlands and Shelf Zones and Comprehensive Utilisation of Shelf Resources, 2000, pp. 163–173.

12. Lee M.E., Marty'nov O.V. Izmeritel' koeffitsienta iarkosti dlia podsputnykovy'kh izmerenii' bioopticheskikh parametrov vod // E'kologicheskaiia bezopasnost' pribrezhnoi' i shel'fovoi' zon i kompleksnoe ispol'zovanie resursov shel'fa, 2000, pp. 163–173.

13. Kuzmin V.N. Development and Study of Devices for Measurement of Parameters and Characteristics of Optical Radiation Sources / Dr. of Tech-

nical science Thesis. Saint-Petersburg: SPbGUITMO, 2007.

13. Kuz'min V.N. Razrabotka i issledovanie priborov dlia izmereniia parametrov i harakteristik istochnikov opticheskogo izlucheniia / Dis. d-ra tekhn. nauk. SPb: SPbGUITMO, 2007.

14. M150 Multi-Purpose Compact Monochromator-Spectrograph. URL: <https://solarlaser.com/ru/products/monochromators-spectrographs/multi-purpose-compact-monochromator-spectrograph-model-m150/> (reference date: 01.11.2017).

14. Universal'ny'i' kompakny'i' monokhromator-spektograf Model' M150. URL: <https://solarlaser.com/ru/products/monochromators-spectrographs/multi-purpose-compact-monochromator-spectrograph-model-m150/> (reference date: 01.11.2017).



Mikhail Yong-gon Lee,

Prof., Dr. of phys.-math. sciences.

In 1965, he graduated from the Leningrad Institute of Precise Mechanics and Optics. At present, he is a Head of the Sea Optics and Biophysics Department of the Marine Hydro-physical Institute of the Russian Academy of Science.

His research interests are optical oceanography, remote sensing of ocean, diffusion of light in marine water, field bio-optical studies, development of devices for hydro-optical studies



Sergei V. Fedorov

is a Head of the Remote Study Methods Department of the Marine Hydro-physical Institute of the Russian Academy of Science. His research interests are optical oceanography, remote sensing of ocean, development of devices for hydro-optical studies

ON THE ISSUE OF TRANSFORMATION OF SPATIAL PHOTOMETRIC SYSTEMS

Olga E. Zheleznikova and Sergei V. Prytkov

Ogarev Mordovia State University, Saransk, Russia
E-mail: sarstf@mail.ru

ABSTRACT

Method of transition between the $A\alpha$, $B\beta$ and $C\gamma$ photometric systems are introduced on basis of their rotation adjustment in the Cartesian coordinate system and on subsequent interpolation of luminous intensity values in given nodes. This allows us to reasonably define all meridian angle values in the whole range of taken values: $[-\pi, \pi]$ for A and B , and $[0, 2\pi]$ for C .

Keywords: illumination device, photometric systems, luminous intensity curve, goniophotometry, interpolation

Spatial angular distribution of luminous intensity is defining by measurements with goniophotometer and can be prescribed in 1 of 3 photometric systems: $A\alpha$, $B\beta$, and $C\gamma$ [1, 2]. There are no strict regulations on how to select a certain system for certain light sources or illumination devices (IDs). However, there are some recommendations. According to [1, 2], spotlights should be measured in the $B\beta$ system, headlamps should be measured in the $A\alpha$ [2] system, office lamps and street lamps should be measured in the $C\gamma$ system. If the goniophotometer kinematic diagram implies a rotation of the measured discharge lamp, you should select a system that does not change the operating position of the lamp.

The case is that people often select the most measure-convenient system.

There are cases in lighting experience when you have to take photometric measurements in one system and you have to present your results in another

system. For instance, you need to compare the measuring results of 2 goniophotometers, which kinematic diagrams use different photometric systems. There are transition equations between photometric systems in [1, 2]. As you can see below, they are not totally correct.

The photometric systems are spherical coordinate systems that are specifically oriented to the first axis, the longitudinal axis, and the transverse axis of the ID [1]. The photometric systems are combined by means of either main definitions and rules of spherical geometry [3] or matrix transitions in the Cartesian coordinate system. Both methods show the same results. In this paper, we prefer the last method because of more effective and intuitive notation.

Transition from spherical coordinates to Cartesian coordinates and vice versa is accomplished as per the following equations:

$$\begin{aligned}x &= r \sin \theta \cos \varphi, \\y &= r \sin \theta \sin \varphi, \\z &= r \cos \theta,\end{aligned}\tag{1}$$

where θ is the vector angle, φ is the azimuth angle, r is the radius vector (Fig. 1).

Let us clear up the process of transition to Cartesian coordinates connected to $C\gamma$, $B\beta$, and $A\alpha$. Coordinate axes in all 3 systems are the transverse axis, the longitudinal axis, and the first axis of the ID. The positive directions of coordinate axes in $C\gamma$, $B\beta$, and $A\alpha$ define triple unit vectors $(\mathbf{i}_C, \mathbf{j}_C, \mathbf{k}_C)$, $(\mathbf{i}_B, \mathbf{j}_B, \mathbf{k}_B)$, and $(\mathbf{i}_A, \mathbf{j}_A, \mathbf{k}_A)$ (Figs. 2–4).

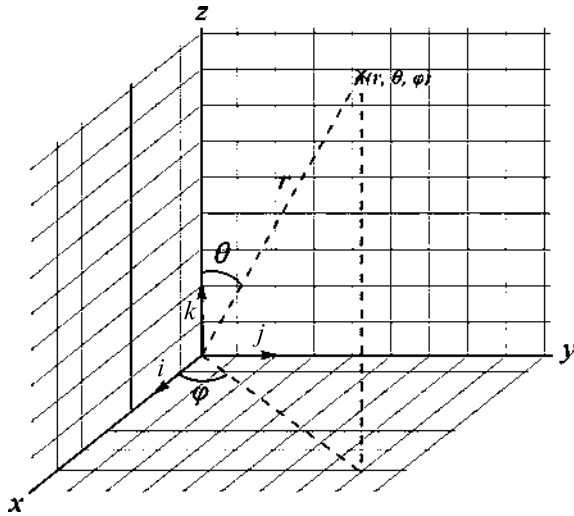


Fig. 1. Spherical coordinates system

Figs. 1–4 show that θ and φ are connected to the meridional angle and the equator angle of $C\gamma$, $B\beta$, and $A\alpha$ as follows: $\theta_C = 180^\circ - \gamma$, $\varphi_C = C$; $\theta_B = 90^\circ - \beta$, $\varphi_B = B$; $\theta_A = 90^\circ + \alpha$, $\varphi_A = A$. If we substitute the data in Eqn. (1), we get the following coordinate transition equations of $C\gamma$, $B\beta$, and $A\alpha$ to Cartesian systems:

$$\begin{cases} x_C = \sin \gamma \cos C, \\ y_C = \sin \gamma \sin C, \\ z_C = -\cos \gamma; \end{cases} \begin{cases} x_B = \cos \beta \cos B, \\ y_B = \cos \beta \sin B, \\ z_B = \sin \beta; \end{cases} \begin{cases} x_A = \cos \alpha \cos A, \\ y_A = \cos \alpha \sin A, \\ z_A = -\sin \alpha. \end{cases}$$

Now we have to rotate the coordinate axes or the basis of the systems. Referring to Figs. 2–4: at

$C\gamma \rightarrow B\beta$, rotation to \mathbf{j}_C is 270° counter-clockwise; at $B\beta \rightarrow A\alpha$, rotation to \mathbf{i}_B is 270° counter-clockwise. These are the transition data matrices:

$$R_{cb} = \begin{pmatrix} \cos 270^\circ & 0 & \sin 270^\circ \\ 0 & 1 & 0 \\ -\sin 270^\circ & 0 & \cos 270^\circ \end{pmatrix} = \begin{pmatrix} 0 & 0 & -1 \\ 0 & 1 & 0 \\ 1 & 0 & 0 \end{pmatrix};$$

$$R_{ba} = \begin{pmatrix} 1 & 0 & 0 \\ 0 & \cos 270^\circ & -\sin 270^\circ \\ 0 & \sin 270^\circ & \cos 270^\circ \end{pmatrix} = \begin{pmatrix} 1 & 0 & 0 \\ 0 & 0 & 1 \\ 0 & -1 & 0 \end{pmatrix}.$$

As you can see below, these 2 matrices are enough to completely describe the relations of the photometric systems. Let us give a matrix designation to these transitions:

$$c = \begin{pmatrix} x_C \\ y_C \\ z_C \end{pmatrix}, b = \begin{pmatrix} x_B \\ y_B \\ z_B \end{pmatrix}, a = \begin{pmatrix} x_A \\ y_A \\ z_A \end{pmatrix}.$$

The transition between the photometric systems should be described as follows:

$$C\gamma \rightarrow B\beta : b = R_{cb}c, \tag{2}$$

$$B\beta \rightarrow A\alpha : a = R_{ba}b, \tag{3}$$

$$C\gamma \rightarrow A\alpha : a = R_{ba}R_{cb}c = R_{ca}c, \tag{4}$$

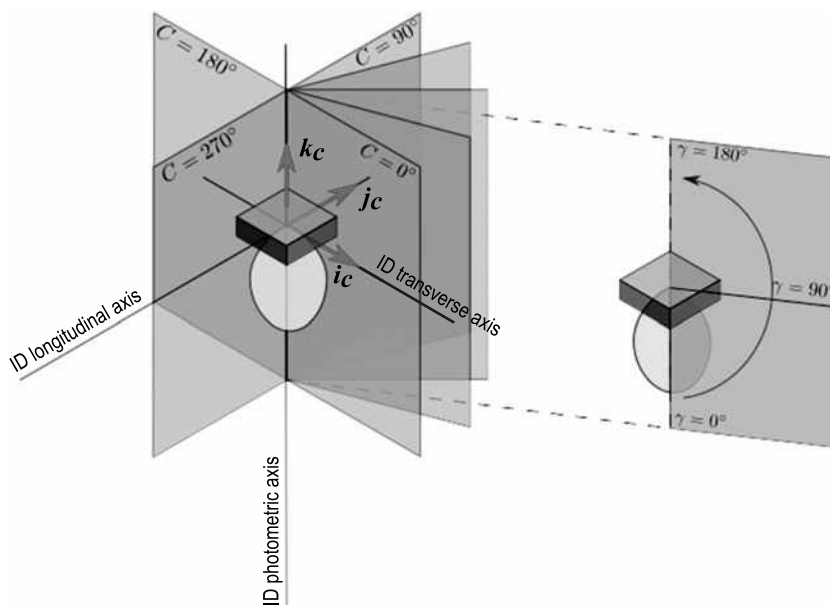


Fig. 2. $C\gamma$ photometric system

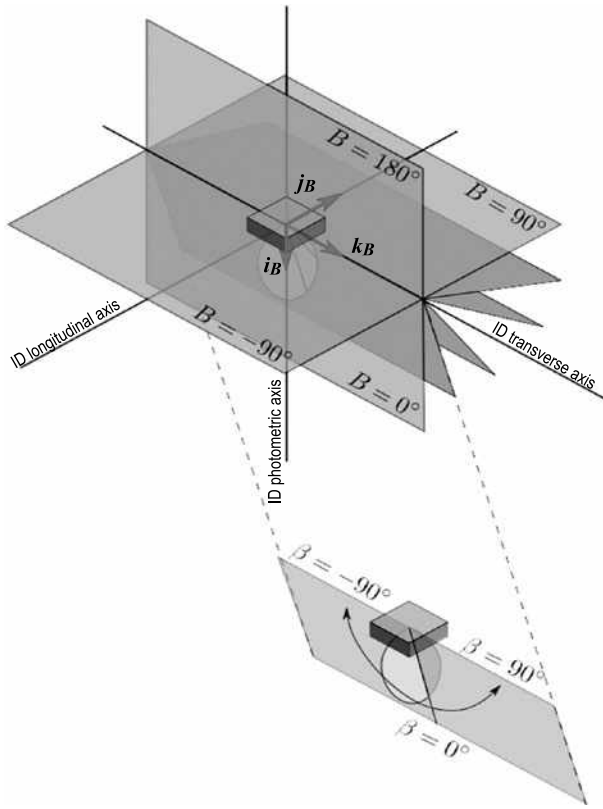


Fig. 3. $B\beta$ photometric system

$$B\beta \rightarrow C\gamma : c = R_{cb}^{-1}b, \quad (5)$$

$$A\alpha \rightarrow B\beta : b = R_{ba}^{-1}a, \quad (6)$$

$$A\alpha \rightarrow C\gamma : c = R_{ca}^{-1}a. \quad (7)$$

Eqns. (2–7) define the relations between the photometric systems. Explicitly solving these equations, we are finding the following angle correlations:

$$C\gamma \rightarrow B\beta : B = \arctg(\sin C \cdot \tg\gamma),$$

$$\beta = \arcsin(\cos C \cdot \sin\gamma), \quad (8)$$

$$B\beta \rightarrow A\alpha : A = \arctg(\tg\beta / \cos B),$$

$$\alpha = \arcsin(\sin B \cdot \cos\beta), \quad (9)$$

$$C\gamma \rightarrow A\alpha : A = \arctg(\cos C \cdot \tg\gamma),$$

$$\alpha = \arcsin(\sin C \cdot \sin\beta), \quad (10)$$

$$B\beta \rightarrow C\gamma : C = \arctg(\sin B / \tg\beta),$$

$$\gamma = \arccos(\cos B \cdot \cos\beta), \quad (11)$$

$$A\alpha \rightarrow B\beta : B = \arctg(\tg\alpha / \cos A),$$

$$\beta = \arcsin(\sin A \cdot \cos\alpha), \quad (12)$$

$$A\alpha \rightarrow C\gamma : C = \arctg(\tg\alpha / \sin A),$$

$$\gamma = \arccos(\cos A \cdot \cos\alpha). \quad (13)$$

These correlations are introduced in [1]. After analysing these correlations according to Figs. 1–4, we conclude that use of the main arctangent line is not enough to find the A equator angle, the B equator angle, and the C equator angle as $-\pi \leq A \leq \pi$, $-\pi \leq B \leq \pi$, $0 \leq C \leq 2\pi$ and $-\pi/2 < \arctg x < \pi/2$. This leads to loss of half data after transition. To reasonable define all meridian angle values you should consider the meridian angle as an argument of a complex number:

In case of A and B , we have

$$\varphi(y, x) = \begin{cases} \arctg(y/x), x > 0; \\ \pi + \arctg(y/x), x < 0, y \geq 0; \\ -\pi + \arctg(y/x), x < 0, y < 0; \\ \pi/2, x = 0, y > 0; \\ -\pi/2, x = 0, y < 0; \end{cases}$$

And in case of C , we have

$$\varphi^*(y/x) = \begin{cases} \arctg(y/x), x > 0, y \geq 0; \\ \pi + \arctg(y/x), x < 0; \\ 2\pi + \arctg(y/x), x > 0, y < 0; \\ \pi/2, x = 0, y > 0; \\ 3\pi/2, x = 0, y < 0. \end{cases}$$

Let us consider this and rewrite Eqns. (8–13) as follows:

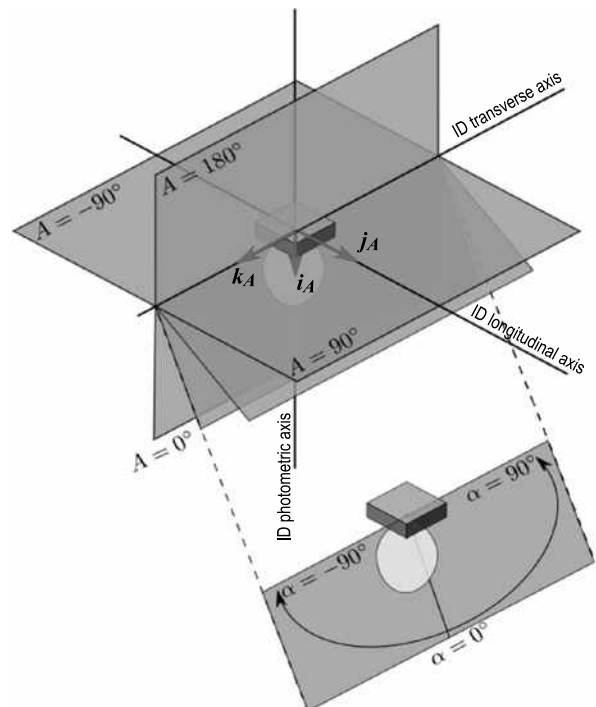


Fig. 4. $A\alpha$ photometric system

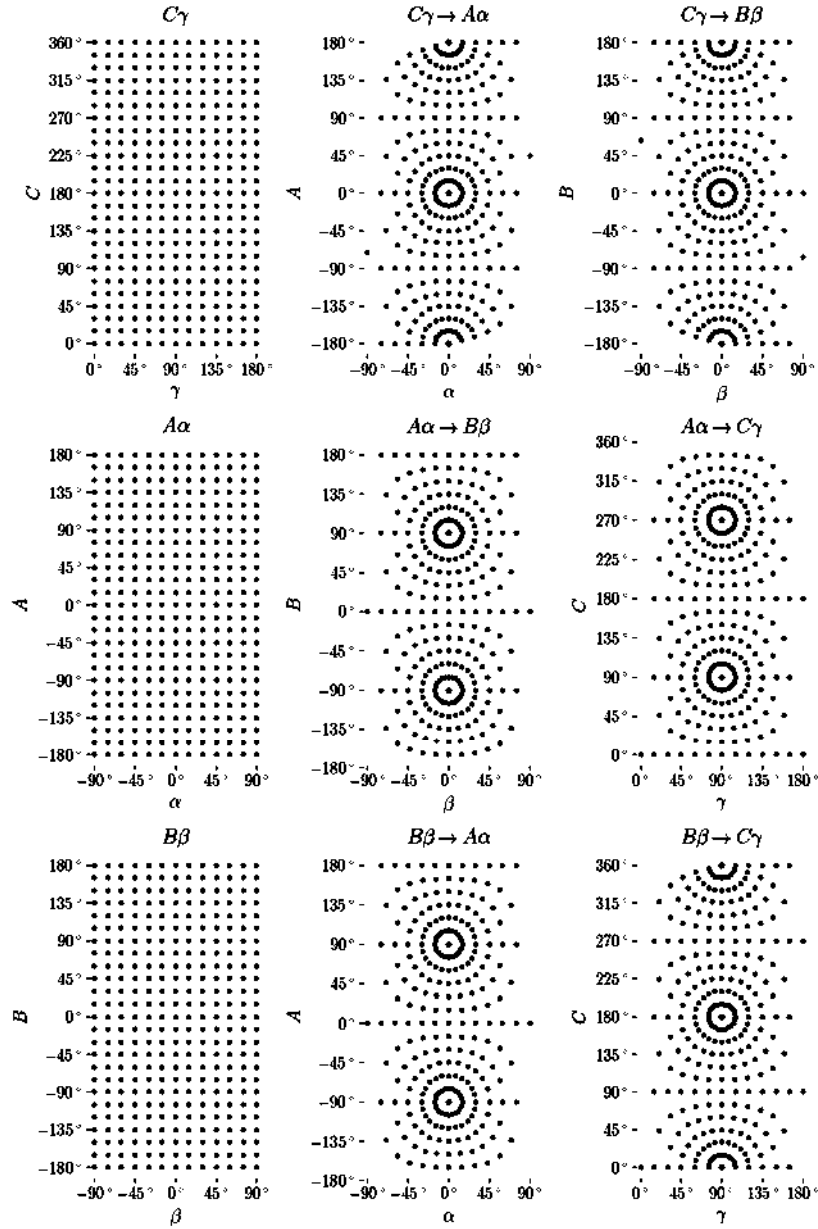


Fig. 5. Photometric systems nodes before and after transition in accordance with Eqns. (14–19)

$$\begin{aligned}
 C\gamma \rightarrow B\beta : B &= \varphi(\sin C, \text{ctg}\gamma), \\
 \beta &= \arcsin(\cos C \cdot \sin \gamma),
 \end{aligned}
 \tag{14}$$

$$\begin{aligned}
 B\beta \rightarrow C\gamma : C &= \varphi(\sin B, \text{tg}\beta), \\
 \gamma &= \arccos(\cos B \cdot \cos \beta),
 \end{aligned}
 \tag{15}$$

$$\begin{aligned}
 B\beta \rightarrow A\alpha : A &= \varphi(\text{tg}\beta, \cos B), \\
 \alpha &= \arcsin(\sin B \cdot \cos \beta),
 \end{aligned}
 \tag{16}$$

$$\begin{aligned}
 A\alpha \rightarrow B\beta : B &= \varphi(\text{tg}\alpha, \cos A), \\
 \beta &= \arcsin(\sin A \cdot \cos \alpha),
 \end{aligned}
 \tag{17}$$

$$\begin{aligned}
 A\alpha \rightarrow C\gamma : C &= \varphi(\text{tg}\alpha, \sin A), \\
 \gamma &= \arccos(\cos A \cdot \cos \alpha),
 \end{aligned}
 \tag{18}$$

$$\begin{aligned}
 C\gamma \rightarrow A\alpha : A &= \varphi(\cos C, \text{ctg}\gamma), \\
 \alpha &= \arcsin(\sin C \cdot \sin \gamma).
 \end{aligned}
 \tag{19}$$

According to the transition result (Fig. 5), the data structure becomes a non-regular structure after transpositions as per Eqns. (14–19), and we need additional interpolation of luminous intensity values. There are 2 alternatives:

- If we combine the old system (source data system) with the new system, luminous intensity values are then interpolated in the new system. Interpolation nodes form a non-regular grid, and this is the reason why you should use appropriate interpolation (e.g. Delaunay triangulation) [4];

• If we combine the new system (where we want to get luminous intensity values) with the old system, luminous intensity values are then interpolated in the old system. Interpolation nodes form a rectangular grid, and this is the reason why you can use bilinear interpolation to find luminous intensity values [5].

This article introduces a transition method between photometric systems based on their combination by means of rotations in the Cartesian coordinate system and on subsequent interpolation of luminous intensity values in given nodes. Unlike the formulas given in [2], Eqns. (14–19) allow us to reasonably define all meridian angle values in the area of taken values: $[-\pi, \pi]$ for A and B , and $[0, 2\pi]$ for C . After transposition in Eqns. (14–19), the angle grid becomes a non-regular grid that prevents exporting files to LDT and IES which are widely used photometric data formats [6, 7]. It is found that [2] for $A\alpha \rightarrow C\gamma$ does not give any equation that could conform to either [1] or the solution given in this article. According to [2], $A\alpha \rightarrow C\gamma$ is transited as follows:

$$\gamma = \alpha + 90^\circ, C = \begin{cases} -A, & -180^\circ < A < 0^\circ; \\ 360^\circ - A, & 0^\circ < A < 180^\circ; \\ 0^\circ, 360^\circ, & A = 0^\circ. \end{cases} \quad (20)$$

According to the analysis of Eqn. (20), there is no rotation of $A\alpha$ relative to the ID before it combines with $C\gamma$. This means that the polar axis of $C\gamma$ (photometric semi-planes intersection line) does not combine with the optical axis of the ID after transition in Eqn. (20), which infringes one of the requirements for given system building [1, 2].

REFERENCES

- GOST R54350–2015. Illumination Devices. Lighting Specifications and Testing Methods.
- GOST R54350–2015. Pribory osvetitelnyye. Svetotekhnicheskiye trebovaniya i metody ispytaniy.
- IESNA LM-75–01. Goniophotometer Types and Photometric Coordinates.
- Alekseevsky, D. V., Vinberg, E. B., Solodovnikov, A.S. Constant Curvature Space Geometry // Science and Engineering Results. Modern Mathematics Challenges. Fundamental Directions. Moscow: VINITI, 1988, Vol. 29, pp. 1–146.
- Skvortsov, A.V. Delaunay Triangulation and Its Use. Tomsk: Tomsk University Press, 2002, 128 p.
- Skvortsov, A.V. Triangulyatsiya Delone i yeye primeneniye. – Tomsk: Izd-vo Tomskogo un-ta, 2002, 128 p.
- GOST R55708–2013. Outdoor Utility Lighting. Rate Parameters Calculation Methods.
- GOST R55708–2013. Osveshcheniye naruzhnoye utilitarnoye. Metody rascheta normiruyemykh parametrov.
- IESNA: LM-63–1995. Standard File Format for Electronic Transfer of Photometric Data.
- Stockmar, A. W. EULUMDAT/2 – Extended Version of a Well Established Luminaire Data Format // CIBSE National Lighting Conference, 1998, pp. 353–362.



Olga E. Zheleznikova,
Ph.D. in Technical Science,
Assistant Professor,
graduated from the Ogarev
Mordovia State University
in 1989, the Faculty for
Lighting Engineering. She
is now the Head of the

Chair for Lighting Engineering at the National Research University – the Ogarev Mordovia State University. She is also an Honorary Figure of Mordovian Higher Education and a Member of the Editorial Board of Light & Engineering Journal



Sergei V. Prytkov,
Ph.D. in Technical Science,
graduated from the Ogarev
Mordovia State University
in 2010. He is now the
Assistant Professor of
the Lighting Engineering
Faculty at the National

Research University – the Ogarev Mordovia State University. Field of his interests includes lighting design

CONTENTS

VOLUME 27

NUMBER 4

2019

LIGHT & ENGINEERING (SVETOTEKHNIKA)

Alexander V. Bogdanov and Vladimir A. Smirnov

Why it is Necessary to Revise the Standards of Exhibition Lighting

Boris G. Kuzyakin

Aspects of Exhibition Lighting in the State Hermitage

Anubrata Mondal and Kamalika Ghosh

Studies on Germicidal Benefit of Ultra Violet Ray upon Old Paper Documents

Lyubov E. Volgina

Light in the Museum: Experiences and Challenges

Leonid G. Novakovsky

Illumination of Paintings, Architectural Lighting in Museums

Nicolai I. Shchepetkov

Graphic Arts, Printed Products, Photographs: Problems and Possible Solutions

**Anna G. Shakhparunyants, Eugene I. Rozovsky, Anatoly Sh. Chernyak,
and Pavel A. Fedorishchev**

LEDs in Museums: New Opportunities and Challenges

Karsten Winkels

Implementation of Exhibition Lighting Concept as Means of Artistic Expression
through Example of "Russian Insomnia" Exhibition

Anatoly Sh. Chernyak, Alyona B. Kuznetsova, Alexandra A. Bartseva

Measurement of Illumination Parameters of the Halls and Exhibited Items of the State
Hermitage and the State Tretyakov Gallery

Sergei S. Bayev, Vladimir N. Kuzmin, and Konstantin A. Tomsky

Study of Impact of Optical Radiation on Materials of Museum Exhibits and Requirements
to Measurement Devices

Andrei V. Aladov, Alexander L. Zakgeim, and Anton E. Chernyakov

LED Museum Lighting: Back to Natural Light

Margarita P. Belyakova

Upgrade of Lighting in Hall 277 of the State Hermitage

Sergei V. Koynov and Dmitry M. Hodyrev

Museum Lighting: Approach, Example and Direction

Sergei A. Stakharny

Organic LED's is an Innovative Light Source

Nicolai R. Vorobyov

Light Dramaturgy as an Element of an Integrated Approach to the Creation
of Museum Expositions and Exhibition Projects

NECROLOGY

Professor Nicolay Ivanov Vasilev

May 10, 2019, after a short illness, at the age of 89 died



We have lost a remarkable scientist, one of the founders of Lighting Engineering as a science in Bulgaria. Professor Nicolay Vasilev was graduated from the State Polytechnic University in Sofia with a degree in electrical networks and systems and specialized in electricity supply and lighting equipment. His professional career began as a designer in ENERGOPROEKT - SOFIA with large-scale power supply systems for new residential areas Yavorov, Iztok and Hipodrum in Sofia. At the same time, he was part-time assistant at MEI-Sofia. As an assistant on an ongoing basis (1959), associate professor (1966) and professor of industrial lighting (1969), he introduces the subjects of electrical equipment and lighting equipment and develops these courses at the Department of Electrical Networks and Systems. In 1981, Prof. Nicolay Vasilev founded an industrial research lighting laboratory in the department of electrical engineering and power supply. For 38 years now this laboratory has been a national scientific centre with international popularity and is accredited in the field of testing and calibration. The first scientific team of lighting technicians was created in this laboratory: 13 Doctors, many Assistant Professors and three Professors. We will remember his active public, organizational and managerial activities as Deputy Dean of the Electrical Engineering Department, Chairman of the Scientific and Technical Union in Bulgaria, Founder, Chairman and Honorary Chairman of the National Committee on Illumination. From 2006 to 2013, Nicolay Vasilev led the national

team participating in the European Adaptive Street Lighting Program. The scientific work of Professor Vasilev, published in world-famous journals and presented at international symposia, are highly valued abroad. He is the author of over 200 publications and most books and textbooks in the field of lighting engineering in Bulgaria. In 2013, the Light & Engineering Journal recognized Professor Nicolay Vasilev as one of the world-renowned scientists in the field of lighting engineering and invited him to participate in an interview organized at the international level.

**HE KNEW, HE COULD, AND HE GAVE
TO US VERY MUCH, REST IN PEACE,
DEAR TEACHER!
LAST FORGEST...**

*Bulgarian National
Lighting Committee*

The editorial board of Light & Engineering /Svetotekhnika Journal express their sincere condolences to the family of the deceased and his staff in connection with the death of Nicolay Vasilev, a member of the editorial board of Light & Engineering Journal, an outstanding Bulgarian scientist.

I am grieving, the death of my friend. We were associated with activities in the field of lighting, international activities within the framework of the CIE and IEC, as well as a great personal friendship for many decades. Nicolay was a great scholar, organizer of science and a wonderful person.

Ju.B. Aizenberg

PARTNERS OF LIGHT & ENGINEERING JOURNAL

Editorial Board with big gratitude would like to inform international lighting community about the Journal Partners Institute establishment. The list with our partners and their Logo see below. The description of partner's collaboration you can found at journal site www.sveto-tehnika.ru

